REDUCTIVE DEHALOGENATION OF GAS-PHASE TRICHLOROETHYLENE USING HETEROGENEOUS CATALYTIC AND ELECTROCHEMICAL METHODS

by

Xiumin Ju

A Dissertation Submitted to the Faculty of the

DEPARTMENT OF CHEMICAL AND ENVIRONMENTAL ENGINEERING

In Partially Fulfillment of the Requirements
For the Degree of

DOCTOR OF PHILOSOPHY
WITH A MAJOR IN ENVIRONMENTAL ENGINEERING

In the Graduate College

THE UNIVERSITY OF ARIZONA

2 0 0 5

THE UNIVERSITY OF ARIZONA
GRADUATE COLLEGE

As members of the Dissertation Committee, we certify that we have read the dissertation prepared by Xiumin Ju

entitled Reductive Dehalogenation of Gas-Phase Trichloroethylene Using Heterogeneous Catalytic and Electrochemical Methods

and recommend that it be accepted as fulfilling the dissertation requirement for the Degree of Doctor of Philosophy

_____ Date: 11/28/05
Robert G. Arnold, Ph.D

_____ Date: 11/28/05
A. Eduardo Sáez, Ph.D.

_____ Date: 11/28/05
James Farrell, Ph.D.

_____ Date: 11/28/05
Eric A. Betterton, Ph.D.

_____ Date: 11/28/05
J. Brent Hiskey, Ph.D.

Final approval and acceptance of this dissertation is contingent upon the candidate's submission of the final copies of the dissertation to the Graduate College.

I hereby certify that I have read this dissertation prepared under my direction and recommend that it be accepted as fulfilling the dissertation requirement.

_____ Date: 11/28/05
Dissertation Director: Robert G. Arnold, Ph.D.

STATEMENT OF AUTHOR

This dissertation has been submitted in partial fulfillment of requirement for an advanced degree at The University of Arizona and is deposited in the University Library to be made available to borrowers under rules of the Library.

Brief quotations from this dissertation are allowable without special permission, provided that accurate acknowledgment of source is made. Requests for permission for extended quotation form or reproduction of this manuscript in whole or in part may be granted by the head of the major department or the Dean of the Graduate College when in his or her judgment the proposed used of the material is in the interest of scholarship. In all other instances, however, permission must be obtained from the author.

SIGNED**:** Xiumin Ju

ACKNOWLEDGEMENTS

I would like to thank my advisor Dr. Robert G. Arnold for his academic guidance and support. It has been a very rewarding experience working with him, and I am always grateful to him for the time, effort, and attention he devoted to me.

For their excellent academic guidance and supervision, I would like to express my gratitude to Dr. A. Eduardo Sáez, Dr. Eric A. Betterton, Dr. Wendell P. Ela, and Dr. J. Brent Hiskey. The moments they spent with me will always be remembered.

I am also grateful to Dr. James A. Field and Dr. Reyes Sierra for their patience, support, and understanding I received in the past years.

For the excellent teaching, suggestions, and criticisms I received for these many years, thank you to Dr. James Farrell.

Thanks to Dr. Srini Raghavan for his teaching and the valuable time he spent for me from his very busy schedule.

I would like to thank Ozer Orbay for initiating the research project, and training me to take over. The assistance I received from Autumn Ela, Matthew Wallen, Rosemary A. Galhotra in performing the experimental work will always be remembered. Special thanks go to Brian Barbaris, Ron Leblanc, and Mathias Hecht for their technical support in this research.

I am also very thankful for the support and help I received from all other faculty members, staff, and students in the University of Arizona, especially the Department of Chemical and Environmental engineering. Thank you all for being there for me, so nicely!

Finally, I would like to acknowledge funding support for this research by the NIEHS Superfund Program at the University of Arizona (under NIH ES04940).

TABLE OF CONTENTS

TABLE OF CONTENTS - *Continued*

LIST OF FIGURES

LIST OF FIGURES - *Continued*

LIST OF FIGURES- *Continued*

ABSTRACT

The first part of this work investigates catalytic hydrodechlorination (HDC) of gas-phase trichloroethylene (TCE) using 0.5 wt.% Pt/γ-Al_2O_3 and 0.0025 wt.% Pt/SiO_2 in packed-bed reactors. TCE was efficiently transformed on the platinum surface using H_2 as reducing agent. The main products of the reaction were ethane and chloroethane. In the case of Pt/Al_2O_3, more than 94% TCE conversion efficiency was maintained for over 700 hours of operation at 100ºC at a residence time of 0.37 seconds. At 22ºC, severe catalyst deactivation was observed. Catalyst deactivation was attributed to coking and chlorine poisoning. A series of treatments including (i) hydrogen gas addition at high temperature (oxygen free) to remove chlorine and (ii) oxygen addition at 500ºC to remove coke were attempted to regenerate the deactivated catalyst. Only hydrogen treatment partially restored catalyst activity. When using Pt/SiO_2, catalyst deactivation was severe even at 100ºC, probably due to low surface area of Pt and the silica support. Adding KOH to the packed Pt/SiO_2 catalyst during (otherwise) normal operation slowed catalyst deactivation. Adding O_2 to the influent improved catalyst activity and slowed deactivation.

The second part of this research involves the destruction of gas-phase TCE using an electrochemical reactor similar in design of a polymer electrolyte membrane (PEM) fuel cell. With a proton-conducting membrane in the middle, the anode and cathode comprised of carbon cloth and carbon-black-supported Pt were hotpressed together to form a membrane electrode assembly (MEA). TCE contaminated gas streams were fed to the cathode side of the fuel cell, where TCE was reduced to ethane and hydrochloric

acid. The results suggest that TCE reduction occurs via a catalytic reaction with atomic hydrogen that is reformed on the cathode's surface rather than an electrochemical reduction via direct electron transfer. Substantial conversion of TCE was obtained, even in the presence of molecular oxygen in the cathode chamber. The process was modeled successfully by conceptualizing the cathode chamber as a plug flow reactor with a continuous source of H_2 (g) emanating from the boundary.

CHAPTER 1

LITERATURE REVIEW

1.1 Introduction

Chlorinated solvents are among the most persistent and widespread classes of hazardous contaminants in groundwater and soil. Common chlorinated solvents such as trichloroethylene (TCE), perchloroethylene (PCE), carbon tetrachloride (CT), and chloroform (CF) were widely used by industries for cleaning and degreasing machinery. Due to inadequate disposal practices, these solvents are now common groundwater and soil contaminants. Sixty-nine percent of national priority list (NPL) sites contain chlorinated solvents [1]. Nine chlorinated solvents were among twenty-five most frequently detected groundwater contaminants at hazardous waste sites: TCE, PCE, dichloromethane (DCM), 1,1,1-trichloroethane (1,1,1-TCA), CF, 1,1-dichloroethane (1,1-DCA), trans 1,2-dichloroethene (trans 1,2-DCE), 1,1-dichloroethene (1,1-DCE), vinyl chloride (VC), and 1,2-dichloroethane (1,2-DCA) [2]. Exposure to these chemicals is linked to severe deleterious health effects such as skin, liver, and kidney cancers; impairment to central nervous system [3]; and fetal heart defects [4].

Pump-and-treat is the most commonly used technology for groundwater remediation. In this process, above ground treatment of contaminated groundwater frequently involves granular activated carbon (GAC) adsorption or air stripping followed by GAC treatment of the contaminated gas stream. For contaminated soil, excavation, incineration, landfill disposal, and solidification in place with cementing agents are conventional treatment technologies.

The inadequacy of conventional technologies for remediation of chlorinated solvents has become apparent. A survey of 77 sites under remedial action using pump-and-treat strategies found that only 8 achieved their cleanup goals. It was determined that 34 of the sites would probably never achieve restoration objectives because of subsurface heterogeneity and consequent slow desorption of contaminants to the bulk groundwater [2].

The inefficiency of conventional treatment technologies and market demand provide incentives to develop non-conventional (innovative) treatment technologies. It was estimated that alternative methods for waste site investigation and remediation could cut costs by 50 percent or more [5]. Widely studied innovative treatment technologies include soil vapor extraction (SVE), bioventing, *in-situ* bioremediation, pulsed and variable pumping, surfactant and co-solvent enhanced flushing, *in-situ* chemical treatment, passive treatment using reactive permeable barriers containing zero valent iron, and electrochemical methods. For example, soil vapor extraction is frequently selected to recover semi-volatile pollutants when they are present in the vadose zone. The technology is particularly attractive when depth to aquifer is relatively large. Both air stripping and soil vapor extraction produce gas streams that require further treatment before they can be discharged to the atmosphere. Incineration and catalytic oxidation are frequently selected to destroy these compounds. However, potential generation of more toxic compounds such as dioxin limits the application of very high temperature technologies [6].

In contrast, reductive dehalogenation using heterogeneous catalytic and electrolytic methods can dehalogenate chlorinated gas-phase contaminants while avoiding the generation of trace contaminants like dioxins because of the absence of oxygen. Due to the electronegative character of halogen substituents, heavily chlorinated aliphatics are thermodynamically disposed for reductive dehalogenation by electron donors such as elemental hydrogen and zero valent metals [7,8]. Electrochemical reduction of such compounds has also been explored [9-11].

1.2 Catalytic hydrodechlorination

In catalytic hydrodechlorination (HDC), chlorinated organic compounds are reduced to corresponding hydrocarbons on the catalyst surface using molecular hydrogen. For instance, TCE can react with H_2 on a platinum catalyst to form ethane. The overall reaction is represented by:

$$C_2HCl_3 + 4\,H_2 \xrightarrow[Catalyst]{} C_2H_6 + 3HCl \qquad (1.1)$$

The characteristics of catalytic HDC as a treatment alternative include: (i) it is effective for a variety of chlorinated organic compounds; (ii) reaction kinetics are typically fast; (iii) it produces no toxic intermediates such as dioxins and phosgene that are formed via oxidative transformations including combustion; (iv) its products are environmentally benign hydrocarbon compounds that can be recycled as fuel or chemical stocks; (v) transformation conditions (temperature and pressure) are typically mild; (vi) there is no NO_x formation due to relatively low reaction temperatures.

Research on catalytic HDC has focused on catalyst screening and its applicability to different types of organochlorine compounds. Among the varieties of catalysts investigated including supported and unsupported precious metals (Pt, Pd, Rh) [12-15], transition metals such as Ni and Mo [16], and metal oxides such as Cr_2O_3 [17], supported precious metals are superior to other catalysts. Representative support media include carbon, alumina, zeolite, silica, titanium oxides, zirconium oxides [18], and polymers [19]. Types of chlorinated organic compounds evaluated include chlorofluorocarbons (CFCs) [20-22], chlorinated aromatics [23-25], and chlorinated aliphatics [14,26,27] in organic matrices, aqueous, and gas phases. Complete dechlorination is generally achieved. Other than elemental hydrogen, hydrogen-donors such as alcohols and formates have also been investigated in this context, but to a lesser extent [28-30].

1.2.1 Reaction mechanisms

While dehalogenation of heavily chlorinated aromatics often proceeds through sequential removal of chlorines [31-33], the dehalogenation of aliphatics containing multi-chlorine substituents often occurs via a concerted mechanism in which fully dehalogenated hydrocarbons are formed without desorption of chlorinated intermediates [34-36].

The first step in catalytic HDC for chlorinated methanes begins with the scission of an initial carbon-chlorine bond on the catalyst surface, forming adsorbed chlorine and intermediates. Irreversible carbon-chlorine bond breakage is thought to be the rate-determining step (RDS) [15,37,38]. The adsorbed intermediates then react with atomic hydrogen to form different products via parallel reaction pathways. The reaction

mechanism is illustrated in Figure 1.1 using CT as the model compound [39-41]. Adsorption of CCl_4 on the metal catalyst resulted in the formation of adsorbed trichloromethyl radical (CCl_3^*) and chlorine (Cl^*). The adsorbed trichloromethyl radical may react with adsorbed atomic hydrogen (H^*) to form chloroform, combine with a second trichloromethyl radical to produce hexachloroethane, or undergo complete dechlorination to form methane. The pathway leading to methane formation may involve further dechlorinated radicals such as $CHCl_2^*$ and CH_2Cl^*, but these radicals stay on the catalyst surface without desorption.

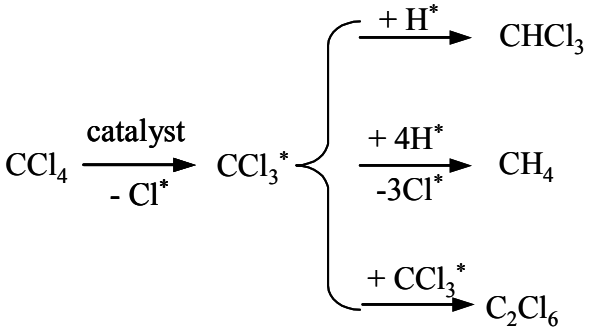

Figure 1.1 Carbon tetrachloride hydrodechlorination reaction scheme

The relative importance of CCl_4 reaction pathways depends on selection of both the catalyst and support material. Supported Pd leads predominantly to CH_4 production. When supported Pt is the catalyst, $CHCl_3$ is frequently a major product [42-45]. The formation of oligomerization products such as C_2Cl_6 and C_2Cl_4 has been related to surface acidity of metal oxides support [18]. Surface acidity is attributed to protons on surface hydroxyl group (Brønsted acid) and surface cations that can accept electron charge from donor molecules (Lewis acid). The surface acidic sites promote formation of

oligomerization products. Reaction rates of chlorinated methanes decrease in the order of CCl_4 > $CHCl_3$ > CH_2Cl_2 > CH_3Cl, well correlated with the bond dissociation energies that increase in the order of CCl_4 < $CHCl_3$ < CH_2Cl_2 < CH_3Cl, suggesting the rate-determining step involves carbon-chlorine bond cleavage [41,44,45].

Hydrodechlorination of chlorinated alkenes involves saturation of the carbon-carbon double bond and replacement of chlorine substituents with hydrogen. Fully dechlorinated hydrocarbons are major products. Ethane, for example, is the major product from chlorinated ethylenes such as PCE and TCE. The formation of hydrocarbons was held to involve a concerted mechanism without desorption of chlorinated intermediates, and parallel reaction pathways were proposed for the production of trace amounts of chlorinated intermediates [34,46].

Ordonez et al. [27,47,48] proposed that catalytic hydrodechlorination of chlorinated ethylenes began with hydrogenation of double bonded carbons, which was also the rate determining step. Hydrocarbons were then formed via concerted mechanisms.

On the other hand, Weiss et al. [49] proposed that HDC of *cis*- and *trans*- DCE proceeded mainly by sequential removal of chlorines from DCE isomers to ethane with VC as an intermediate product. The rate constant for reduction of DCE to VC was approximately twice that of VC conversion to ethane. Side reactions included hydrogenation of DCE to produce DCA, and VC to chloroethane. However, rates of these reactions were apparently orders of magnitude lower than the rates of hydrodechlorination reactions.

1.2.2 Catalyst deactivation and regeneration

Loss of catalyst activity as a function of operation time is common in catalytic HDC. Since the most effective catalysts so far studied are supported precious metals such as Pt and Pd, catalyst life has a great effect on process economics. Mechanisms for catalyst deactivation and means to regenerate catalysts have been studied extensively, but are not yet well established.

Possible mechanisms for catalyst deactivation include catalyst sintering, poisoning, and coking [50]. Sintering refers to aggregation of catalyst particles with a consequent decrease in surface area. Poisoning causes activity loss by strong chemisorption of chemical elements to active sites. Coking refers to the deposition of carbonaceous compounds on the catalyst, which reduces the number of effective catalyst sites either by direct deposit of carbonaceous products or by blockage of pathways that provide access to internal sites.

In the fairly extensive literature pertaining to catalyst deactivation as a consequence of HDC of chlorinated compounds, deactivation is usually attributed to chlorine poisoning of the catalyst surface (Pt or Pd) or coking. Although uncommon, catalyst sintering and leaching of metal from the catalyst support have also been observed [51,52].

1.2.2.1 Chlorine poisoning

Chlorines can be strongly adsorbed onto transition metals via covalent bonds, and thus reduce HDC reaction rates by limiting the number of sites available for adsorption of target compounds and hydrogen. Catalyst will continue to decay if chlorine-bonded sites

accumulate during catalyst use. Desorption of adsorbed chlorine as HCl gas or aqueous phase HCl increases the number of available catalyst sites. The kinetics of HDC reactions are often inversely proportional to the concentration of gas phase HCl, reflecting the inhibition of HDC reaction by the presence of HCl [15,36,53-56].

Accumulation of HCl inside a HDC catalytic reactor may eventually stop the reaction. It was frequently observed that the addition of strong base was necessary to fully convert the chlorinated organics to dehalogenated products [33,57,58]. Base addition also assisted HDC reactions by scavenging protons, keeping the metal catalyst in reduced state, and reducing the interaction of chloride with catalyst.

In continuous flow reactors, fluids continually carry HCl out of the reactor, and catalyst activity is expected to eventually stabilize. However, a typical deactivation pattern consists of an initial period of rapid deactivation followed by a longer period of continuous slow deactivation. The sequential periods of rapid and slow deactivation apparently result from different deactivation mechanisms.

HDC-deactivated catalysts usually have increased chlorine content. Bozzelli et al. [14] found that chlorine content of the catalyst increased from 0.11% to 0.46 wt% after 600 minutes of operation for the HDC of 1,2-DCA on Rh/SiO_2. Using deionized (DI) water, Gampine et al. [51] extracted 4.5 chloride ions for each Pd atom from used catalyst. Shin et al. [59] showed that catalyst deactivation was proportional to the total amount of chlorine removed from the chlorinated target compounds.

Transition metals covalently bound to chlorine are reduced to elemental metal at high temperature in the presence of H_2. However, catalysts deactivated by HDC processes

could not be restored by hydrogen treatment, even at 400°C [55,59]. Sometimes partial regeneration of catalyst is achieved by hydrogen treatment [14,54]. The ineffectiveness of H_2 treatment indicates that catalyst deactivation is caused not only by chemisorbed chlorine. Bozzelli et al. [14] studied the hydrogenation of ethylene using $RhCl_3/SiO_2$ and deactivated Rh/SiO_2. The activity of deactivated Rh/SiO_2 was significantly lower than $RhCl_3/SiO_2$. To explain this irreversible catalyst deactivation, Coq et al. [55] proposed the existence of tightly bound chloride species that could not be removed by hydrogen. Shin et al. [59] suggested that an irreversible modification of electronic structure of the metal occurred during long-term exposure to HCl. However, the hypothesized tightly bound chloride species may have been chlorine-containing coke.

1.2.2.2 Coking

Carbonaceous deposits commonly form on catalysts during HDC processes [18,26,48,60-63]. For example, Frankel et al. [60] observed 23-29 wt.% of carbon deposited on used Pt/ηδ-alumina after 7 hours of operation for reduction of 1,1,1-TCA. These deposits contained chlorine, suggesting that both the chlorinated target compound and chlorinated intermediates are coke precursors [44,64,65].

The quantity, chemical composition, and temperature of combustion of carbonaceous deposits can be tested using techniques such as thermogravimetry (TG), differential scanning calorimetry (DSC), temperature programmed reduction (TPR), and temperature programmed oxidation (TPO). TG gives coke content and temperature of combustion by measuring change in mass with temperature. DSC measures the flux of heat energy as a

function of temperature to yield information about the temperature of combustion. Using mass spectrometry to identify the substances produced, TPR and TPO reveal chemical composition and temperature of combustion.

Temperature of combustion is an important factor for coke identification. Research indicated that the temperature of combustion of coke varies in the range 250-500ºC, reflecting differences in formation mechanism, composition and reactivity [44,64,66]. Marecot et al. [66] found three coke oxidation peaks at near 250ºC, 400ºC, and 500ºC, which were correlated to the coke deposits on Pd metals with different coordination number and silica support. Creyghton et al. [63] observed two peaks in the region 269-312ºC and near 400ºC. They attributed the low temperature peak to burning of carbonaceous deposits on the metal surface and the peak at 400ºC to the burning of carbonaceous deposits on Brønsted acid sites of the support material. The peak at lower temperature might also be attributed to the burning of coke at the external surface and pore mouth of the catalyst [67].

Coke deposits can be burned off under oxidizing conditions, and thus restore catalyst activity. Bae et al. [44] observed almost complete regeneration of catalyst in the presence of O_2 at 500ºC followed by H_2 reduction at 300ºC. The same catalyst treated with O_2 at 300ºC did not recover its activity, which was in agreement with their finding that coke combustion was initiated at 477ºC. Kim et al. [18] reported the recovery of catalyst activities after treatment with O_2 at 300ºC for 2 hours. Complete catalyst regeneration was not generally achieved due to changes in catalyst and support structure during high temperature operation. Ren et al. [68] reported that even the complete combustion of

coke could not restore the catalyst activity due to changes in pore size distribution and tortuosity. They also found that higher coke content led to less effective regeneration during equivalent recovery steps.

1.2.2.3 Factors affecting catalyst deactivation

As mentioned above, HCl poisoning and coking are the two primary mechanisms for catalyst deactivation in the literature. It is likely that strong chemisorption of chlorine causes the initially rapid drop of catalyst activity, and that the deposition of carbonaceous compounds continues to reduce catalyst activity, although more slowly, thereafter. It has also been demonstrated that chemisorbed chlorine species alter the electronic properties of the catalyst surface, which promotes carbon deposition [69,70]. Bae et al. [44] observed that catalyst activity dropped dramatically when catalysts were pretreated with HCl. They also found that a large amount of coke formed on the same catalyst.

Catalyst decay rate has also been examined as a function of catalyst particle size. Small metal particles (<5 nm) on the support are intrinsically more electron deficient than large particles due to the interaction of metals with acid sites of the support material [71,72]. These electron-deficient particles interact strongly with chorine, resulting in fast catalyst deactivation. Zhang et al. [71] observed that the conversion efficiency of CCl_4 dropped from 90% to 1% within an hour when most of the catalyst particles were smaller than 1.5 nm. However, when the particle size was increased to 5-8 nm, the catalyst activity was stable for more than 2000 h at about 75% removal efficiency. Bae et al. [26] also reported that small particles (2.76 – 4.10 nm) promoted the formation of carbonaceous

deposits due to strong adsorption of chlorinated single carbon species. Among metal particles of sufficient size, catalyst deactivation is structure insensitive. Ribeiro et al. [56] studied the HDC of CFC 114a on Pd(111) and Pd(100) single crystal surfaces and on Pd foil, and found that reaction rates were similar. Thompson et al. [36] also found that the HDC of CFCs was structure insensitive on Pd/C with particle sizes in the range of 6.2 - 13.3 nm.

The nature of the catalyst support has great influence on the catalyst performance. The acidity of the metal oxide support is believed to promote coke formation [18,63]. Studying the HDC of CCl_4 on Pt supported on a series of metal oxides, Kim et al. [18] found that Pt/MgO was the least deactivated catalyst due to the basicity of MgO. The rate of coke formation on that support was also the lowest. Activated carbon is resistant to HCl and may be a better catalyst support in HDC processes [73]. However, blockage of micropores by coke is of particular concern among activated carbon supports [48].

There are different opinions on the effects of temperature on catalyst deactivation. In the study of HDC of PCE on Pd/Al_2O_3 and Pt/Al_2O_3, Ordonez et al. [48] observed higher catalyst initial activity, but faster deactivation rates with increasing temperatures in the range of 250ºC -350ºC. Conversely, for HDC of chlorophenols on Ni/SiO_2, Shin et al. [59] found that higher temperatures increased catalyst activity and slowed deactivation at temperatures from 150ºC to 300ºC. The difference suggests that there are different deactivation mechanisms and/or that there is an optimal operating temperature for the minimization of coke deposition.

1.2.3 Catalytic hydrodechlorination for contaminated groundwater

Only recently has catalytic HDC been investigated as an alternative remediation technology for organochlorine contaminated groundwater. This research area has grown rapidly, progressing from laboratory to pilot scale [46].

Aqueous-phase catalytic HDC has unique characteristics. First, it is unlikely that this technology will be used at elevated temperatures. Considering the beneficial effect of high temperature to process kinetics, this could be a disadvantage. Nevertheless, the reaction rate is acceptable for TCE destruction at ambient temperature, and field study has established the feasibility of in-situ treatment by forcing contaminated water through catalyst packed wells [74-76]. Second, hydrogen insolubility may be a barrier for field application. Two stage reactors have been proposed in which the first reactor generates H_2 by the electrolysis of water and the second reactor transforms chlorinated organics [76].

Another important aspect of aqueous-phase hydrodechlorination is the role that solutes play. Bicarbonate reacts with H_2 on the surface of Pd catalyst to form formate via the following reaction [74]:

$$HCO_3^- + H_2 \rightarrow HCO_2^- + H_2O \qquad (1.2)$$

This reaction competes with chlorinated organics for catalyst sites, and formate stimulates the growth of microorganisms causing biofouling of the catalyst. Similarly, nitrite interferes with chlorine transformation by reacting with hydrogen to generate nitrogen and ammonia on the catalyst surface. Dissolved oxygen is also a concern due to its rapid reaction with hydrogen on the catalyst surface.

Catalyst deactivation is also recognized in aqueous-phase HDC [74]. Deactivation occurred even in DI water, probably due to the inhibition by HCl and modification of catalyst active sites. Sulfide severely inhibited catalyst activity. The catalyst was regenerated via oxidative treatment, by either exposure to air or flushing with a solution containing hypochlorite [74].

1.3 Electrochemical reduction of trichloroethylene

Several studies have illustrated that trichloroethylene can be reductively transformed to fully dechlorinated hydrocarbons such as ethane, ethene, and acetylene at the cathode of electrochemical reactors [9-11,77-84]. Reaction mechanisms and kinetics depend on cathode material, pH, solvent composition, and applied cathode potential. Two frequently mentioned reaction mechanisms for TCE electrochemical reduction are β-elimination, which involves elimination of two chlorine substituents with concomitant formation of a new carbon-carbon bond, and hydrogenolysis, in which a carbon-chlorine bond is broken and hydrogen replaces the chlorine substituents.

In aprotic solvents such as acetonitrile, TCE was primarily transformed via β-elimination to chloroacetylene on a cathode consisting of oxidatively pretreated glassy carbon particles (GCO) [85]. Chloroacetylene was rapidly reduced to acetylene via hydrogenolysis when using a composite cathode consisting of GCO and stainless steel (SS) particles. A cathode made of SS particles was insensitive to TCE dechlorination, but caused rapid hydrogenolysis of chloroacetylene. The ability of the SS electrode to

transform chloroacetylene was attributed to the presence of Ni and Cr that could concentrate protons from the traces of water in the acetonitrile solvent.

Costentin et al. [81] investigated the reduction of TCE in *N*,*N*'-dimethylformamide (DMF) at a glassy carbon rotating disk electrode using cyclic voltammetry and dissociative electron transfer theory. From cyclic voltammetry evidence, the authors concluded that TCE was transformed via chloroacetylene. By applying modified dissociative electron transfer models, a reaction scheme for TCE dechlorination was proposed as follows (Figure 1.2).

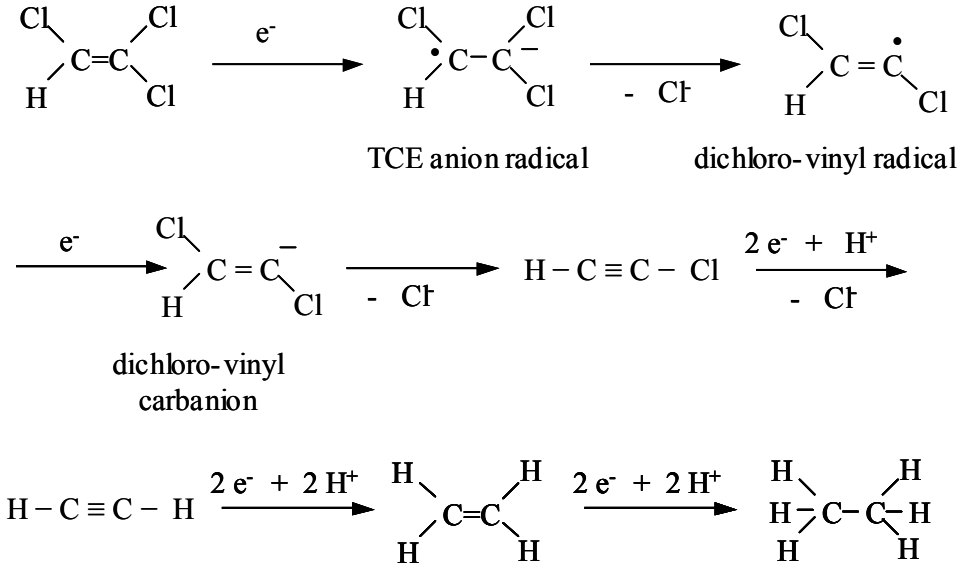

Figure 1.2 TCE electrochemical reduction via β-elimination

The reaction begins with a one-electron transfer step to form TCE anion radical, which then expels one chloride to give rise to dichloro-vinyl radical. Dichloro-vinyl radical

accepts a second electron to form dichloro-vinyl carbanion. This dichloro-vinyl carbanion eliminates a second chloride to yield chloroacetylene. When proton sources are available, chloroacetylene can be rapidly transformed to acetylene via hydrogenolysis, and ethene and ethane via hydrogenation.

When water is present, the dichloro vinyl carbanion can be protonated, leading to the hydrogenolysis of TCE to DCE isomers. For instance, Tezuka et al. observed both DCE isomers and chloroacetylene for TCE reduction in hexamethylphosphoramide/water at Pt and Hg electrodes [86]. Liu et al. investigated aqueous-phase TCE reduction at a porous Ni cathode and suggested that the electrochemical reduction of TCE was primarily via hydrogenolysis [77]. In his work, Liu observed trace amounts of DCE isomers and both C_4 and C_6 hydrocarbons in addition to primary products ethane and ethene. No acetylene was detected. The formation of C_4 and C_6 hydrocarbons suggested that radicals were involved in the reaction mechanisms.

Hydrogenolysis of TCE proceeds via the reaction scheme in Figure 1.3. The reaction starts with two-electron, one-proton transfer to TCE to form DCE isomers. This two-electron, one-proton transfer is a multi-step process that may proceed via formation of TCE anion radical, dichloro-vinyl radical, and dichloro-vinyl carbanion as depicted in Figure 1.2. Hydrogenolysis then converts DCE isomers to vinyl chloride and vinyl chloride to ethene. Ethene may undergo a two-electron, two-proton transfer to form ethane.

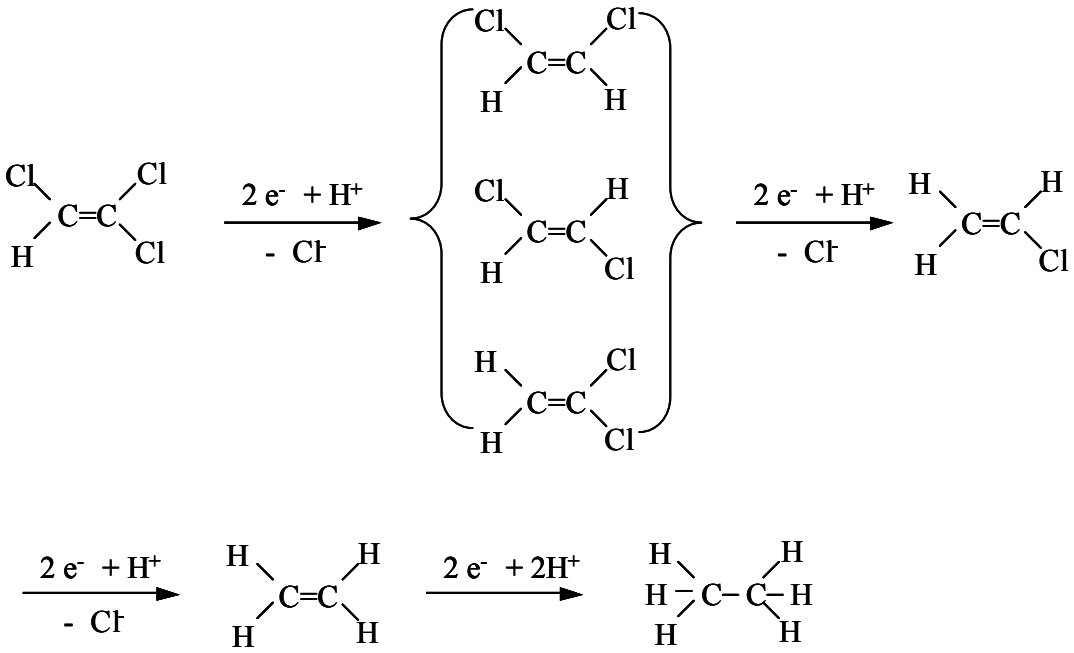

Figure 1.3 TCE electrochemical reduction via hydrogenolysis

In aqueous systems, TCE reduction occurs in parallel with hydrogen evolution from water reduction, which usually occurs via the Volmer-Heyrovsky-Tafel reaction mechanism [87]:

$$H_2O + e^- \leftrightarrow H^* + OH^- \quad \text{(Volmer reaction)} \quad (1.3)$$

$$H^* + H_2O + e^- \leftrightarrow H_2\,(g) + OH^- \quad \text{(Heyrovsky reaction)} \quad (1.4)$$

$$2\,H^* \leftrightarrow H_2\,(g) \quad \text{(Tafel reaction)} \quad (1.5)$$

In this mechanism, atomic hydrogen adsorbed on electrode surface (Volmer reaction) can be desorbed electrochemically (Heyrovsky reaction) or chemically (Tafel reaction) depending on the electrode material, potential, and solution pH.

On the surface of a metal electrode, adsorbed atomic hydrogen may react with TCE, resulting in fully dechlorinated hydrocarbons. In weakly acidic aqueous systems, or at sub-millimolar concentration at iron and palladized iron electrodes, TCE reduction is mainly via reaction with atomic hydrogen instead of direct electron transfer [9,11,80]. The contribution of the reaction with atomic hydrogen decreases with increasing TCE concentration and pH values. The direct electron transfer mechanism and atomic hydrogen reaction mechanism proposed by Wang et al. [11] are illustrated in Figure 1.4.

The two proposed reaction mechanisms begin with chemisorption of TCE on the metal surface to form di-σ-bonded surface intermediates. The reaction then undergoes β-elimination on the metal surface via direct electron transfer or via reaction with atomic hydrogen. The di-σ-bonded surface chloroacetylene intermediate may desorb to yield chloroacetylene, or further react via hydrogenolysis without desorption to form di-σ-bonded surface acetylene. Similarly, surface bonded acetylene may desorb, or further react to yield ethene, and ethane via hydrogenation. Chloroacetylene and acetylene was not observed in the system of Wang et al. [11], suggesting that the predominant pathway involves further reaction of these compounds without desorption.

a)

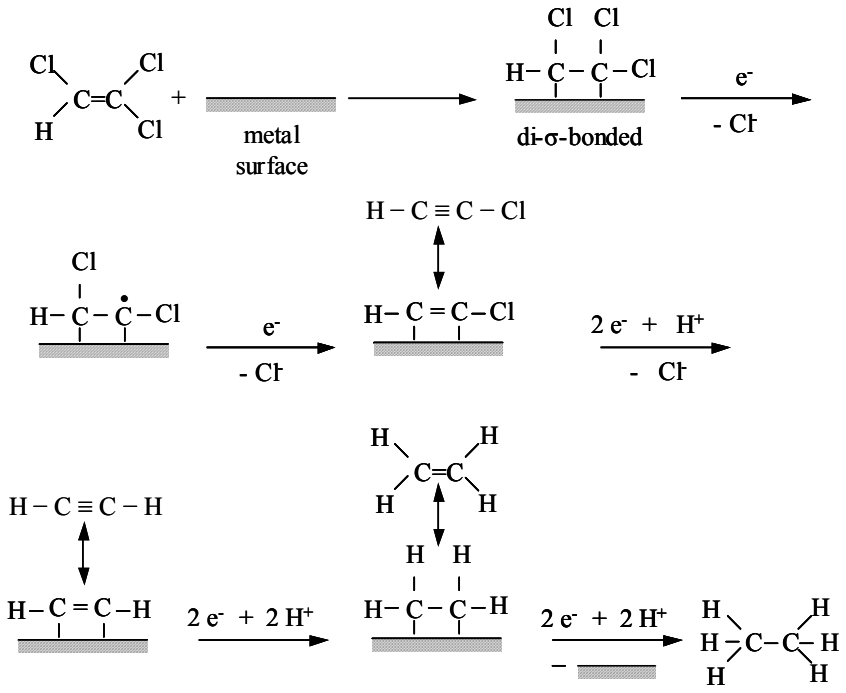

b)

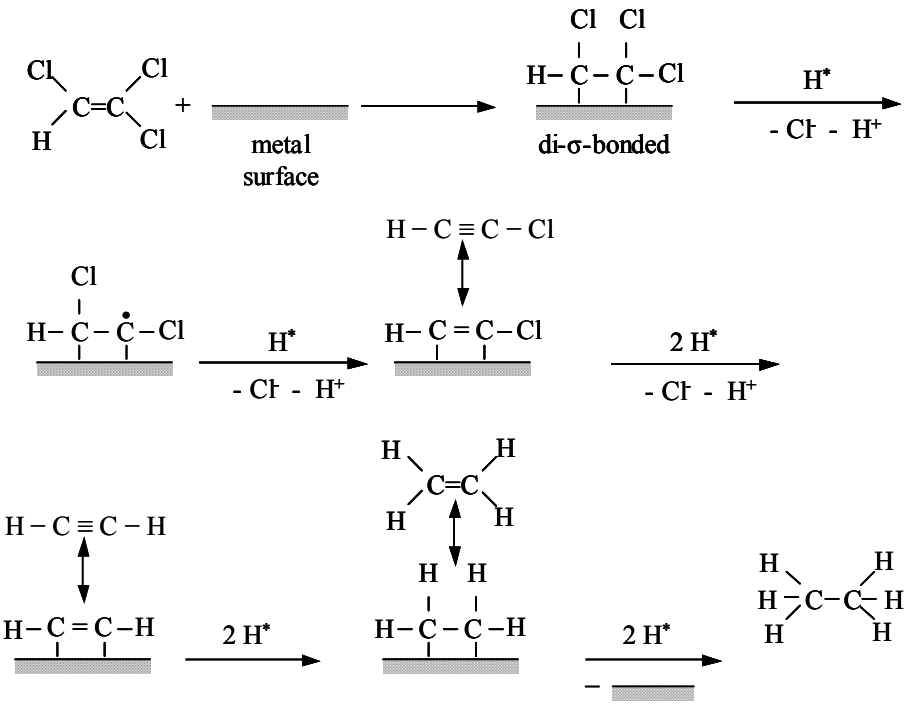

Figure 1.4 TCE reduction on metal electrode surface via a) direct electron transfer b) reaction with adsorbed atomic hydrogen

Reduction rates of TCE usually increase with decreasing pH values [11,78,80]. However, protons are not directly involved in the rate-determining step. The effect of pH on TCE reaction rates has been attributed to (i) an increase in active electrode surface area due to dissolution of metal oxide film, (ii) an increase in exchange current density by modifying surface properties, (iii) an increase in the amount of adsorbed atomic hydrogen causing faster dechlorination via reaction with atomic hydrogen, and (iv) involvement of the proton in pre- and post- rate-determining steps.

Remediation of TCE contaminated groundwater could be complicated due to side reactions. Roh et al. [84] tested TCE contaminated groundwater at a cathode packed with palladized iron oxides using a flow-through electrolytic reactor. At an applied potential of 30V between cathode and anode, TCE was completely degraded to ethane and ethene without detection of DCE isomers or VC even after 250 pore volumes. However, C_2 forms of carbon produced were 10x larger than the mass of TCE degraded. When using granular graphite as the cathode in a mixed electrochemical reactor, TCE was rapidly reduced to ethane at an applied cell voltage of 10V, and a trace amount of *cis*-DCE was observed [82] . However, chloromethane was formed as a product of chloride oxidation at the graphite anode in aqueous acetate electrolyte.

Electrochemical reduction of chlorinated volatile and semi-volatile contaminants using gas diffusion electrodes (GDEs) has received some attention recently [10,88,89]. Gas diffusion electrodes consist of a gas-diffusion region and a reactive (catalytic) region. The reactive gas must diffuse through a liquid layer that separates the gas phase and solid electrode. This transport step frequently limits the overall transformation rate for the

target compound [90]. Sonoyama et al. [89] investigated the kinetics of dichlorofluoromethane (CFC-12) reduction on GDEs comprised of various candidate metals. Both dehalogenation kinetics and product selectivity were functions of electrode material. Production of hydrogen gas on Pt, Pd and Ni electrodes interfered with CFC-12 reduction. Current efficiency, defined as the fraction of total current utilized for reduction of CFC-12, ranged from 0.044 (Pt) to 1.0 (Pb). Current efficiency was directly related to metal-dependent overpotential requirements for the reduction of water to hydrogen gas.

Liu et al. [10] studied the reductive dechlorination of TCE in a GDE that was identical in design to a polymer electrolyte membrane (PEM) fuel cell. Dehalogenation rates and product selectivity were functions of primarily cathode material selection, temperature, and the cathode potential. Under the most favorable experimental conditions, half-times for TCE destruction were on the order of tenths of a second.

1.4 Research Objectives

This research explores reductive dehalogenation of gas-phase chlorinated contaminants using (i) heterogeneous catalytic hydrodechlorination and (ii) reductive electrochemical methods.

During the investigation of catalytic hydrodechlorination, H_2 served as reducing agent for TCE destruction on Pt supported on alumina or silica in packed-bed reactors. The aims of this study were:

(1) to establish the feasibility of catalytic hydrodechlorination as a treatment alternative based on process kinetics and product identification.

(2) to evaluate effects of process variables such as gas flow rate, temperature, and H_2/TCE (molar) ratio on kinetics and product distribution,

(3) to investigate the mechanisms of catalyst deactivation and explore catalyst recovery procedures.

(4) to develop a mathematical model to quantitatively represent reactor performance and support extrapolation for design purposes.

Electrochemical dechlorination of gas-phase TCE was studied on a cathode consisting of platinum on carbon black using a polymer electrolyte membrane (PEM) fuel cell design. Hydrogen was oxidized on an anode that also consisted of Pt/C. The membrane electrode assembly (MEA) consisting of cathode, membrane electrolyte, and anode was manufactured as a part of the study. The aims of the investigation were:

(1) to characterize laboratory-made MEAs in which H_2 is oxidized at the anode and O_2 is reduced at the cathode,

(2) to investigate the effects of process parameters such as cell potential and gas flow rate on gas-phase TCE destruction efficiency and product selectivity,

(3) to establish a mathematical model for process simulations,

(4) to evaluate O_2 effects on gas-phase TCE reduction, and

(5) to investigate catalyst deactivation mechanisms and regeneration strategies.

1.5 Dissertation format

There are five chapters. The first chapter provides background information to motivate the research described subsequently. A review of relevant literature on catalytic

hydrodechlorination and electrochemical reduction of chlorinated organic compounds is also included. In Chapter 2, catalytic hydrodechlorination of gas-phase TCE on Pt/Al_2O_3 in a packed-bed reactor is described. Chapter 3 describes a parallel investigation of gas-phase TCE reduction on Pt/SiO_2. Electrochemical reductive dehalogenation of gas-phase TCE in a PEM fuel cell device is described in Chapter 4. Key findings from this research are summarized in Chapter 5.

CHAPTER 2

GAS-PHASE HYDRODECHLORINATION OF TRICHLOROETHYLENE OVER Pt/Al_2O_3 IN PACKED BED REACTOR

2.1 Abstract

Catalytic hydrodechlorination (HDC) of gas-phase trichloroethylene (TCE) was investigated using 0.5 wt.% Pt/γ-Al_2O_3 in packed-bed reactors. TCE was efficiently transformed on a platinum surface using H_2 as reducing agent. The main products of the reaction were ethane and chloroethane. At temperatures above 60ºC, ethane was the sole measurable organic product. Catalyst deactivation was observed. Long-term (700 hours) experiments at 100ºC were marked by relatively slow catalyst deactivation, while catalyst deactivation at 22ºC was much faster. The observed deactivation rate constant at 22ºC (0.039 h^{-1}) was 162 times larger than at 100ºC (0.00024 h^{-1}). That is, high temperature operation tended to extend catalyst life while improving both process kinetics and selectivity (for ethane as a product). A series of treatments was attempted to restore the activity of the deactivated bed including reduction under hydrogen and oxidation under oxygen at 500ºC. Hydrogen treatment partially restored catalyst activity, while oxygen treatment caused permanent loss of catalyst activity.

2.2 Introduction

Catalytic hydrodechlorination (HDC) of chlorinated organic compounds using molecular hydrogen is mechanistically straightforward and kinetically attractive at ambient pressure and mild temperatures. Additionally, catalytic HDC of common environmental

contaminants such as trichloroethylene (TCE) and perchloroethylene (PCE) produces environmentally benign products. Chlorinated alkanes and alkenes are mainly converted to hydrocarbons and hydrogen chloride (HCl) with no chlorinated intermediates under optimal reaction conditions. The corrosive HCl generated can be easily neutralized in base. In contrast to thermal incineration of chlorinated organic compounds, no dioxins and other toxic compounds are formed. The absence of toxic intermediates is attributed to the reducing environment provided by elemental hydrogen and the mild temperature and pressure conditions.

Catalytic HDC has been extensively studied as a remediation technology under laboratory conditions. Some pilot-scale field applications have also been initiated. A variety of chlorinated organic compounds have been examined as targets including chlorofluorocarbons (CFCs) [20-22], chlorinated aromatics [23-25], and chlorinated aliphatics [14,26,27] in organic matrices, aqueous-, and gas phases. Most of the studies have focused on the HDC of gas-phase CFCs to hydrofluorocarbons (HFCs) and on the HDC of other chlorinated compounds in organic matrices within the context of industrial waste treatment. The catalysts used in these studies include supported/unsupported precious metals (Pt, Pd, Rh) [12-15], transition metals (Ni, Mo) [16,34], and metal oxides [17]. Supported precious metals, especially Pd and Pt, are superior to other catalysts in terms of reaction kinetics and selectivity to non-chlorinated products [47]. Various catalyst supports have been used including carbon, alumina, zeolite, silica, titanium oxides, and zirconium oxides [18].

Among the disadvantages associated with catalytic HDC is catalyst deactivation, as evidenced by the decrease of removal efficiency of target compounds with operation time. Catalyst poisoning and coking are the two main mechanisms discussed in related literature. Catalyst poisoning refers to the loss of active surface sites by forming strong covalent bond between active metals and chlorine. Hydrogen chloride, the major inorganic product of catalytic HDC process, is believed to cause catalyst poisoning [15,36,53-56]. The evidence includes the inhibition of HDC in the presence of HCl and recovery or delay in the development of poisoning effects by addition of base. For instance, in the study of catalytic HDC of chloroethane using evaporated metal films of Pd, Pt, Ni, Rh, Fe, and W, Campbell et al. [15] found that the reaction order was inversely proportional to the partial pressure of HCl, as suggested by the following semi-empirical equation:

$$-\frac{dP_{EtX}}{dt} = \frac{k P_{EtX}}{1 + k_1 P_{HCl}} \approx \frac{k P_{EtX}}{k_1 P_{HCl}} \qquad (2.1)$$

Where P_{EtX} and P_{HCl} are the partial pressures of ethyl chloride and HCl; k_1 is a constant related to adsorption strength of HCl; k is the observed reaction constant. This equation is a good kinetic approximation only when HCl is strongly adsorbed to the catalyst.

Coking refers to the formation of carbonaceous material (coke) on the surface of the catalytic metals or in the pores of the catalyst support, which blocks the access of reactants to active sites. In some investigations, coking was identified as the main mechanism of catalyst deactivation during HDC [18,48,60-62]. Large amounts of coke can be deposited on the catalyst in some applications. In a study of catalyst deactivation

during HDC of 1,1,1-trichloroethane (1,1,1-TCA), Frankel et al. [60] found that the 3.0 wt.% Pt/ηδ-Al_2O_3 catalyst and support was covered by up to 29 wt.% carbon. This carbon content was measured after less than 8-h operation, during which 1,1,1-TCA conversions dropped from 100% to less than 80%. While catalyst life is of practical importance for HDC economics, the mechanism of catalyst deactivation and the regeneration methods for deactivated catalyst are not well established.

Catalytic HDC of light chlorinated carbons such as TCE and PCE has not been widely studied as an alternative remediation technology for contaminated groundwater and soil. Ordonez et al. [47] studied the HDC of these compounds but in an organic matrix (heptane). Bozzelli et al. [14] studied HDC of gas phase TCE using Rh/SiO_2, a catalyst that is easily deactivated by chlorine. Lowry et al. [74,75] established the feasibility of catalytic HDC of TCE in groundwater using Pd/γ-Al_2O_3. With a retention time of 4.3 min, >24% TCE conversion was maintained over a 60-day period of continuous treatment in a packed bed reactor. Slow catalyst deactivation was reversed by treatment with a dilute sodium hypochlorite solution. Compared with gas-phase catalytic HDC, aqueous-phase catalytic HDC suffers from the difficulty of supplying elemental hydrogen to the catalytic surface, due primarily to the limited solubility of H_2 (1.7 mg/L at 20ºC) in water. To make the best use of catalytic HDC to treat groundwater and soil contaminated by semi-volatile chlorinated solvents, contaminants should be presented in the gas phase. That is, waste streams derived from contaminated groundwater or soil via air sparging or soil vapor extraction could be directly treated in this manner. Waters derived from pump-and-treat operations could be stripped (many are already) with the resultant gas streams

being treated with catalytic HDC instead of carbon adsorption. Catalytic HDC provides the advantage of destroying or limiting the toxicity of waste streams while transforming the halogenated targets. The cost savings when carbon adsorption/recovery or disposal is avoided is obvious.

The purpose of this work is to investigate the feasibility of gas-phase catalytic HDC of semi-volatile chlorinated hydrocarbons under mild experimental conditions such as low temperatures and ambient pressure. TCE was chosen as a model compound. It is among the most widespread contaminants in the environment, and representative of other chlorinated alkenes in terms of probable reaction mechanisms during catalytic HDC. Commercial 0.5 wt.% Pt/γ-Al_2O_3 was used as catalyst in this work. Catalytic HDC of TCE using Pt/γ-Al_2O_3 was fast even at room temperature, and product selectivity was heavily biased towards production of ethane. Catalyst deactivation was observed, mainly attributed to coking and chlorine poisoning. The deactivated catalyst was treated via reduction under hydrogen and oxidation under oxygen. Hydrogen treatment partially restored catalyst activity, while oxygen treatment caused permanent loss of catalyst activity.

2.3 Materials and methods

2.3.1 Catalyst and chemicals

The catalyst used was 0.5 wt.% Pt supported on spherical γ-alumina with a diameter of 3.2 mm (Englehard, Inc.). The Pt metal is predominantly distributed at the exterior of the spheres as a thin layer, which is referred as an eggshell or edge- type catalyst. This

catalyst has a BET surface area of 80 m^2/g, and a bulk density of 0.7 g/cm^3 (manufacturer's data). The total bed porosity of randomly packed catalyst was 0.5, measured as the water volume necessary to fill the void space.

Trichloroethylene (Sigma-Aldrich, 99.5% purity), H_2 (Airgas, 99.95%), N_2 (Airweld, 99.99%), ethane, ethylene, and methane (Scotty, 99.9% purity) were all used as received.

2.3.2 Experimental setup

Figure 2.1 is a schematic diagram of the experimental setup. The reactions were carried out in a continuous fixed-bed reactor, consisting of a 60 cm long, 2.54 cm i.d. glass tube held vertically in a tubular electric furnace (Thermolyne 21100). A glass frit was placed within the tube reactor to hold the catalyst in position. The temperature was controlled by adjusting the electric furnace setting and measured *in situ* using a thermocouple.

TCE vapor was added to the mixture of influent gases by passing nitrogen through a wash bottle filled with pure TCE liquid. The flow of nitrogen was varied as necessary to produce the target concentration of TCE in the recombined influent gas stream. H_2 and/or O_2 were added in different amounts or ratios as dictated by experimental objectives. Flow rates for all gases were controlled using mass flow controllers (Aalborg). Several stainless steel three-way valves were used to direct the gas stream to the column or bypass the column, so that influent and effluent concentrations of target compounds could be conveniently monitored. A wash bottle filled with 800mL deionized water was used to scrub HCl from the effluent gas stream. The time-dependent chloride concentration in the wash bottle was monitored in experiments where a chloride balance

was attempted. PTFE tubing and stainless steel fittings were used to prevent HCl corrosion.

2.3.3 Catalytic hydrodechlorination

Long-term catalytic HDC of TCE was evaluated at 22ºC and 100ºC using 3 g of 0.5 wt.% Pt/Al_2O_3. The experiments were conducted at ambient pressure (~0.92 atm at Tucson, AZ). Hydrogen flow rate was fixed at 0.059 L/min, and the total volumetric flow rates to the reactor were 0.31 L/min at 22ºC, and 0.35 L/min at 100ºC, for residence times of 0.41 seconds for the experiment at 22ºC and 0.37 seconds for the experiment at 100ºC. The influent TCE concentration was 3900 ppmv at 22ºC, and 4800 ppmv at 100ºC.

In addition to the long-term experiments described above, short-term experiments with durations less than 2 hours were performed to evaluate the effects on reaction kinetics and product selectivity of temperature (22º -100ºC) and molar ratio of H_2/TCE (1.5-150). The same (short-term) experimental procedure was used to investigate chloride balances. Experiment-specific conditions are included with the results of each set of experiments.

2.3.4 Catalyst regeneration

Reactivation was attempted through a series of *in situ* treatments after the catalyst deactivated in the long-term experiment performed at 22ºC. The deactivated catalyst was first treated under hydrogen at 500ºC to reduce the oxidized form of the metal or to vaporize volatile compounds that may be responsible for the decay. With hydrogen gas flowing at 0.035 L/min through the reactor, reactor temperature was ramped from 22ºC to

500ºC at a rate of 3ºC/min, and held at 500ºC for 3 hours. After allowing the catalyst to cool to 22ºC overnight with continuous hydrogen flow, a standard TCE HDC experiment, under conditions similar to the operation with the fresh catalyst, was performed to examine the effectiveness of the treatment. Again time-dependent catalyst deactivation was monitored.

The twice-deactivated catalyst was then subjected to a second treatment, in this case using nitrogen to vaporize the compounds that are responsible for catalyst deactivation. Temperature setting and nitrogen flow rate were the same as in the hydrogen treatment. Again, the standard TCE HDC experiment was performed. Similarly, the catalyst was treated under oxygen in an attempt to restore catalyst activity by burning any coke formed on the catalyst surface. More treatments with nitrogen, hydrogen, and oxygen followed by hydrogen were sequentially conducted for the same bed. In each case, the objectives were to establish the level of catalyst reactivation and subsequent longevity during continuous use. Results were used to speculate on the mechanism of catalyst deactivation.

2.3.5 Analytical methods

Influent and effluent concentrations of TCE, and reaction products (chlorinated and non-chlorinated hydrocarbons) were monitored periodically using GC-FID (Hewlett Packard 5840A; GS-Q 30.0 m; He carrier gas; isothermal (180^{o}C); Hewlett Packard 5840A integrator). A 200-μL sampling loop was used to withdraw gas samples from the reactor inlet and outlet. Individual data points represent the average of 3 to 5 measurements. The

detection limits were 10 ppmv for TCE and reaction products. Products were identified by comparing the chromatogram retention times with those of authentic standards. Standards for TCE and other chlorinated liquid compounds were prepared by injecting 2, 4, 6, and 8 μL of pure liquid into 160 mL sealed borosilicate bottles. After the liquid was completely evaporated, a 50-μL gas sample was withdrawn from each bottle and injected into the GC. Standards for ethane and chloroethane were prepared by injecting 2, 4, 6, and 8 mL pure gas into 160 mL sealed borosilicate bottles. After complete mixing, a 50-μL gas sample was withdrawn from each bottle and injected into the GC. Ethene could not be separated from ethane using the GC method specified above. Product distribution (ethane vs. ethene) was occasionally determined by lowering the GC oven temperature to 70ºC. In each such case, ethane was the dominant product and ethene was absent or present in trace amounts.

Chloride concentration in the HCl scrubber was monitored using ion chromatography (IC) with a conductivity detector (Dionex 500, AG-11 and AS-11 column). The relative amount of chlorine deposited on the catalyst was tested using scanning electron microscopy (SEM) with energy dispersive spectroscopy (EDS) (Hitachi S-2460N /Thermo-Noran Digital Imaging).

2.3.6 Method for evaluating reaction and deactivation kinetics

Assuming that TCE was not lost by alternative mechanisms, TCE conversion through the reactor was calculated using equation (2.2):

$$x = \frac{C_p}{C_p + C_{eff}} \tag{2.2}$$

Where x is the conversion of the TCE, and C_{eff} and C_p are the effluent concentrations of TCE and all products. The error introduced by the mass balance assumption was less than 10%, probably due to coke formation on the catalyst and experimental errors.

Product selectivity was calculated using equation (2.3):

$$S_i = \frac{C_{p_i}}{\sum C_{pi}} \tag{2.3}$$

Where S_i and C_{p_i} are the selectivity and effluent concentration of organic product i, respectively. In these experiments, ethane and chloroethane always comprised >99% of the measurable products. Therefore, in the calculation of product selectivity, only ethane and chloroethane were considered as organic products.

Based on the following assumptions: first-order reaction kinetics, plug flow, no change in gas volume due to reaction, isothermal operation, and no mass transfer limitation, reactor performance was modeled using

$$\ln(1 - x) = -k_{obs} \cdot \frac{V_{cat} \cdot \theta}{Q} \tag{2.4}$$

Where V_{cat} is the volume of the catalyst bed (L), Q is the total volumetric flow rate to the reactor (L/min), θ is the porosity of packed catalyst, and k_{obs} is the observed pseudo first-order rate constant (min^{-1}).

Normalizing the observed first order rate constant to catalyst density yields

$$k = k_{obs} \cdot \frac{V_{cat} \cdot \theta}{W_{cat}} \tag{2.5}$$

Where W_{cat} is the mass of catalyst (g), and k is the pseudo first-order rate constant normalized to catalyst concentration ($L \cdot g_{cat}^{-1} \cdot min^{-1}$).

Substituting equation (2.5) into equation (2.4) yields

$$\ln(1 - x) = -k \cdot \frac{W_{cat}}{Q} \tag{2.6}$$

Catalyst deactivation can be modeled in terms of exponential decay of the reaction constant [74]. The expression was given by

$$k = k_0 \exp(-k_d \cdot t) \tag{2.7}$$

Where t is operation time (h), k_0 is the initial reaction rate constant for fresh catalyst, and k_d is the deactivation rate constant (h^{-1}).

Inserting equation (2.7) into equation (2.6) gives

$$\ln(1 - x) = -k_0 \exp(-k_d \cdot t) \cdot \frac{W_{cat}}{Q} \tag{2.8}$$

2.4 Results and Discussion

2.4.1 Long-term catalyst performance

At 22ºC, TCE conversion efficiency dropped rapidly from 87% to 77% during the first three hours of operation then decreased at a much slower rate through the remainder of the experiment (Figure 2.2). After 80 h of operation, TCE conversion efficiency was only 5%, indicating severe catalyst deactivation.

At 22ºC, the major gas-phase organic products observed were ethane and chloroethane (CA). There were also trace amounts of *cis*-dichloroethene (*cis*-DCE) and 1,1,2-trichloroethane (1,1,2-TCA), but they constituted less than 1% of the products. A number of previous investigations have identified ethane as the major product from HDC of TCE [14,34,47,91]. Carbon balances were usually within 90%. The product selectivity between ethane and chloroethane varied with time. In the first three hours of operation, ethane selectivity dropped from 88% to 83%, followed by a slower decrease from 83% to 79% during the next 77 h of operation.

At 100ºC, high TCE conversion efficiency was sustained over the entire duration of the experiment (Figure 2.3). At the beginning of the experiment, 97% of TCE was converted to ethane, and TCE conversion remained at 94% after 700 h of operation. The high temperature increased the apparent rate constant for TCE disappearance, and slowed the kinetics of catalyst deactivation. In this experiment, ethane was the sole organic product observed.

The first-order rate constant (k) for TCE loss, estimated by equation (2.6), decreased from 0.214 to 0.0058 $L \cdot g_{cat}^{-1} \cdot min^{-1}$ during the 80 h operation at 22ºC. Following an initial period of rapid rate decrease, slow catalyst inactivation was modeled based on exponential decay with time as shown in equation (2.7). The estimated rate constant (k_d) for catalyst deactivation at 22ºC was 0.039 h^{-1} based on a linear regression of log-transformed k with operation time. At 100ºC, reaction rate constants dropped from 0.416 $L \cdot g_{cat}^{-1} \cdot min^{-1}$ to 0.347 $L \cdot g_{cat}^{-1} min^{-1}$ after 700 h of operation, and the estimated deactivation rate constant was 0.00024 h^{-1}.

The reaction rate constants estimated here were higher but of the same order of magnitude as those obtained by Bozzelli et al. [14] using 3 wt. % Rh/SiO_2. The pseudo first-order rate constants measured in liquid-phase reactions [34,74] were usually two orders of magnitude lower (Table 2.1).

Table 2.1 Comparison of rate constants and activation energy for TCE hydrodechlorination in literature.

T ºC	k $L \cdot g_{cat}^{-1} \cdot min^{-1}$	E_a $kJ \cdot mol^{-1} \cdot K^{-1}$	Experimental Conditions	Ref.
200	0.0047	62.7	C_{inf} ~ 13 mM, liquid phase in hexadecane, 1500 psig, 0.04 g $NiMo/Al_2O_3$	[34]
250	0.016			
300	0.078			
25	0.00077-0.00056		C_{inf} ~ 27 μM, aqueous phase in DI water, 10 psig, 0.5 g 1 wt.% $Pd/\gamma\text{-}Al_2O_3$	[74]
92	0.048	57.4	C_{inf} ~1.2 mM, gas phase, atmospheric pressure, 0.15 g 3 wt.% Rh/SiO_2	[14]*
102	0.103			
112	0.136			
122	0.196			

* Data were recalculated based on original data using pseudo first-order kinetic and plug flow reactor (PFR) model

The rate of catalyst deactivation was much slower at 100ºC compared with 22ºC. This may be due to the relatively high surface reaction rate at 100ºC while the total reaction kinetics were controlled by diffusion. While studying the HDC of chlorophenol on Ni/SiO_2, Shin et al. [59] observed higher catalyst activity and slower catalyst deactivation rate with increasing temperature between 150ºC and 300ºC. Ordonez et al. [48] measured higher initial catalyst activity, but faster deactivation during PCE HDC on Pd, Pt/Al_2O_3 at temperatures from 250-350ºC. This inconsistency suggests that the deactivation

mechanism may differ at very high temperature and/or there is an optimal temperature for avoidance of catalyst deactivation.

At 22ºC, the ratio of ethane/chloroethane production was essentially constant (independent of TCE conversion rate or efficiency) at fractional conversion from 80% to 5%. This result suggests that ethane and chloroethane are formed via parallel reaction pathways, as opposed to sequential formation of ethane from chloroethane. That is, ethane was directly formed from TCE dechlorination, without release of chlorinated intermediates from the catalyst surface. This is consistent with the observation of Kim et al. [34] that TCE dechlorination occurred through the removal of multiple halogen substituents without desorption of partially halogenated intermediates.

2.4.3 Effects of temperature

Effects of temperature on reaction kinetics and product distribution were further studied at 22-100ºC, to complement the information obtained from the long-term experiments at 22ºC and 100ºC. TCE HDC was performed over 80-120 minute increments starting at 100ºC and decreasing temperature at each step.

TCE conversion efficiency increased with temperature from 84% at 22ºC to 95% at 100ºC. Ethane and to a lesser extent, chloroethane were the main organic products of TCE conversion. However, ethane was the only observable product at 60ºC and above (Figure 2.4). At temperatures lower than 60ºC, chloroethane was observed indicating that low temperature favors the formation of chloroethane.

An apparent activation energy for TCE conversion was calculated using the Arrhenius equation as follows:

$$k_{obs} = A \cdot \exp\left(-\frac{E_a}{RT}\right) \tag{2.9}$$

Where E_a is the apparent activation energy ($J \cdot mol^{-1}$), A is the pre-exponential constant (s^{-1}), R is the gas constant (= 8.31 $J \cdot mol^{-1} \cdot K^{-1}$), and T is absolute temperature (K).

The log transformation of equation (2.9) yields:

$$\ln k_{obs} = \ln A - \frac{E_a}{R} \cdot \frac{1}{T} \tag{2.10}$$

A plot of $\ln k_{obs}$ vs. $\frac{1}{T}$ gives a slope of $\frac{E_a}{R}$ (Figure 2.5). From this analysis, an apparent activation energy of 4.73 kJ/mol was obtained. This low value of apparent activation energy suggested that the reaction was controlled by external diffusion. From related literature, the estimated activation energy for TCE catalytic HDC is around 60 kJ/mol (Table 2.1) [14,34].

2.4.4 Effects of H_2/TCE (molar) ratios

The effects of H_2/TCE (molar ratios) on TCE conversion and product selectivity were investigated using 21.5 g of 0.5 wt.% Pt/Al_2O_3 at 22ºC. The total gas flow rate ranged from 0.35-0.44 L/min, the retention time was between 2.1-2.6s, the influent TCE concentration varied from 1000 to 5000 ppmv, and the hydrogen flow rate varied from 0.002-0.07 L/min to produce a range of H_2/TCE (molar) ratios from 1.3 to 150.

Experiment duration at each ratio was approximately 60 minutes. These abbreviated experiments were designed to ensure minimal catalyst deactivation.

The overall reduction of TCE to ethane by hydrogen is given by:

$$C_2HCl_3 + 4H_2 \rightarrow C_2H_6 + 3HCl \quad (2.11)$$

When complete TCE conversion was observed (before TCE breakthrough), a stoichiometric ratio of H_2/TCE from 4 to 150 resulted in complete TCE dechlorination (Figure 2.6). At ratios lower than 4, TCE conversion was less than 100% and was directly related to the influent H_2/TCE ratio, suggesting that TCE conversion stopped after H_2 was exhausted.

At all ratios tested, product selectivity for ethane was in the range 85-90%, independent of the H_2/TCE ratios, providing further evidence that ethane and chloroethane were formed from TCE through parallel reaction mechanisms.

The effect of H_2/TCE ratio on catalyst deactivation was not studied in this series of experiments. It is possible, however, that relatively high H_2/TCE ratios hinder the formation of oligomerization products and thus increase catalyst life. Bae et al. [44] found that high H_2/CCl_4 ratios increased the useful life of Pt/γ-Al_2O_3. Frankel et al. [60] also observed slower catalyst deactivation at higher H_2/1,1,1-TCA ratio using Pt/η-Al_2O_3.

2.4.5 Chloride balance

A chloride balance was attempted for TCE degradation at 22ºC and 150ºC. The amount of chloride captured from the effluent of the gas stream was compared to the chlorine content of transformed TCE. At 22ºC, ethane and chloroethane accounted for 85% and

15% of the TCE converted, respectively. The theoretical limit to chloride formation was thus 2.85x the moles of TCE converted. At 150ºC, ethane was the sole organic product; the upper limit to chloride recovery would be 3x the moles of TCE converted. Figure 2.7 contains a summary of chloride ion recovered and TCE losses at 22ºC and 150ºC. In each experiment, approximately one-third of the expected chloride was present in the water trap. A large fraction of the chloride must have been retained on the catalyst surface or in the lines of the experimental apparatus.

Surface composition analysis by SEM/EDS of both fresh and used catalysts indicated that chlorine did in fact accumulate on the used catalyst surface (Figure 2.8). The used catalyst had undergone TCE hydrodechlorination at 100ºC for over 700 h. The x-ray intensity counts were collected on a representative surface of 54 μm x 44 μm for both catalysts. Compared to the fresh catalyst, a larger Cl/Pt ratio was obtained in the SEM/EDS for the used catalyst, qualitatively suggesting that used catalyst contains chlorine that resulted from TCE reduction. In addition, the Cl/Pt ratio was much less than one when the intensity of x-ray energy was collected on a Pt particle, indicating that large portion of accumulated chlorine stays on the catalyst support. By visualization, some of the used catalyst turned black. However, carbon was not detected by SEM/EDS, possibly due to the light weight of the carbon atom.

2.4.6 Catalyst regeneration

Catalyst deactivation during the HDC of chlorinated organic compounds has been attributed to chlorine poisoning and/or carbonaceous deposits. Chlorine poisoning forms

strong Pt-Cl covalent bonds and thus reduces the available Pt atoms for the adsorption of hydrogen and target compounds. Oxidized noble metals bound to chlorine can be reduced to their zero valent forms in the presence of hydrogen. Therefore, restoration of the deactivated catalyst was expected in the presence of hydrogen at high temperature. Carbonaceous deposits on the catalyst surface or in the pores of the support impede the access of reactants to active sites, and thus reduce the catalytic activity. Carbonaceous deposits (coke) can be removed by oxidizing them to carbon monoxide or carbon dioxide. Both reductive and oxidative processes have been used to regenerate deactivated metal catalysts. However, related observations have been inconsistent. Some investigators found that H_2 treatment of deactivated catalyst did not restore catalyst activity, even at 400ºC [55,59]. Others observed partial catalyst restoration under similar circumstances [14,54]. Bae et al. [44] observed almost complete catalyst regeneration after oxidation by O_2 at 500ºC followed by H_2 reduction at 300ºC. The same catalyst treatment with O_2 at 300ºC did not restore catalyst activity. Kim et al. [18] found that catalyst activity returned to original levels after treatment with O_2 at 300ºC for 2 h. In general, however, complete catalyst regeneration has been hard to achieve due to the change of catalyst structure (e.g. pore size distribution and tortuosity) at high temperatures [68]. Long-term catalyst operation and higher coke content causes less effective regeneration.

Treatment of deactivated catalyst with hydrogen at 500ºC partially restored catalyst activity. Figure 2.9a shows initial TCE conversion efficiency (80%) was only slightly lower than the 87% conversion obtained with the fresh catalyst. However, performance of recovered catalyst quickly showed evidence of deactivation (k_d = 0.087 h^{-1}) compared to

that of the fresh catalyst (0.039 h^{-1}). The conversion of TCE dropped from 80% to 16% within 22 hours.

The patterns of catalyst activity/deactivation before and after the nitrogen treatment at 500ºC were identical, suggesting that the partial recovery of catalyst activity under hydrogen treatment may result from the removal of volatile species.

The subsequent treatment with oxygen and heat dramatically changed catalyst properties, as the initial TCE was only 26% and dropped to 3% within just two hours. Two subsequent treatments with N_2 and H_2 at 500ºC produced no recovery of catalyst activities (Figure 2.9b). The permanent loss of catalyst activity during oxidative treatment may have resulted from aggregation of active metal or phase change in the alumina support at the high temperature in an oxidizing environment.

2.5 Summary

Gas-phase TCE was efficiently transformed on a platinum surface with H_2 as reducing agent. The main products of the reaction were ethane and chloroethane. At temperatures above 60ºC, ethane was the sole measurable organic product. Catalyst deactivation was observed. Long-term (700 hours) experiments at 100ºC were marked by relatively slow catalyst deactivation, while catalyst deactivation at 22ºC was much faster. The catalyst deactivation rate constant in TCE hydrodechlorination at 22ºC (0.039 h^{-1}) was 162 times larger than at 100ºC (0.00024 h^{-1}). That is, high temperature operation tended to extend catalyst life while improving both process kinetics and selectivity (for ethane as a product). A series of treatments was attempted to regenerate deactivated catalyst,

including reduction under hydrogen and oxidation under oxygen at 500ºC. Hydrogen treatment partially restored catalyst activity, while oxygen treatment caused permanent loss of catalyst activity.

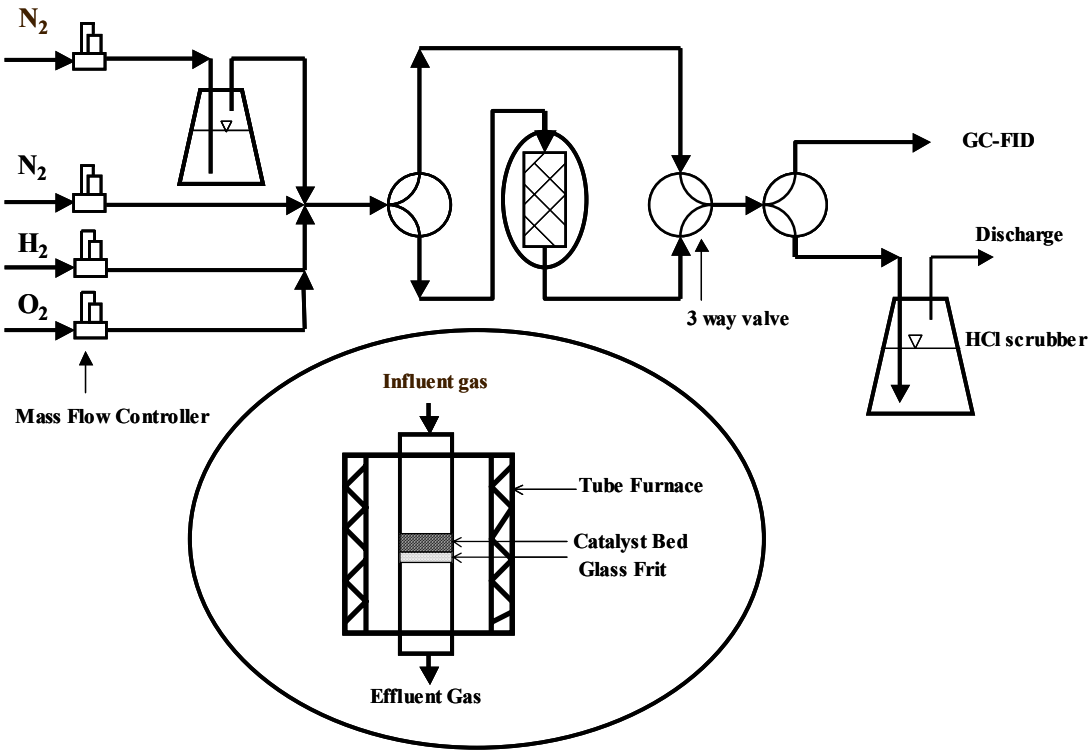

Figure 2.1 Experimental setup for gas-phase TCE hydrodechlorination on 0.5 wt.% Pt/Al_2O_3. The reactions were carried out in a continuous packed-bed reactor. TCE vapor was obtained by passing nitrogen through a wash bottle filled with pure TCE liquid. H_2 and/or O_2 were added in different amounts as dictated by experimental objectives. Gas chromatography with FID was used to monitor TCE and products. HCl was scrubbed from the effluent gas stream using a wash bottle filled with water.

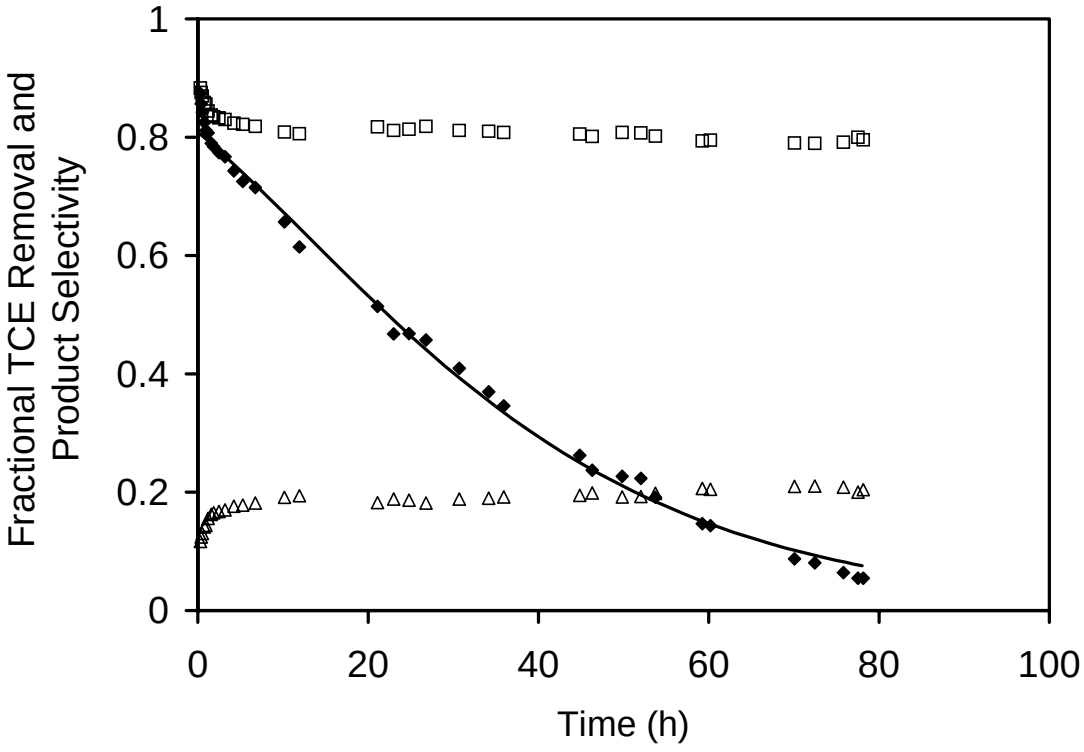

Figure 2.2 TCE hydrodechlorination as a function of time over 0.5 wt.% Pt/Al_2O_3 at 22ºC. (♦) factional TCE removal; (□) selectivity to ethane; (Δ) selectivity to chloroethane; (-) model simulation using equation (2.8). Experiment was conducted at ambient pressure (~0.92 atm) with ~4800 ppmv TCE in the influent, 0.059L/min hydrogen and 0.31 L/min total gas flow. Residence time in the packed bed was 0.41 seconds

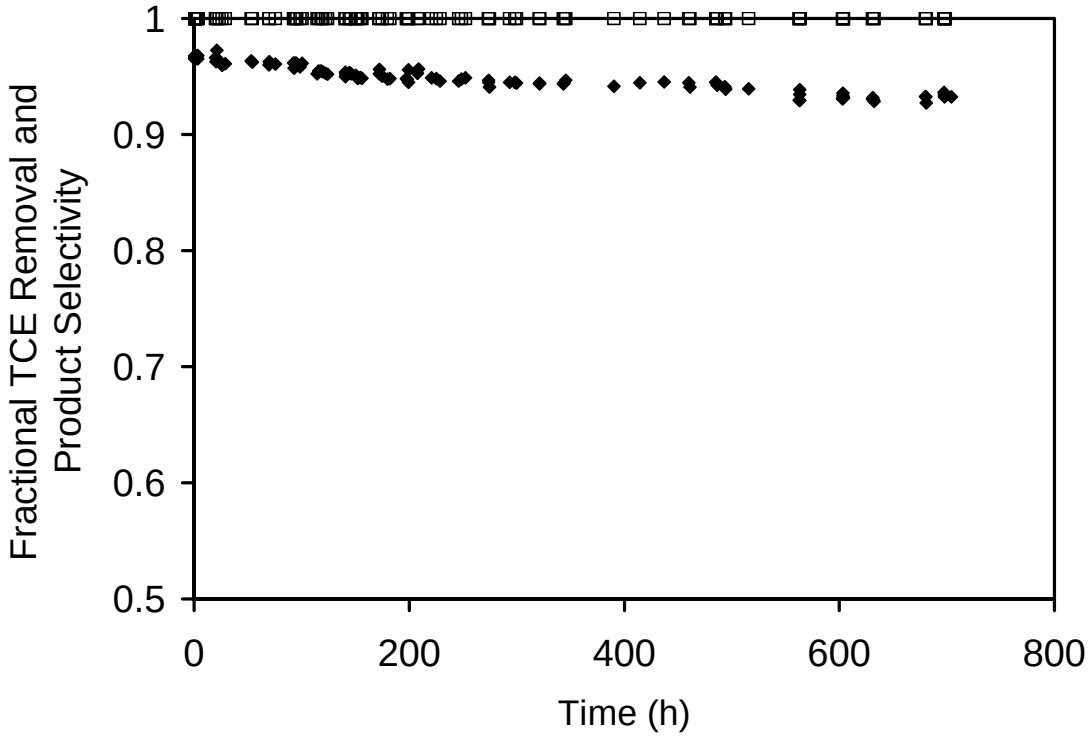

Figure 2.3 TCE hydrodechlorination as a function of time on 0.5 wt.% Pt/Al_2O_3 at 100ºC. (♦) factional TCE removal; (□) selectivity to ethane. Experiment was conducted at atmospheric pressure with ~4400 ppmv TCE in the influent, 0.059 L/min hydrogen and 0.35 L/min total gas flow. The residence time was 0.37 seconds.

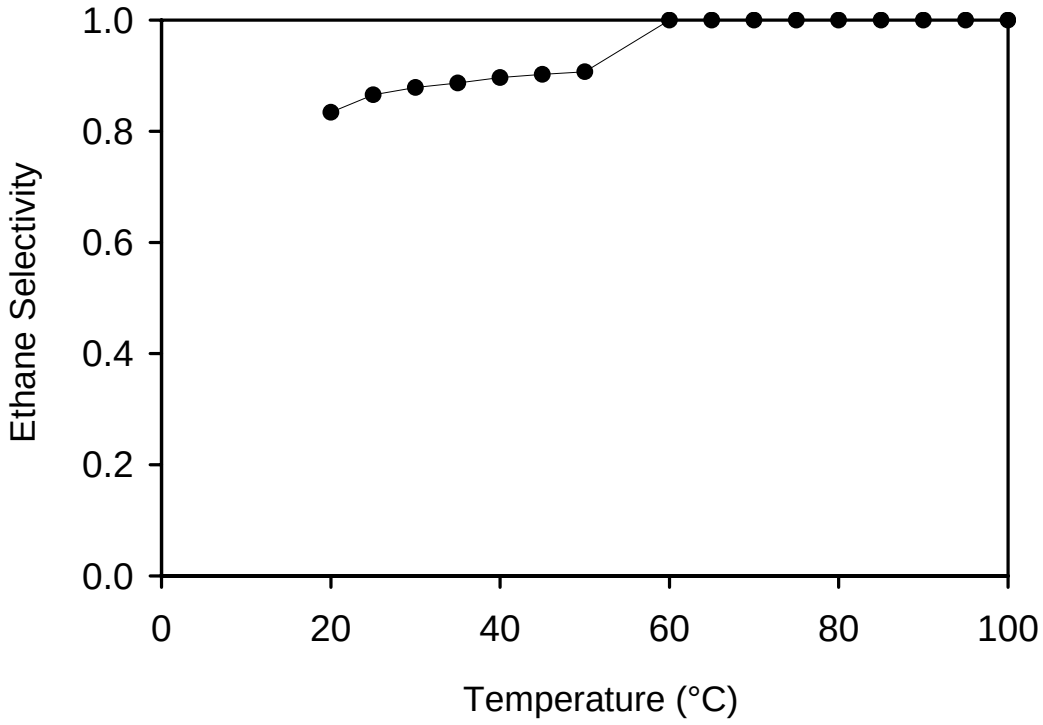

Figure 2.4 Effect of temperature on ethane selectivity in TCE hydrodechlorination on 0.5 wt.% Pt/Al_2O_3. Ethane and chloroethane were the observable compounds counted. Ethane was the sole organic product above 60ºC. Experiments were conducted under ambient pressure (~ 0.92 atm) with ~4400 ppmv TCE in the influent, 0.059 L/min hydrogen and 0.35 L/min total gas flow. Residence tome of TCE in packed bed was 0.37 seconds.

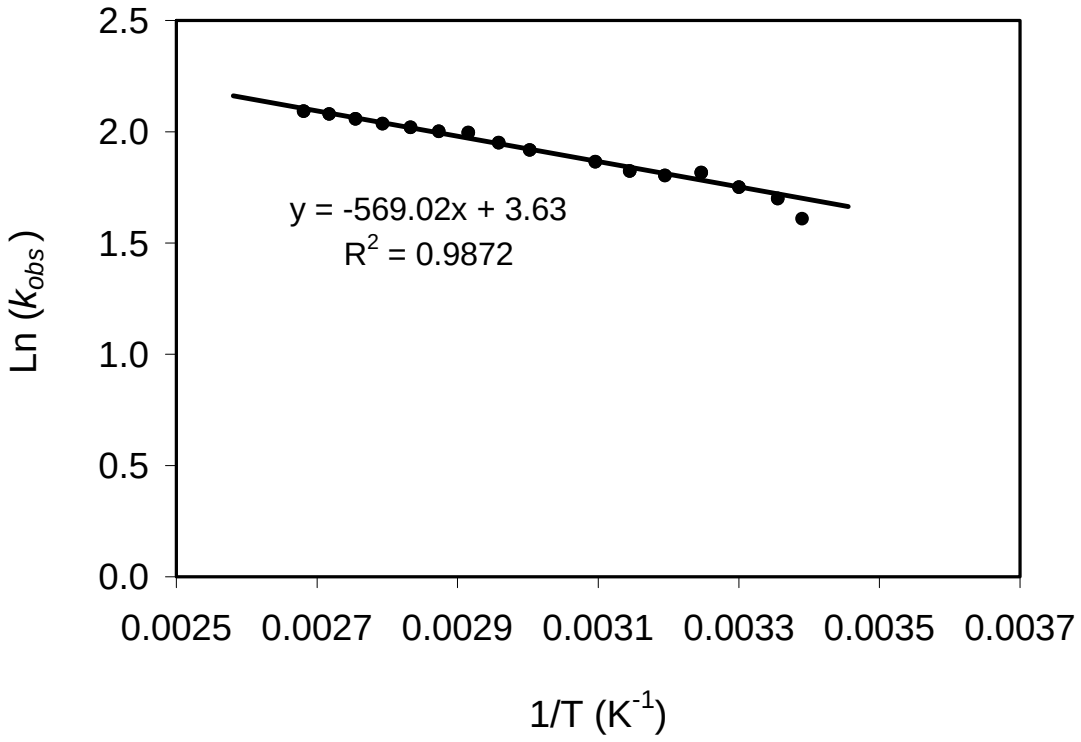

Figure 2.5 Linear regressions of log-transformed rate constants with inversion of temperature in TCE hydrodechlorination on 0.5 wt.% Pt/Al_2O_3. Experimental conditions were the same as in Figure 2.4. Apparent activation energy Ea = 4.73 kJ/mol, calculated according to equation (2.10). This low apparent activation energy suggests the reaction kinetics were limited by diffusion.

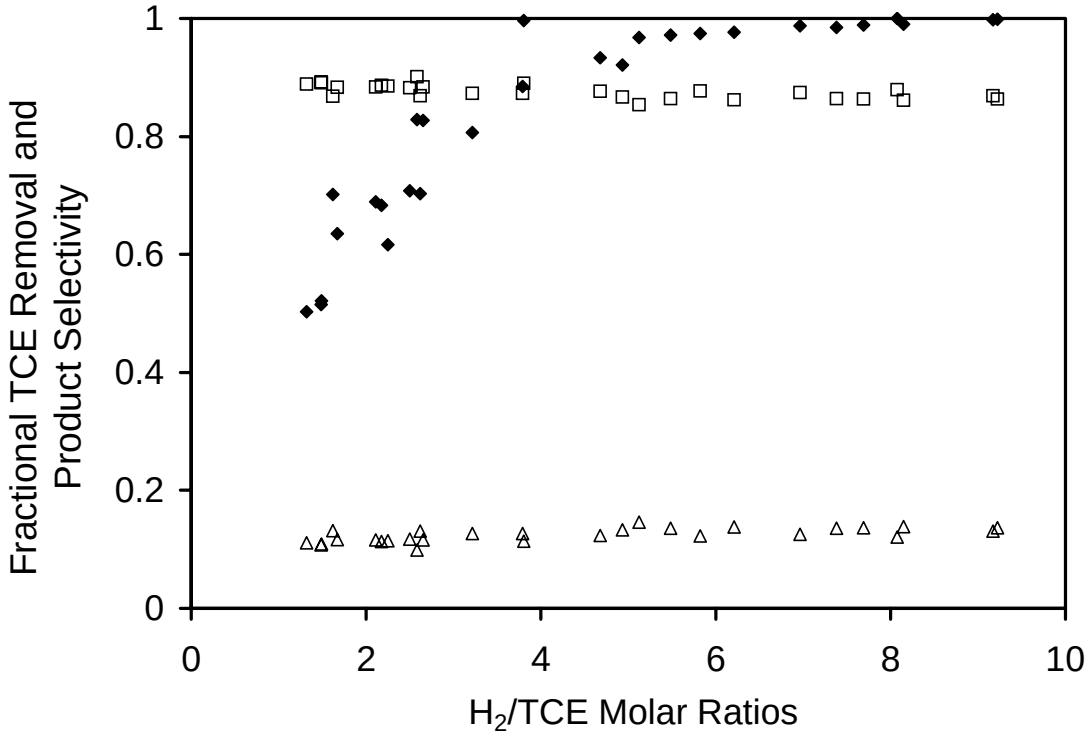

Figure 2.6 Effects of H_2/TCE ratio on TCE conversion efficiency and product selectivity in TCE hydrodechlorination on 0.5 wt.% Pt/Al_2O_3 at 22ºC. (♦) factional TCE removal; (□) selectivity to ethane; (Δ) selectivity to chloroethane. Experiments were conducted at atmospheric pressure (~0.92 atm, Tucson, AZ) with TCE influent concentration ranging from 1000 - 3900 ppmv and total volumetric flow rate ranging from 0.35 – 0.44 L/min (at 22ºC). Residence times ranged from 2.1 – 2.6 seconds.

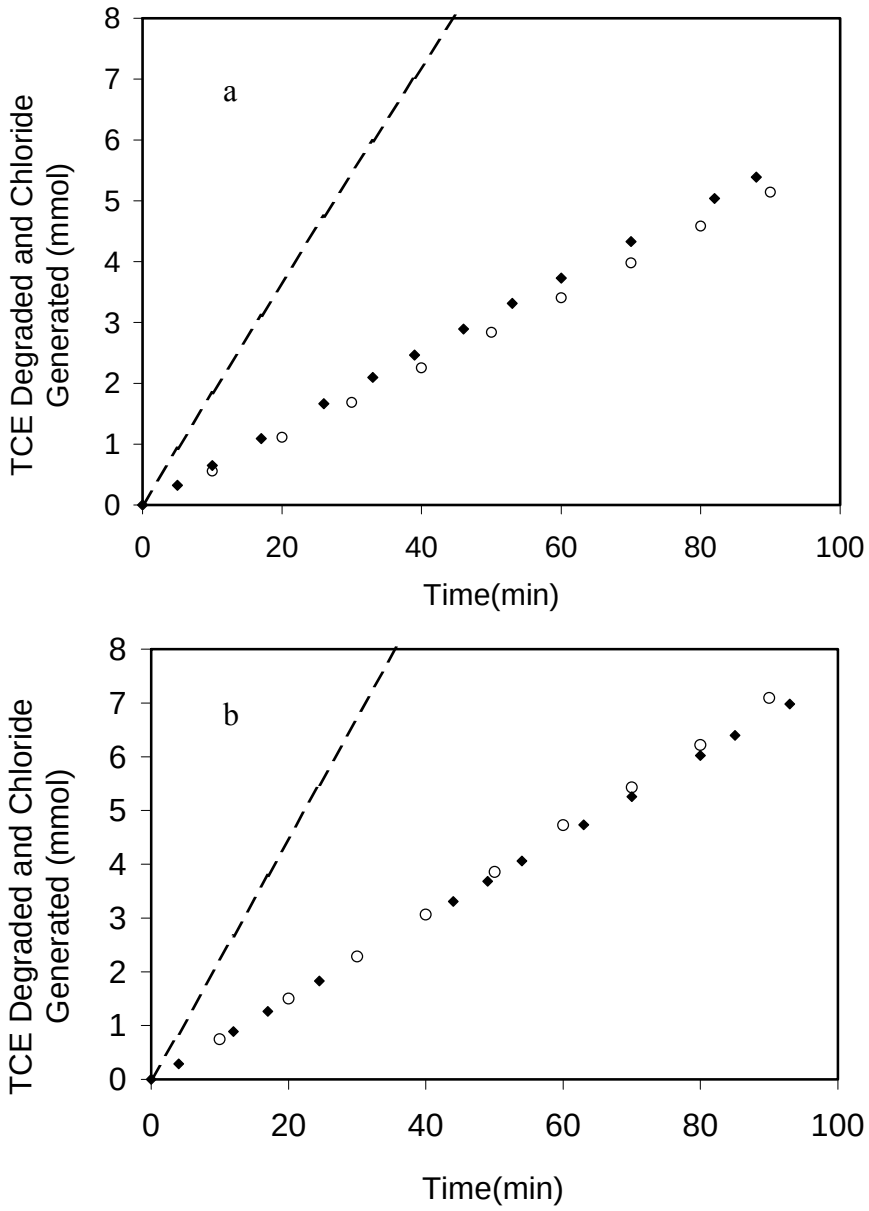

Figure 2.7 Chloride balance – moles of TCE converted and that of chloride captured from the effluent as a function of time for TCE hydrodechlorination on 0.5 wt.% Pt/Al_2O_3 at: a) 22ºC; b) 150ºC. (♦) moles of TCE converted; (○) moles of chloride captured; (--) moles of chloride obtained theoretically from converted TCE. Experiments were conducted at ~0.92 atm with ~ 4900 ppmv TCE in the influent, 0.059 L/min hydrogen and 0.37 L/min total gas flow.

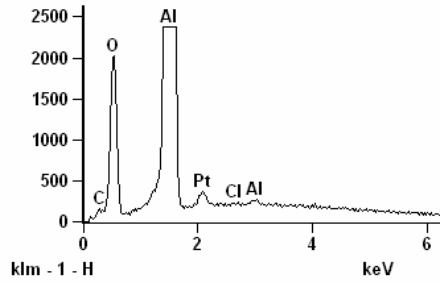

(a)

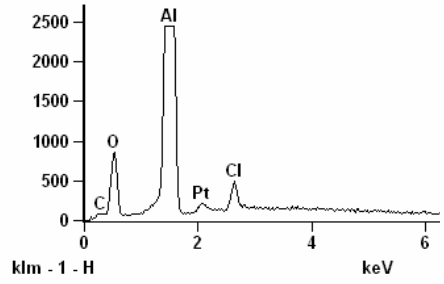

(b)

Figure 2.8 SEM/EDS of a) fresh catalyst and b) used catalyst. The intensity of x-ray energy was collected on a surface area of 54 μm x 44 μm. The used catalyst was examined after 700 hours of operation in TCE hydrodechlorination at 100ºC. The larger Cl/Pt ratio in used catalyst suggests that the scanning area contains chlorine-containing species.

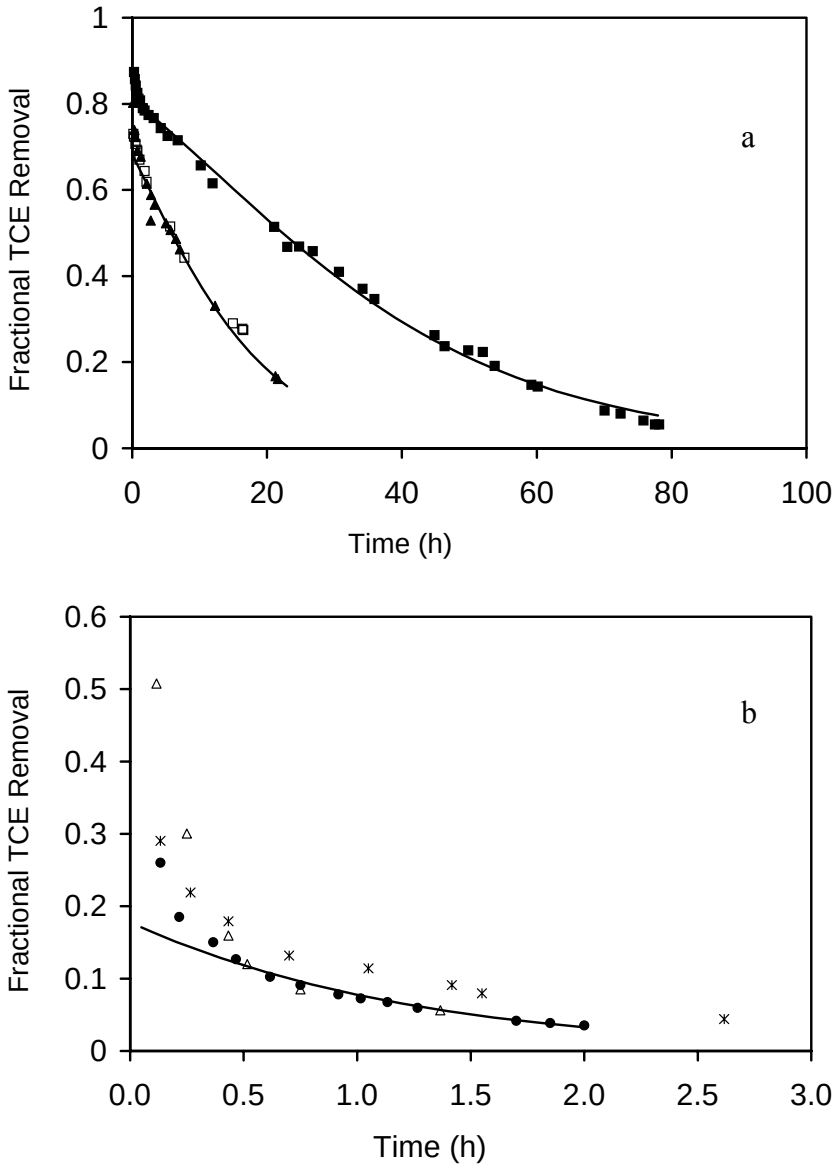

Figure 2.9 Catalyst performances in TCE hydrodechlorination on 0.5 wt.% Pt/Al_2O_3 at 22ºC after regeneration treatments: a) (■) TCE hydrodechlorination using fresh catalyst; (▲) after hydrogen treatment at 500ºC; (□) after nitrogen treatment at 500ºC; b) (●) after oxygen treatment at 500ºC; (*) after nitrogen treatment at 500ºC; (Δ) after hydrogen treatment at 500ºC; (-) model simulation using equation (2.8).

CHAPTER 3

GAS-PHASE HYDRODECHLORINATION OF TRICHLOROETHYLENE OVER Pt/SiO_2 IN PACKED-BED REACTOR

3.1 Abstract

Catalytic hydrodechlorination of gas-phase TCE was studied in a packed-bed catalytic reactor using a silica supported platinum catalyst. Silica sand was impregnated with platinum black to obtain the design loading of catalyst. An extremely low catalyst loading (0.0025 wt.%) was used to maximize the effects of catalyst deactivation in a subset of these experiments. Catalyst activity and durability were studied as a function of temperature. Higher temperature increased the initial catalyst activity. Among the temperatures 50ºC, 90ºC, and 100ºC, the catalyst deactivation rate was the lowest at 90ºC. Addition of KOH to the packed catalysts resulted in slower catalyst deactivation. The presence of O_2 in the gas stream had beneficial effects on TCE removal, increasing the temperature of the catalyst surface due to the reaction with H_2, and preventing deposition of carbonaceous compounds on the catalyst.

3.2 Introduction

Trichloroethylene (TCE) is a common solvent for metal degreasing. It was widely used in textile processing industries. Due to historical improper disposal and resistance to environmental degradation, TCE is one of the most widespread contaminants in groundwater and soil. Exposure to high levels of TCE causes nervous system effects,

liver and lung damage, and death. Based on a combination of frequency, toxicity, and potential for human exposure at National Priority List sites, TCE is ranked as the 16th most important pollutant in the 2003 Comprehensive Environmental Response, Compensation, and Liability Act (CERCLA) list, maintained by the U.S. Environmental Protection Agency (EPA) and the U.S. Agency for Toxic Substance and Disease Registry (ATSDR). TCE has been detected in at least 861 of 1,428 National Priority List (NPL) sites, which are among the most polluted hazardous waste sites in the U.S. [92]. Recycling and recovery is now emphasized in the manufacture and application of TCE. According to the U.S. EPA Toxic Release Inventory (TRI) [93], 161 million pounds of TCE was recycled and 10 million pounds were combusted for energy recovery from the 185 million pounds of TCE waste produced in 2003. Nevertheless, remediation of TCE contaminated groundwater and soil is one of the most important issues in environment and public health protection.

Traditional remediation technology for TCE contaminated groundwater is based on pump-and-treat methods. In this process, contaminated groundwater is pumped from subsurface for above ground treatment. The treated groundwater is re-injected or discharged on the surface. The most commonly applied above-surface treatment technologies are granular activated carbon (GAC) adsorption and air stripping. Air stripping is generally followed by some forms of treatments for the contaminated gas, including GAC adsorption. In GAC adsorption and air stripping, TCE is transferred from the aqueous phase to solid phase or gas phase, respectively. Treatment or disposal of spent GAC and contaminated gas is required. Contamination of groundwater by TCE is

frequently associated with contamination of soil in the overlying vadose zone. This is particularly true in the semiarid, southwestern United States, where depth to groundwater can be extensive. In spills, leaks, and improper disposal, TCE first contaminates the vadose zone, and then infiltrates to the local unconfined aquifer, driven by gravity. The process leaves TCE behind in the vadose zone as non-aqueous phase liquids, dissolved contaminant and vapor. This TCE contaminated vadose zone will serve as a long-term, continuous source for renewal of groundwater contamination if it is not treated properly. Soil vapor extraction is an appropriate technology for TCE contaminated soil, especially in arid and semi-arid regions with a relatively deep vadose zone, where the cost for excavation of soil is prohibitive. Similar to air stripping, the off gas of soil vapor extraction requires treatment prior to disposal.

Catalytic hydrodechlorination (HDC) is a process in which hydrogen is used to reduce chlorinated organic compounds to corresponding hydrocarbons on the surface of a metal catalyst. Hydrodechlorination has been tested or considered for remediation of a variety of chlorinated organic compounds including chlorofluorocarbons (CFCs) [20-22], chlorinated aromatics [23-25], and chlorinated aliphatics [14,26,27] in organic matrices, aqueous-, and gas phases. Moreover, this technology is simple to construct and operate. Kinetics are rapid for many dehalogenation reactions at ambient temperature and pressure. The products of reductive dehalogenation reactions are generally benign. Chlorinated alkanes and alkenes are mainly converted to hydrocarbons and hydrogen chloride (HCl) with no chlorinated intermediates under optimal reaction conditions. The corrosive HCl generated can be easily neutralized by passage through basic solutions. In

contrast to thermal incineration of chlorinated organic compounds, no dioxins and other toxic compounds are formed. The absence of toxic intermediates is attributed to the reducing environment provided by H_2(g) and to the mild temperature and pressure conditions.

This work focuses on the feasibility of catalytic HDC of TCE using a Pt/SiO_2 packed column. In the absence of O_2, gas-phase TCE was mainly reduced to ethane. Chloroethane was the only observable chlorinated intermediate. Catalyst deactivation resulted in decreased TCE removal efficiency with catalyst use. Addition of a small amount of KOH (0.0057 g KOH per gram of Pt/SiO_2 catalyst) to the packed bed increased catalyst life. The presence of O_2 in the influent gas stream also increased catalyst life.

3.3 Materials and methods

3.3.1 Catalyst and chemicals

Accusand® silica sand, 0.60 – 0.84 mm in diameters (Unimin Corp) was washed using DI water and air dried at room temperature. One kilogram of cleaned sand was then impregnated with 25 mg of platinum black (Aldrich) suspended in 500 mL deionized water. The mixture was homogenized and dried at 104ºC. The resultant metal loading was 0.0025 wt.%. The density of silica sand was 2.65 g/cm^3, and the bulk density of randomly packed Pt/SiO_2 was 1.75±0.03 g/cm^3, resulting in a porosity of 0.34±0.01.

Trichloroethylene, chloroethane and other chlorinated compounds were purchased from Aldrich and used as received. H_2 (Airgas, 99.95%), N_2 (Airweld, 99.99%), ethane and ethylene (Scotty, 99.9% purity) were all used as received.

3.3.2 Experimental setup

Figure 3.1 is a schematic diagram of the reactor system. Experiments were carried out in a continuous packed-bed glass reactor surrounded by a water jacket (Ace Glass Inc.). The glass reactor was 60 cm long with an inside diameter of 2.5 cm. Teflon plungers at both ends adjusted the length of packed beds. A water bath was used to control the reactor temperature from 22ºC – 100ºC. At the highest temperatures studied, boiling was avoided by adding 50% antifreeze (Chevron Delo®) to the water bath.

TCE vapor was added to influent gas mixtures by passing N_2 (g) through a wash bottle filled with pure TCE liquid. Another stream of N_2 (g) was introduced ahead of the reactor to produce the target concentration of TCE in the combined influent gas stream. H_2 and/or O_2 was added in different amounts or ratios as dictated by experimental objectives. Flow rates for all gases were controlled using mass flow controllers (Aalborg). Several three-way valves were used to direct the gas stream through the column or bypass the column, so that both the influent and effluent concentrations of target compounds could be monitored. A wash bottle filled with 800mL DI water was used to scrub HCl from the effluent gas stream.

3.3.3 Catalytic hydrodechlorination

Catalytic HDC of TCE was carried out at varying residence times, temperatures, and catalyst conditions. Other experimental conditions were constant: ambient pressure (~0.92 atm, Tucson, AZ), volumetric flow rate of 0.065L/min, influent TCE concentration of ~ 3500 ppmv, and 5% H_2(g) by volume in the influent, resulting in a H_2/TCE molar ratio of 14.

Reaction kinetics were studied at 22ºC and 64ºC by varying the amount of catalyst used. Residence times changed from 1.5 seconds to 9.8 seconds. To minimize the interference of catalyst deactivation with kinetics, fresh catalyst was used in each experiment, and the TCE conversion efficiency was examined for the first 10-minute period.

Long-term catalyst activity was tested at 50ºC, 90ºC, and 100ºC using 175 g of 0.0025 wt.% Pt/SiO_2 (4.38 mg Pt). Effects of base addition on catalyst activity were investigated by mixing 175 g Pt/SiO_2 with 1 g KOH powder. Column residence times were 31.3 seconds for these experiments.

3.3.4 Catalyst reactivation and O_2 effects

The deactivated catalyst, 44 g 0.01 wt.% Pt/SiO_2 (4.4 mg Pt) was washed in DI water, dried at 104ºC, and repacked in the reactor to examine restoration of catalyst activity via a series of treatments. Catalyst activity after each treatment was determined using standard TCE HDC experiments (influent TCE concentration ~4000 ppmv, volumetric flow rate 0.065 L/min, 10% H_2, and T =100ºC). N_2(g) flushing, O_2(g) oxidation, H_2(g) reduction, and O_2(g) oxidation followed by H_2(g) reduction were examined in sequence.

N_2(g) or O_2(g) passed through the packed bed at 0.035 mL/min and H_2(g) at 0.01 mL/min. The treatments were all performed at 100ºC.

Finally, TCE HDC was conducted with 5% O_2 and 10% H_2 (by volume) in the influent. TCE, ethane and chloroethane were monitored through the course of the experiment. No attempt was made to detect carbon monoxide or dioxide in the reactor effluent.

3.3.5 Analytical methods

Refer to section 2.3.5 of Chapter 2.

3.3.6 Methods for evaluating reaction and deactivation kinetics

Refer to section 2.3.6 of Chapter 2

3.4 Results and discussion

3.4.1 Products and kinetics

Ethane and chloroethane were the only observable products from TCE HDC. When carbon balance was attempted, ≥ 90% of carbon in the reactor feed stream was accounted for. Ethane was the major product, typically accounting for more than 80% of the observable products. Although not detected here, other chlorinated intermediates such as $C_2H_4Cl_2$, C_2H_3Cl, and $C_2H_2Cl_2$ may have been present in trace amounts, based on observations by Bozzelli et al. [14] for TCE HDC over Rh/SiO_2.

The linear relationship between log (1-*x*), where *x* is TCE conversion at the outlet of the reactor, and residence time suggested that the rate of TCE conversion was pseudo first-

order in TCE concentration (Figure 3.2). The apparent first-order rate constant (k_{obs}) was 0.029 s^{-1} at 22ºC, and 0.191 s^{-1} at 64ºC. Based on these two rate constants, an activation energy of 37.5 kJ/mol was calculated using the Arrhenius equation.

3.4.2 Effects of temperature

At 50ºC, ethane accounted for more than 83% of the observable products (molar basis) even at TCE conversions as low as 6.5% (Figure 3.3). At 90ºC, ethane selectivity decreased from 94 % to 83%, coincident with a drop of TCE removal efficiency from 77% to 7% during the 780-minute experiment (Figure 3.4). At 100ºC, ethane accounted for more than 90% of the observed products during the first 270 minutes of operation (Figure 3.5). Measurements were discontinued during minutes of 270 - 470. When measurements were reinitiated, ethane selectivity dropped from 83% to 52% during minutes of 475 to 600 of the overall experiment. Notice that ethane selectivity dropped at a much faster rate when TCE conversion was below 5% (Figure 3.5).

Catalyst deactivation was observed at all three temperatures tested here, following the typical time-dependent pattern: initial rapid decrease in catalyst activity followed by continuous deactivation at a much slower rate. Rapid initial deactivation might be due to physical changes in the catalyst such as losses of hyperactive corner and edge sites and loosely bound Pd particles [74], or the establishment of equilibrium with products, especially HCl, that compete with TCE for active catalyst sites [15,53-55]. The slow catalyst deactivation might be due to surface blockage by continuous coke deposition.

The catalyst decayed rapidly at 50ºC as TCE transformation dropped from 60% to 10% during the first 30 minutes of operation. At that point, however, catalyst activity stabilized, changing little over the remainder of the experiment. At 90ºC, catalyst deactivation occurred much more slowly. At 100ºC, complete TCE conversion was observed for the first 20 minutes, indicating that the initial activity of the catalyst was high enough to allow complete conversion of TCE before it reached the end of the packed bed. From that point, decay of catalyst activity followed a pattern similar to that observed at 90ºC.

Figure 3.6a contains the plots of the time-dependent TCE removal efficiencies at reactor temperatures of 50ºC, 90ºC, and 100ºC. The slow catalyst deactivation at 90ºC and 100ºC was simulated using the pseudo first-order rate equation and PFR transport model with exponential catalyst decay as described in equation (2.8). The procedure for the simulation begins by calculating the time-dependent apparent rate constant k for each TCE conversion using equation (2.6). Linear regression of log-transformed k values with time (equation 2.7) provides an initial reaction rate constant (k_0) and deactivation rate constant (k_d). At 90ºC, k_0 was 0.043 $L \cdot g_{cat}^{-1} \cdot min^{-1}$ and k_d was 0.0028 min^{-1}, while at 100ºC, k_0 was 0.070 $L \cdot g_{cat}^{-1} \cdot min^{-1}$ and k_d was 0.0050 min^{-1}.

Note that although the initial first-order rate constant for TCE conversion was taken as the rate constant for fresh catalyst, the catalysts were already subjected to a small amount of deactivation because measurements were always taken after a finite period of time had elapsed. In the case of the experiment at 100ºC, the initial rate constant was underestimated, possibly significantly, because the full conversion of TCE during the

initial experimental period could not support the procedure used for estimation of k_0 and k_d.

To further illustrate the kinetics of deactivation, TCE removal efficiencies were plotted with respect to the moles of TCE converted (Figure 3.6b). The slopes of these plots represent the normalized inactivation rate, or loss of reactivity per unit mass of TCE converted. The higher rate of catalyst deactivation at 100ºC is readily apparent. Results suggest that the mechanism of inactivation of Pt catalyst is temperature dependent.

3.4.3 Effects of KOH on catalyst deactivation

For each mole of TCE transformed to ethane, three moles of HCl are produced. The presence of HCl in the system has several potential effects. First, HCl could corrode the catalyst and support, resulting in the loss of active metal catalyst. Second, chemical interaction of chlorine with Pt may reduce the availability of catalytic sites for the target compounds. The reaction may eventually stop due to the accumulation of HCl and loss of active sites. Accumulation of HCl is more severe in batch systems, and some investigators have found that the addition of base was necessary to mitigate the effects of acid accumulation on the hydrodechlorination rates of target compounds [57].

Figure 3.7 shows TCE removal efficiency as a function of time with and without addition of KOH. The addition of KOH slowed the rate of catalyst deactivation, extending the period during which complete conversion was observed and slowing the rate of loss of TCE conversion efficiency thereafter. Analyzing the experimental data after the period of complete conversion provided an initial rate constant ($k_0 = 0.074$ $L \cdot g_{cat}^{-1} \cdot min^{-1}$) and

deactivation rate constant (k_d = 0.0013min^{-1}). The deactivation rate constant (k_d) in the absence of KOH was 0.0050 min^{-1}, about four times faster. Apparently, the role of KOH was to neutralize HCl and thus prevent the accumulation of HCl at or near the catalyst surface.

Figure 3.8 shows the fraction of total chlorine in TCE converted to ethane/chloroethane that was recovered in the water trap. Data correspond to experiments with and without addition of KOH to the catalyst bed. In each case, about half the chlorine was accounted for. Missing chlorine could have been retained on the surface of catalyst or elsewhere in the reactor.

3.4.5 Reactivation of catalyst and effects of O_2

Catalyst life is an important economic factor affecting the practicality of HDC application. Therefore, identifying means for reducing catalyst deactivation rate and reactivating the deactivated catalyst is of particular interest.

Figure 3.9 shows the effect of various reactivation strategies on catalyst recovery, in terms of TCE conversion efficiency. None of the treatments including washing, oxidation, and reduction significantly regenerated the deactivated catalyst. The inability to recover catalyst activity was attributed to the low temperature (100º) used here. When insoluble carbonaceous compounds with high temperature of combustion cause catalyst deactivation, the restoration of catalyst activity may require high temperature. Bae et al. [44] observed almost complete regeneration of catalyst in the presence of O_2 at 500ºC

followed by H_2 reduction at 300ºC. The same catalyst treated with O_2 at 300ºC did not recover its activity. Initiation of coke combustion was observed at 477ºC.

Adding O_2 to the contaminated gas stream significantly increased catalyst activity (Figure 3.10). TCE removal efficiency improved from 40% to about 80%, and the high removal rate was sustained for the remainder of the experiment (more than 15 hours). That is, only a very low deactivation rate was observed during this period of time. Interestingly, TCE removal efficiency was improved each time when the contaminated gas steam was deviated from the reactor to monitor the influent TCE concentration. This might be due to a temperature increase on the catalyst surface when no gas passed through the reactor.

The improvement of TCE removal efficiency upon addition of O_2 could be due to several factors. The reaction of O_2 directly with TCE was excluded here because the major carbon product was still ethane, accounting for more than 90% of TCE reduced. The reaction of O_2 with H_2 forming water is exothermic, and the heat released would increase the temperature of the catalyst surface, perhaps improving reaction kinetics. The introduction of O_2 may also burn carbonaceous deposits and increase the availability of active surface area. It was clear that in the presence of O_2, the deactivation rate was slowed, from either the volatilization of HCl or unfavorable conditions for coking. Considering the prevalence of O_2 in contaminated gas stream, the benefit of O_2 in hydrodechlorination should be further explored.

In this experiment, TCE was primarily converted to ethane. Chloroethane was only about 1% of the ethane produced. By just counting ethane and chloroethane, 90% of the

influent carbon was accounted for. CO or CO_2 may be produced, but they are not monitored in this work.

3.5 Summary

This research explored catalytic hydrodechlorination of gas-phase TCE on the surface of 0.0025 wt.% Pt/SiO_2. Low Pt loading was used to facilitate the study of catalyst deactivation and reactivation. Temperature has important effects on reaction kinetics and catalyst deactivation. The apparent activation energy for anaerobic conversion of TCE to products was 37.5 kJ/mol, calculated from the rate constants at two temperatures. The product distribution was essentially independent of target conversion, suggesting that the transformations of TCE to ethane and chloroethane were through parallel reaction mechanisms. Addition of KOH to the packed-bed reactor reduced the rate of catalyst deactivation by neutralizing HCl produced. Addition of O_2 to the influent gas flow increased the efficiency of TCE removal, either by increasing the local temperature (by reacting with H_2 to produce water and heat) or by preventing formation of carbonaceous deposits.

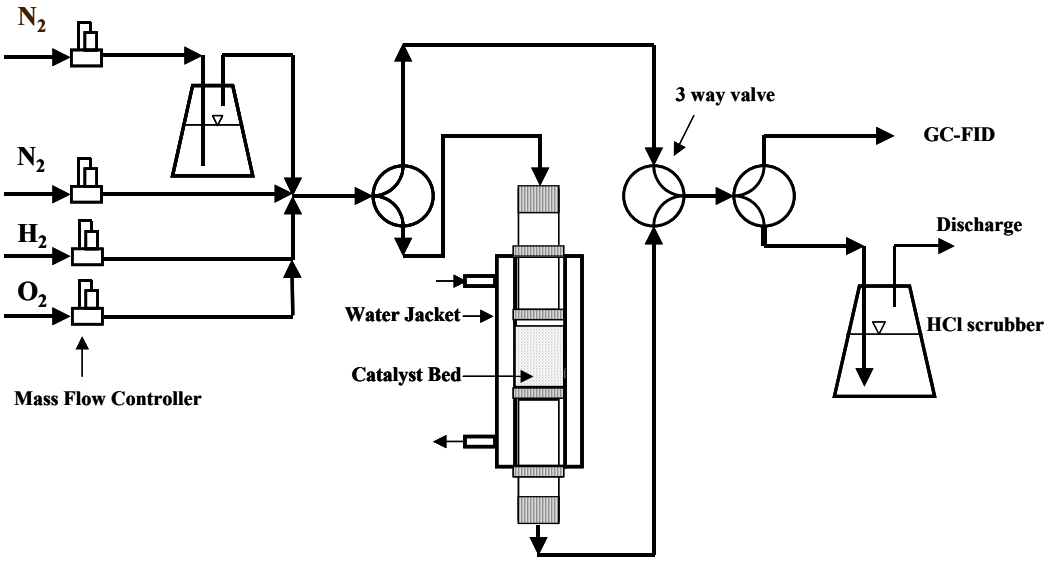

Figure 3.1 Experimental setup for gas-phase TCE hydrodechlorination over 0.0025 wt.% Pt/SiO_2. The reactions were carried out in a continuous packed-bed reactor. TCE vapor was obtained by passing a nitrogen side stream through the wash bottle filled with pure TCE liquid. H_2 and/or O_2 were added in different amounts as dictated by experimental objectives. Gas chromatography with FID was used to monitor target compound and products. HCl was scrubbed from the effluent gas stream using a wash bottle filled with water.

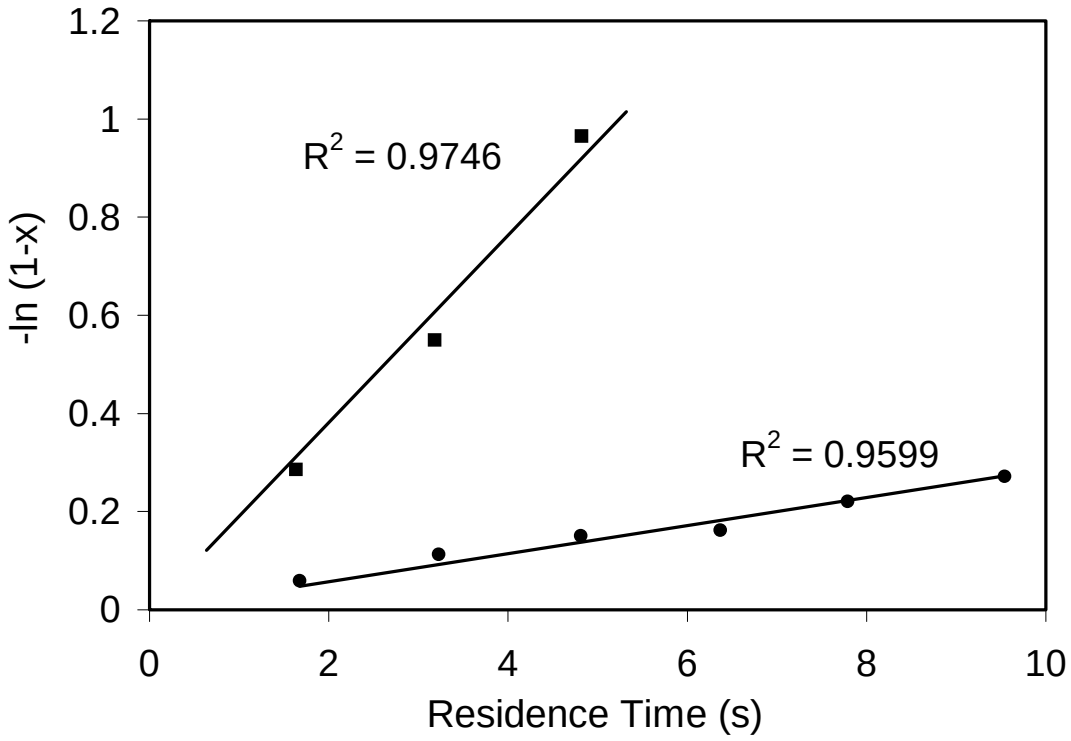

Figure 3.2 Dependence of TCE conversion efficiency on residence time at (●) 22ºC and (■) 64ºC for TCE hydrodechlorination over 0.0025 wt.% Pt/SiO_2. Lines were the linear regression of experimental data using equation (2.4): $\ln(1-x) = -k_{obs} \cdot \tau$ by forcing the solution through origin. Reaction constants k_{obs} were 0.029 s^{-1} and 0.191 s^{-1} for 22ºC and 64ºC. Activation energy calculated by these two rate constants was 37.5 kJ/mol.

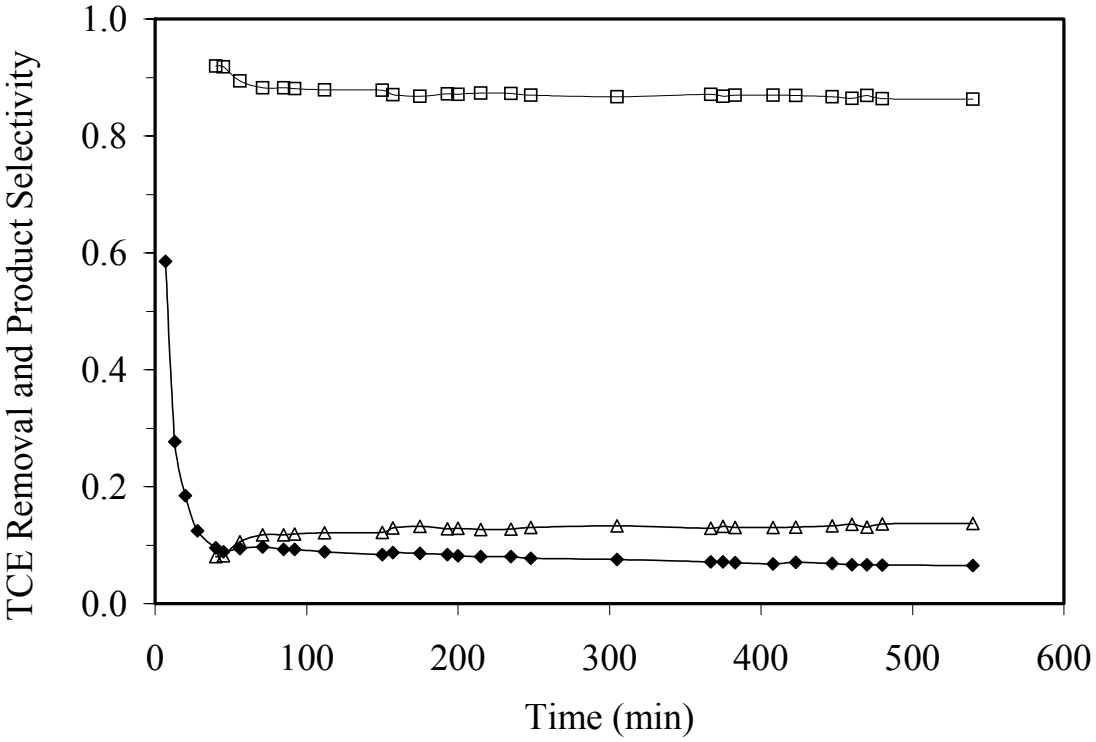

Figure 3.3 TCE removal and product selectivity as a function of time for TCE hydrodechlorination over 0.0025 wt.% Pt/SiO_2 at 50ºC. (♦) fractional TCE removal; (□) selectivity to ethane; (Δ) selectivity to chloroethane. Line is used to guide the eyes. The experiment was conducted at ambient pressure (~0.92 atm, Tucson, AZ) with total volumetric flow rate of 0.065 L/min, influent TCE concentration ~ 3500 ppmv, H_2/TCE molar ratio of 14, and a residence time of 31.3 seconds.

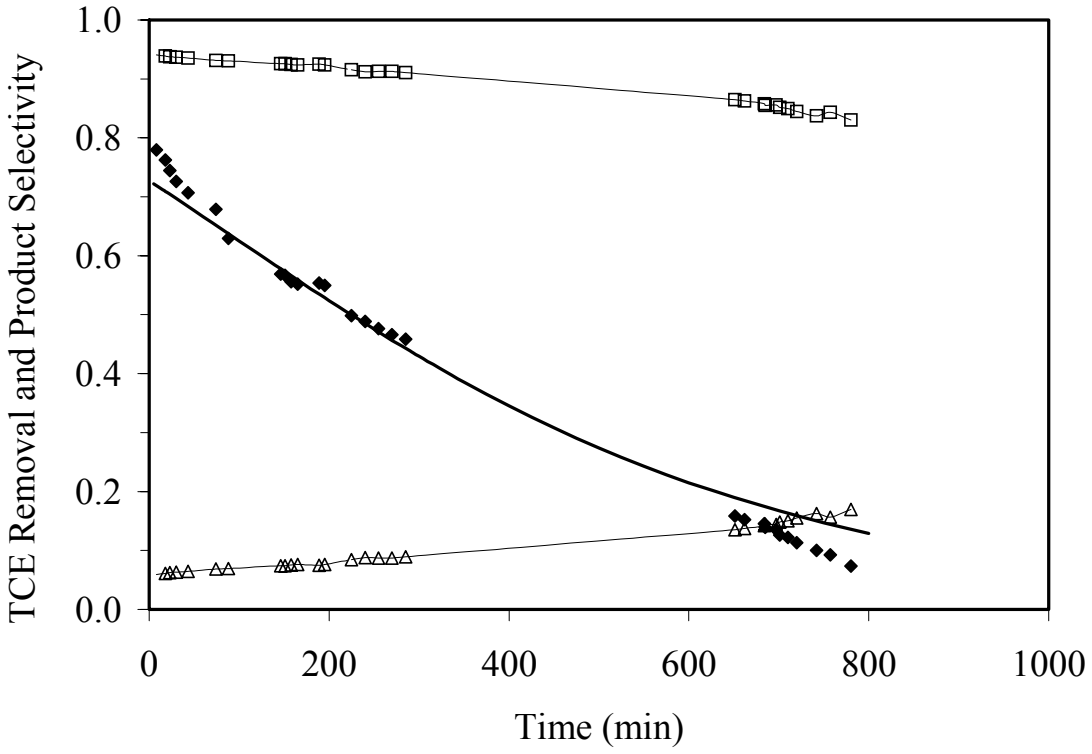

Figure 3.4 TCE removal and product selectivity as a function of time for TCE hydrodechlorination over 0.0025 wt.% Pt/SiO_2 at 90ºC. (♦) fractional TCE removal; (□) selectivity to ethane; (Δ) selectivity to chloroethane; (-) model simulation using design equation (2.8) with $k_0 = 0.043$ $L \cdot g_{cat}^{-1} \cdot min^{-1}$, $k_d = 0.0028$ min^{-1}. Other experiment conditions were described in Figure 3.3.

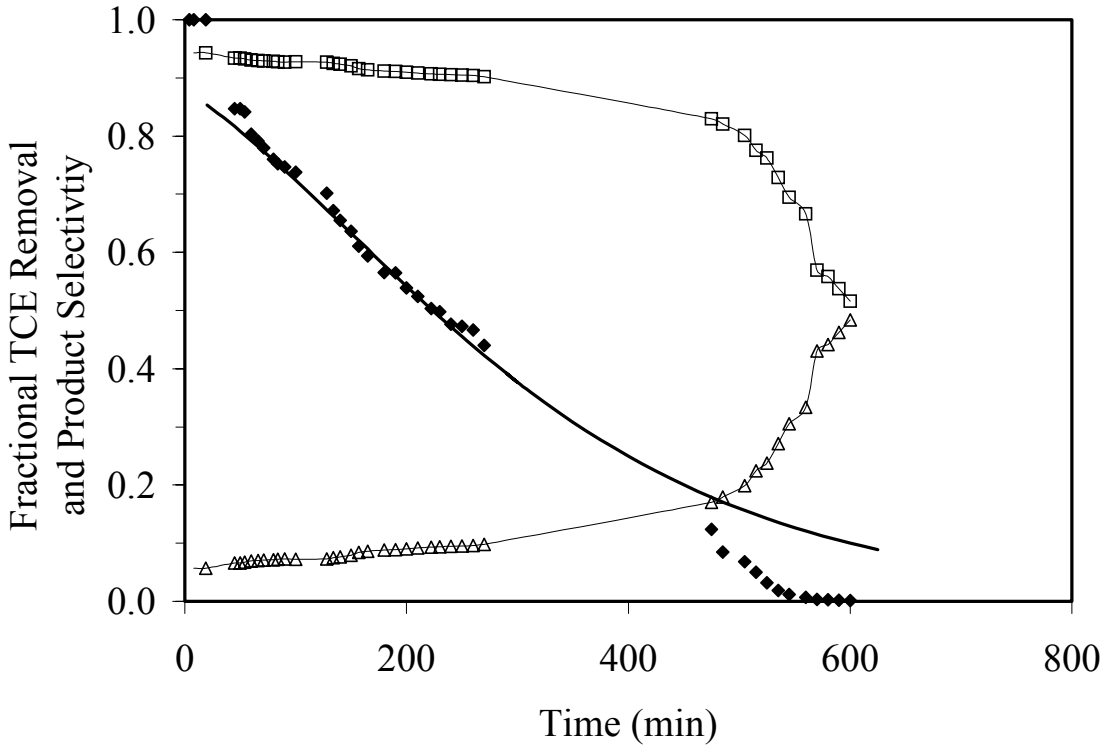

Figure 3.5 TCE removal and product selectivity as a function of time for TCE hydrodechlorination over 0.0025 wt.% Pt/SiO_2 at 100ºC. (♦) fractional TCE removal; (□) selectivity to ethane; (Δ) selectivity to chloroethane; (-) model simulation using design equation (2.8) with $k_0 = 0.070$ $L \cdot g_{cat}^{-1} \cdot min^{-1}$, $k_d = 0.0050$ min^{-1}. Other experiment conditions were described in Figure 3.3.

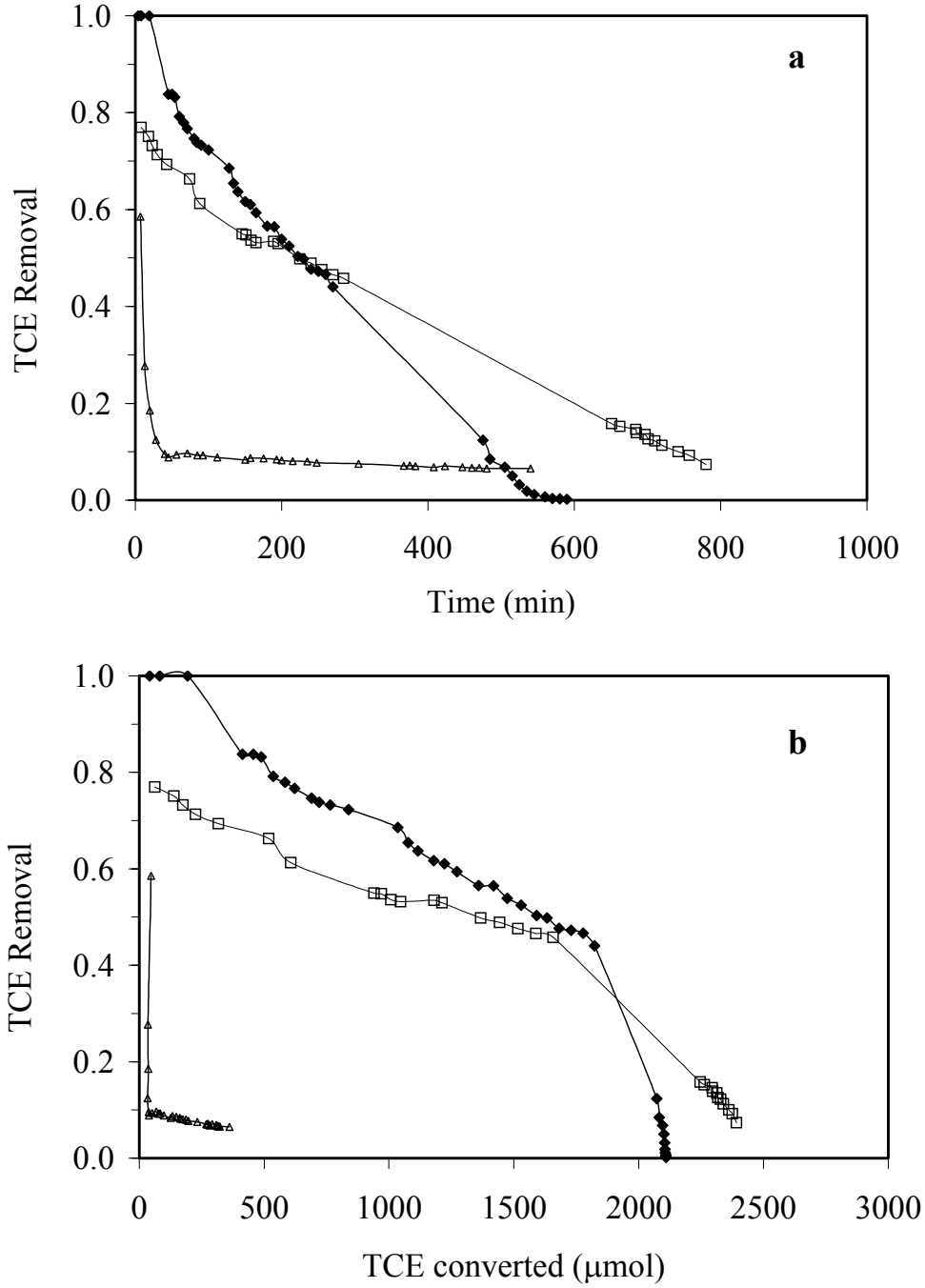

Figure 3.6 TCE removal as a function of a) operation time and b) amount of TCE transformed at (Δ) 50ºC, (□) 90ºC, and (♦) 100ºC. Experiment conditions were described in figure 3.3-3.5.

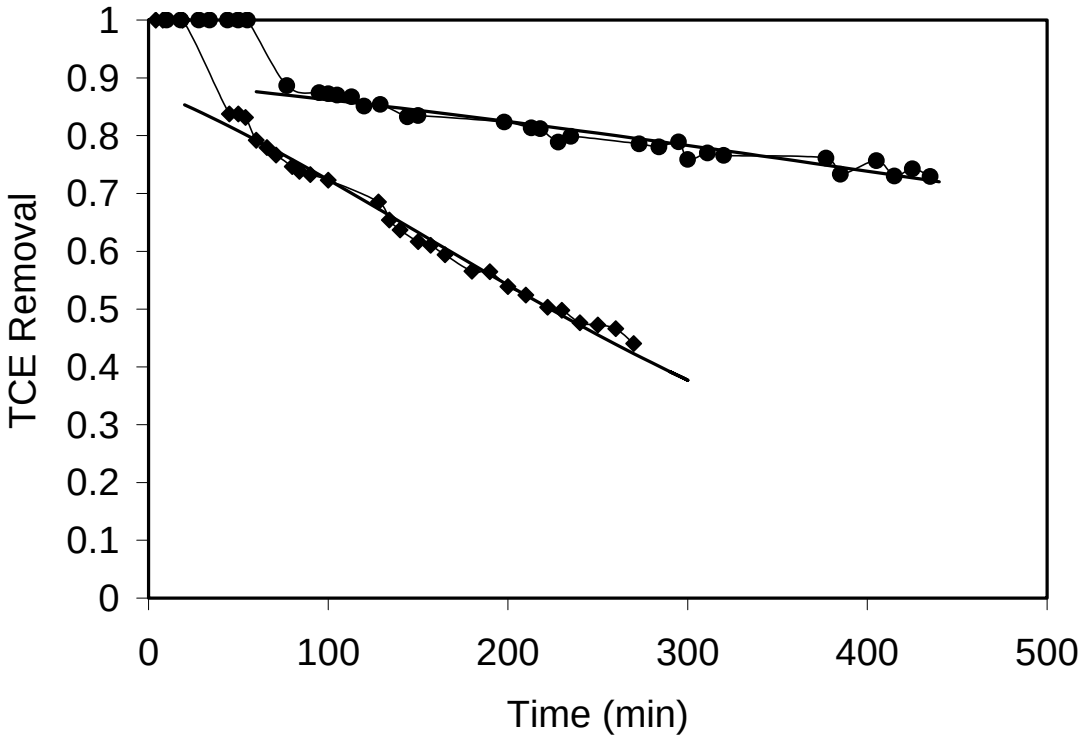

Figure 3.7 Effects of KOH on TCE removal as function of time for TCE hydrodechlorination over 0.0025 wt.% Pt/SiO_2 at 100ºC. (♦) without KOH and (●) with KOH. Without KOH, $k_0 = 0.070$ $L \cdot g_{cat}^{-1} \cdot min^{-1}$, $k_d = 0.0050$ min^{-1} ; with KOH, $k_0 = 0.074$ $L \cdot g_{cat}^{-1} \cdot min^{-1}$, $k_d = 0.0013$ min^{-1}. For the experiment with KOH, 1 gram KOH powder was mixed with catalyst. Other experiment conditions were described in Figure 3.3.

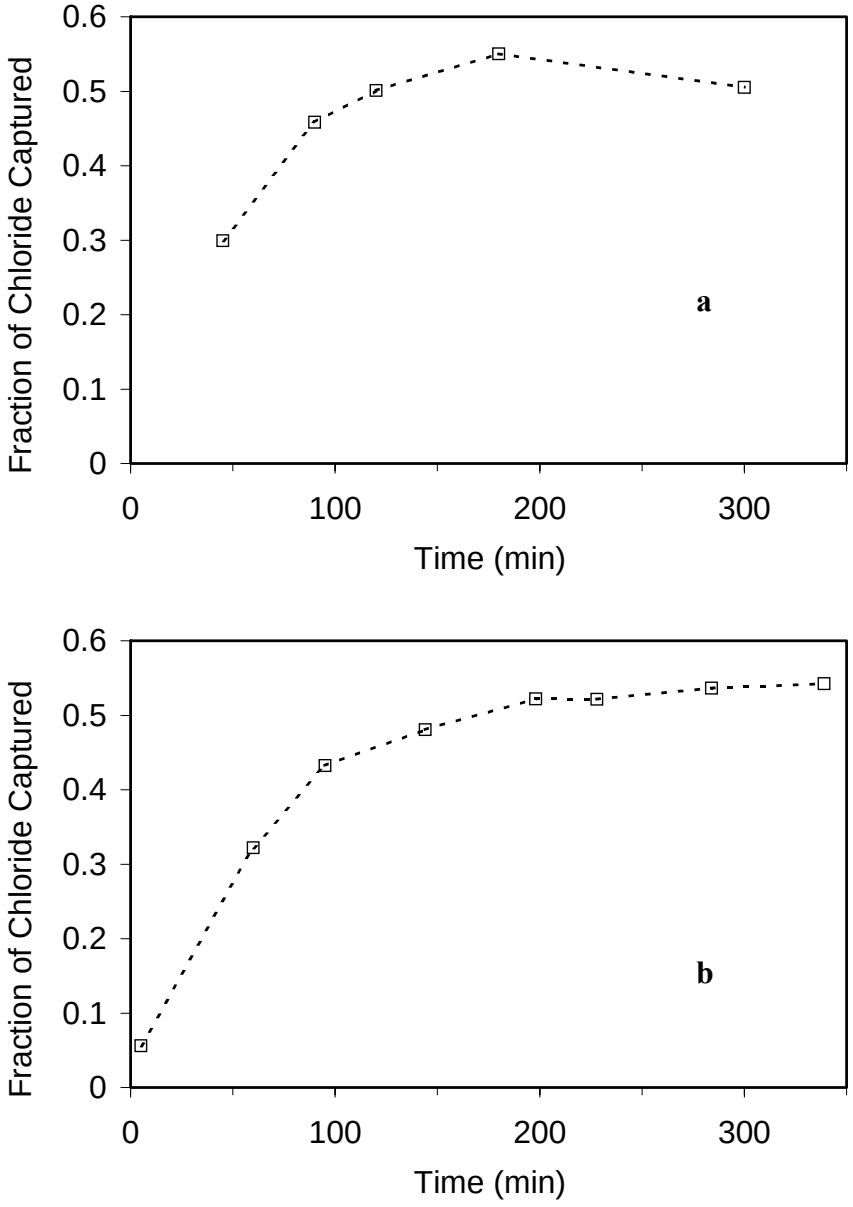

Figure 3.8 Fraction of total chlorine in TCE converted to ethane/chloroethane that was captured in the water trap: (a) without KOH and (b) with KOH. Experiment conditions were described in Figure 3.7.

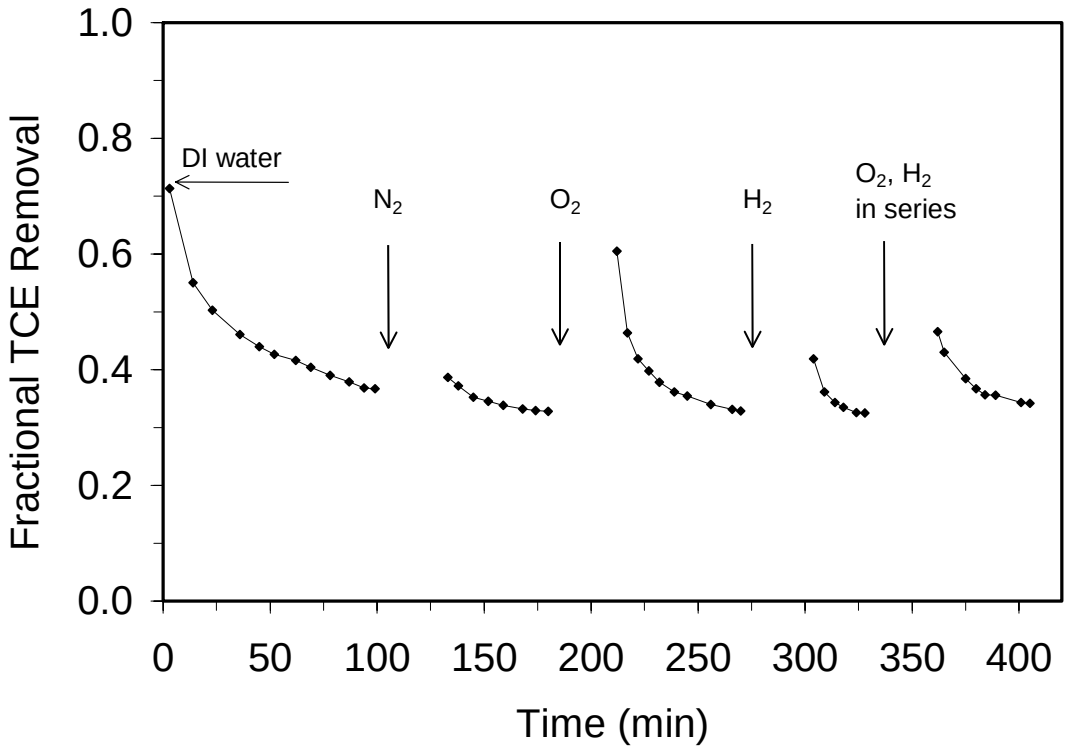

Figure 3.9 Catalyst performances in TCE hydrodechlorination over deactivated 0.01 wt.% Pt/SiO_2 after regeneration treatments. The deactivated catalyst was washed with deionized water *ex situ*, dried, and repacked for the subsequent test. Treatment of further deactivated catalyst was performed *in situ* for 30 minutes at 100ºC using different gas streams. N_2 and O_2 had volumetric flow rates of 0.035 L/min, and H_2 was 0.010L/min.

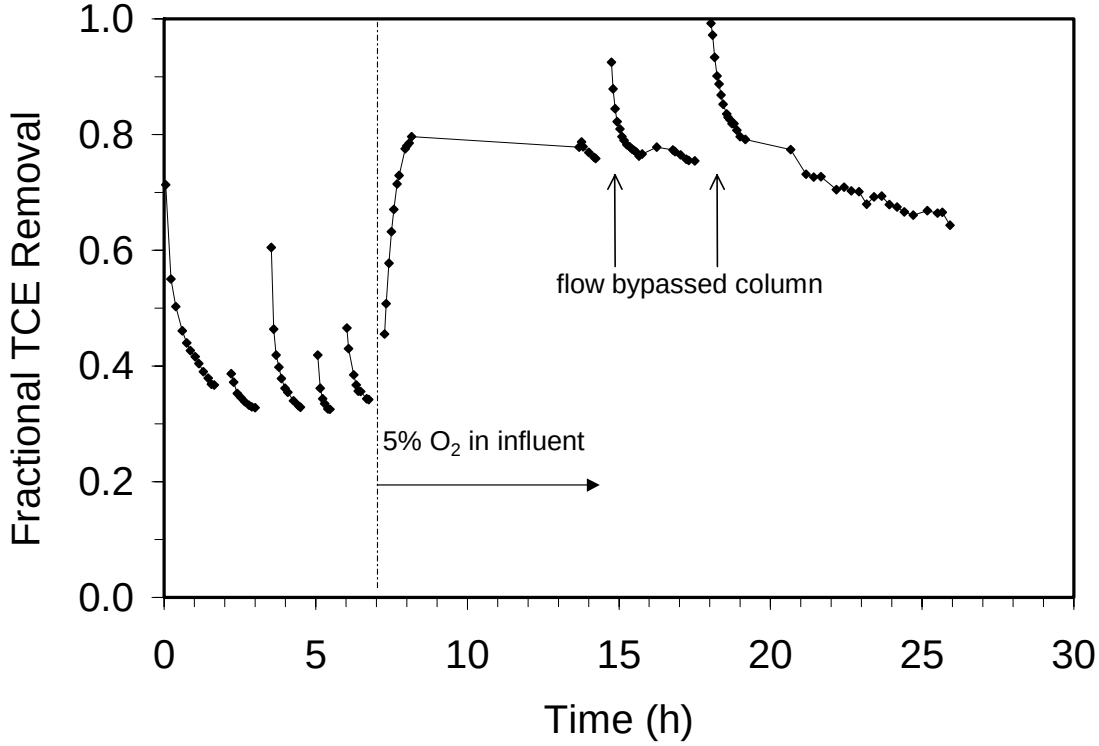

Figure 3.10 TCE removal in the presence of O_2 over deactivated 0.01 wt.% Pt/SiO_2. Catalyst performance after each recovery attempt was included in the left part of the dashed line (Figure 2.9) for comparison. To the right of the dashed line, 5% O_2 was added to the influent that contained 10% H_2 and TCE vapor. TCE removal efficiency was temporarily improved each time after the influent was deviated from the reactor for a short period of time to measure the influent TCE concentration.

CHAPTER 4

REDUCTIVE DEHALOGATION OF GAS-PHASE TRICHLOROETHYLENE IN A MODIFIED FUEL CELL

4.1 Abstract

A conventional polymer electrolyte membrane (PEM) fuel cell has been used as an electrocatalytic reactor to reduce gas-phase trichloroethylene (TCE). The TCE-containing gases are fed to the cathode side of the fuel cell device, where TCE is reduced to ethane and hydrochloric acid. The results obtained suggest that TCE reduction occurs mainly via a catalytic reaction with atomic hydrogen that is reformed on the cathode's surface beyond a certain applied cell potential. Substantial conversion of TCE is obtained, even when competing oxygen reduction occurs in the cathode. The process has been modeled successfully by conceptualizing the flow passage in the fuel cell as a plug flow reactor.

4.2 Introduction

Chlorinated solvents such as trichloroethylene (TCE) and perchloroethylene (PCE) have a history of widespread industrial use and improper disposal. They are among the most common contaminants at United States Superfund sites [2]. Chlorinated solvents have been implicated in skin, liver and kidney cancers; nervous system dysfunction; and fetal heart defects [3]. Their presence in potable water and groundwater or sediments is subject to stringent federal regulations. Pump-and-treat technologies are the most commonly applied methods for remediating or simply managing groundwater contaminated with TCE or PCE. Water is pumped to the surface for cleaning via stripping or carbon

adsorption. The apparent simplicity of pump-and-treat methods is deceptive, however. Contaminant rebound, for example, is frequently observed in field situations. Rebound is the reappearance of relatively high contaminant concentration after seemingly successful pump-and-treat operations for contaminant recovery. There are several plausible mechanisms that could result in contaminant rebound. Commonly, rebound is based on an initial "sweeping" of aqueous-phase contaminants from the affected zone with advective flow, followed by recontamination of bulk groundwater phase via contaminant transfer from solid surface, pores and interstitial zones between adjacent particles into the bulk fluid phase after pumping is discontinued [2]. Pump-and-treat applications do not necessarily involve compound destruction, so that disposal of residuals generally remains problematic. For these reasons, strategies based on pump-and-treat technologies have seldom satisfied remediation objectives at or near anticipated costs.

Where semi-volatile contaminants are present in an extensive vadose zone, soil vapor extraction (SVE) is frequently selected to recover pollutants. Advantages over pump-and-treat technologies lie primarily in energy costs, since pressure driven gas recovery is more economical than water recovery from porous media. SVE applications yield contaminated gas streams that are frequently cleaned up via carbon adsorption before release to the atmosphere. The cost of such operations can be heavily influenced by carbon recovery or replacement costs, particularly when spent carbon must be treated off site as a hazardous waste.

Over the last ten years a number of destructive technologies have been developed and applied for the treatment of fluid streams containing chlorinated solvents. These include heterogeneous catalysis [14,47,75] and electrocatalysis of redox transformations [7,77-79,94-96], and straightforward chemical reduction using zero-valent iron (ZVI) or other reductants [8,97,98]. Each method has unique advantages and disadvantages. ZVI, for example, provides a passive, economically attractive basis for contaminant transport. Surface reactions leading to passivation of the iron surface have not proven to be as great an obstacle to long-term barriers effectiveness, and the technology has been widely deployed in the United Sates and Canada. However, installation costs can be prohibitive when depth to groundwater is significant.

The kinetics and product distribution of chloroalkane and chloroalkene reduction via electrolysis can be strong functions of electrode material, temperature, ionic strength and pH [7,11,77,78,80,94-96,99-101]. In some situations, the kinetics of such reductions are first-order in contaminant concentration, suggesting that electrode materials are far from saturated or that reaction rates are governed by mass transport as opposed to electron transfer kinetics at electrode surfaces.

More recently, investigations have turned toward gas diffusion electrodes (GDEs), particularly for treatment of volatile contaminants. Gas diffusion electrodes consist of a gas-diffusion region and a reactive (catalytic) region. The reactive gas must diffuse through a liquid layer that separates the gas phase and solid electrode. This transport step frequently limits the overall transformation rate for the target compound [90]. Sonoyama et al. [88,89] investigated the kinetics of Freon reduction on GDEs comprised of various

candidate metals. In each case, the surrounding electrolyte consisted of a mixture of water and methanol amended with 1M NaOH to both transfer charge and to suppress hydrogen production. Freons studied were dichlorofluoromethane (CFC-12) and monochlorotrifluoromethane (CFC-13). Both dehalogenation kinetics and product selectivity were functions of electrode material. Production of hydrogen gas on Pt, Pd and Ni electrodes interfered with CFC-12 reduction. Current efficiency, defined as the fraction of total current utilized for reduction of CFC-12, ranged from 0.044 (Pt) to 1.0 (Pb). Current efficiency was directly related to metal-dependent overpotential requirements for the reduction of water to hydrogen gas. Only the Cu- and Ag-supported GDEs effectively reduced CFC-13. Lack of success using other metals was attributed to poor adsorption characteristics. Current efficiencies for CFC-13 reduction were lower than corresponding efficiencies for the reduction of CFC-12. This was attributed to the lower solubility of CFC-13 in water (0.33 g/L for CFC-12 vs. practically insoluble CFC-13 at 20 ºC). Current efficiency increased at high partial pressures of CFC-13.

Liu et al. [10] studied the reductive dechlorination of TCE in a GDE that was identical in design to a polymer electrolyte membrane (PEM) fuel cell. That is, a proton-conducting membrane served as the solid-phase electrolyte, separating the anode and cathode, which were pressed directly onto opposite sides of the membrane. When operated as a fuel cell, hydrogen gas can be introduced to the anode chamber, where it is oxidized to produce protons and electrons. The protons produced are transported through the PEM to the cathode where they participate in the reduction of molecular oxygen to water. The overall reaction is exergonic, and the resulting current, passed through an external circuit, can

perform work. When gas-phase halogenated solvents are supplied to the cathode, instead of or in addition to molecular oxygen, they are reduced to less chlorinated homologues. Liu et al. [10] showed that under these circumstances dehalogenation rates and product selectivity were functions of primarily cathode material selection, temperature, and the cathode potential, which could be lowered (made more negative) in order to increase reaction rate. Under the most favorable experimental conditions, half-times for TCE destruction were on the order of tenths of a second. However, catalyst surface area and a detention time in the cathode chamber could not be determined exactly and only the cell potential (cathode minus anode) was known, so that mechanistically-based reactor simulations are not possible on the basis of these experiments. Although continuous operation resulted in reactor poisoning, kinetic performance could be restored by periodic reversal of electrode polarities. At the most negative cell potentials utilized, hydrogen reformation on the cathode surface was probably observed, but no attempt was made to rationalize reactor kinetic performance based on the contribution of reformed $H_{2(g)}$ to total gas flow rate in the cathode.

Here we explore the kinetics and mechanism of gas-phase TCE reduction under conditions similar to those employed by Liu et al. [10]. Among the questions addressed is whether TCE reduction on the porous graphite/Pt cathode occurs primarily through a thermocatalytic or an electrocatalytic mechanism. The effects of near-atmospheric levels of molecular oxygen, a potential competitor to TCE reduction, on reactor performance were also investigated. Based on those data, process performance was successfully simulated under a variety of operating conditions.

4.3 Materials and methods

4.3.1 PEM Fuel cell fixture

The PEM fuel cell (MP Technologies) used in this research (Figure 4.1) was composed of two gold-plated copper end plates, two graphite plates to collect current and distribute gas within the cathode and anode chambers, and the membrane electrode assembly (MEA). Figure 4.2 shows a schematic of transport and gas flow paths in the fuel cell. Serpentine flow channels with a cross sectional area of 1 mm^2 were cut into the two graphite plates as shown (Figure 4.2b). Three parallel channels formed one flow path. Thus, each segment of the flow path has a total cross sectional area of 3 mm^2. The length of flow path was 220 mm. The MEA consisted of a proton-conducting membrane Nafion-112 (DuPont®) in the middle, onto which the catalyst and gas diffusion layers were mounted (cathode and anode) on opposite sides. The catalyst layers, where the reactions occur, had a geometric area of 10 cm^2 for each electrode.

4.3.2 MEA fabrication

The gas diffusion layer is composed of Teflon-treated carbon cloth and a layer of mixture of acetylene black and Teflon on the top. Teflon-treated carbon cloth was obtained by submerging carbon cloth (Zoltek) into a PTFE solution (Aldrich). After the excess liquid was drained, the carbon cloth was dried at 120ºC for 30 minutes and sintered at 350ºC. The mixture of 1:1 carbon and PTFE was then loaded onto the Teflon-treated carbon cloth to improve the gas diffusion. Acetylene black (Chevron) and PTFE solution were mixed with a small amount of 2-propanol to obtain the mixture paste. The paste was

evenly applied to the top of the Teflon-treated carbon cloth and dried under ambient conditions. The GDE was then cut to electrode size. The catalyst was prepared by mixing 70 mg 20% Pt on Vulcan XC-72 (E-TEK^{SM}) with 5 mL 2-propanol and sonicating for 10 minutes. The surface area of the Vulcan XC-72 was 250 m^2/g, and the Pt metal had a surface area of 110 m^2/g and particle size of 2.5 nm (manufacturer's data). The catalyst suspension was then brushed on the top of the GDE to obtain a catalyst loading of about 1.4 mg/cm^2. The carbon cloth electrodes so produced were placed on both sides of the Nafion-112 membrane, wrapped in aluminum foil, and hot pressed at the glass transition point of the membrane (140ºC) and 130 psig for 90 seconds. The completed MEAs were covered with aluminum foil and stored at room temperature pending use.

4.3.3 PEM fuel cell reactor

The reactor configuration and experimental set up are shown in Figure 4.3. Hydrogen gas was humidified before it was introduced into the cathode chamber. Pressure on the hydrogen side of the reactor was maintained at 10 psig. To test PEM fuel cell performance, humidified oxygen was supplied to the cathode at a rate of 60 mL/min and atmospheric pressure. Electrical current was measured as a function of cell potential, and a reactor performance curve was obtained (current density vs. cell potential). The cell potential, defined here as

$$E_{cell} = E_c - E_a - IR \qquad (4.1)$$

where IR is the IR-drop across the membrane, and E_c and E_a are cathode and anode potentials, respectively, was maintained using a potentiostat (model 410, Electrosynthesis) and a 24-V power supply (model 6201A, Harrison Laboratories).

In the normal mode of operation for TCE conversion (termed here electrochemical operation), the gas stream containing the target contaminant (TCE) replaced the oxygen flow to the cathode, and fractional dechlorination was measured as a function of cell potential. The TCE vapor was obtained by passing a nitrogen side stream through a wash bottle filled with pure TCE liquid. The main stream of humidified nitrogen gas was introduced to dilute gas-phase TCE vapor to the target concentration (500 ppmv) ahead of the cathode chamber. All gases were obtained from US Airweld and used without further purification. All experiments were conducted at room temperature.

4.3.4 Analytical

TCE and reaction products were measured by gas chromatography (SRI 8610 with FID, RTX-5 30m capillary column, oven temperature 100°C, injection temperature 100ºC, carrier gas: 14 mL/min He). A 250-µL sampling loop was used to withdraw gas samples. Data points represent averages of three to five measurements. The lower detection limit was 5-10 ppmv for TCE and reaction products. Products were identified by comparison of retention times with authentic standards. Standards for TCE and less chlorinated homologues (Aldrich) were prepared by injecting known volumes of pure liquid into 70-mL sealed bottles. Standards for ethane and ethylene (Scott gases) were prepared by injecting known volume of pure gas into the sealed bottles.

4.4 Mathematical model

In the PEM fuel cell, an electrochemical reaction occurs where carbon particles, polymer electrolyte, and Pt catalyst are in close contact. A carbon substrate must be present to conduct electrons and serve as support material for both electrodes. The polymer electrolyte conducts protons from anode to cathode, thereby completing the electrical circuit. The Pt surfaces catalyze the reactions of interest on both sides of MEA. In the void space of the gas diffusion electrode, a thin film of water forms around the carbon/platinum particles. Due to the production of hydrochloric acid in TCE reduction, this thin film of water is acidic. In acidic solutions on Pt surfaces, hydrogen evolution occurs via the Volmer-Tafel mechanism [87], consisting of the following elementary reactions,

$$Pt + H^+ + e^- \leftrightarrow Pt - H \quad \text{(Volmer reaction)} \tag{4.2}$$

$$2Pt - H \leftrightarrow 2Pt + H_{2(g)} \quad \text{(Tafel reaction)} \tag{4.3}$$

Because these are surface reactions, the rates can be expressed in terms of the Pt-H surface coverage, θ_H, as follows,

$$\nu_1 = k_1[H^+](1-\theta_H) - k_{-1}\theta_H \tag{4.4}$$

$$\nu_2 = k_2\theta_H^2 - k_{-2}P_H(1-\theta_H)^2 \tag{4.5}$$

where ν_i are reaction rates, and k_i and k_{-i} are the forward and backward rate constants, $[H^+]$ is the proton concentration in the liquid, and P_H is the hydrogen partial pressure.

The surface coverage of atomic hydrogen can be controlled by manipulating the electrode potential. When hydrogen desorption and re-adsorption proceed very fast, reaction 4.3

can be assumed to be at equilibrium and $\nu_2 \approx 0$. Under these circumstances, equation (4.5) yields

$$\theta_H = \frac{(K_H P_H)^{0.5}}{1+(K_H P_H)^{0.5}} \tag{4.6}$$

where $K_H = \frac{k_{-2}}{k_2}$ is the hydrogen adsorption equilibrium constant. The same expression can be derived for a heterogeneous catalytic reaction by using the Langmuir adsorption isotherm where hydrogen is dissociatively adsorbed.

Results obtained in this work suggest that TCE reduction is initiated by reaction with atomic hydrogen on the cathode side. The overall reaction is

$$C_2HCl_3 + 8Pt\text{-}H \rightarrow C_2H_6 + 3HCl + 8\ Pt \tag{4.7}$$

Assuming that TCE and nascent hydrogen do not compete for adsorption sites on Pt and that TCE adsorption is governed by a Langmuir isotherm, the surface coverage of TCE can be expressed as:

$$\theta_T = \frac{K_T P_T}{1+K_T P_T} \tag{4.8}$$

where θ_T is the surface coverage of TCE, K_T is the adsorption equilibrium constant for TCE, and P_T is the partial pressure of TCE. If the reduction rate of TCE is proportional to the surface coverage of both TCE and atomic hydrogen, use of the previous equations allows us to express the rate of TCE disappearance as

$$r = k\theta_H\theta_T = \frac{kK_H^{0.5}K_T P_H^{0.5} P_T}{[1+(K_H P_H)^{0.5}](1+K_T P_T)} \tag{4.9}$$

where k is the rate constant.

Individual flow channels of the fuel cell reactor have a cross sectional area of 1 mm^2. Three flow channels together form one path of flow. Thus, the flow path has a total cross sectional area of 3 mm^2 and a length of 220 mm. These dimensions suggested that the cathode be treated as a plug flow reactor (PFR). In addition, we will assume that gas-phase diffusion into the electrode is fast, and we will consider that hydrogen gas will be reformed in the cathode. Under these conditions, mole balances for TCE and hydrogen gas yield

$$\frac{d(QP_T/RT)}{dz} = -Aa_v r \tag{4.10}$$

$$\frac{d(QP_H/RT)}{dz} = -4Aa_v r + q_H P_a/RT \tag{4.11}$$

where R is the gas constant, T is absolute temperature (assumed uniform along the flow path), A is cross-sectional area of flow path, a_v is the specific surface area of electrode, q_H is the volume of hydrogen reformed per unit length and time, which will be assumed uniform along the flow path, z is the flow direction, and P_a is atmospheric pressure (~0.92 atm). In addition, a total mass balance states that the volumetric flow rate of gas along the flow path will increase due to hydrogen reformation,

$$\frac{dQ}{dz} = q_H \tag{4.12}$$

Note that changes in total flow due to TCE consumption are negligible because of the low influent TCE concentration (500 ppmv).

Subtracting equation (4.10) from (4.11) yields

$$\frac{d(QP_H)}{dz} - \frac{4d(QP_T)}{dz} = \quad q_H P_a \tag{4.13}$$

Equations (4.12) and (4.13) can be directly integrated from 0 to z to obtain

$$Q = Q_0 + q_H z \tag{4.14}$$

$$P_H = P_{H0}\frac{Q_0}{Q} + \frac{q_H P_a z}{Q} - 4(P_{T0}\frac{Q_0}{Q} - P_T) \tag{4.15}$$

where Q_0 is the influent volumetric flow rate, and P_{H0} and P_{T0} are the hydrogen and TCE partial pressures in the influent, respectively.

Equation (4.10) can be rearranged to find a differential equation governing the TCE partial pressure profile in the reactor, as follows,

$$\frac{dP_T}{dz} = -Aa_v r\frac{RT}{Q} - \frac{q_H P_T}{Q} \tag{4.16}$$

Substitution of equations (4.9), (4.14) and (4.15) into this equation yields an ordinary differential equation that can be solved numerically, along with the initial condition

$$P_T = P_{T0}, \text{ at } z=0 \tag{4.17}$$

The only unknown parameters in the formulation are A, a_v, k, K_T and K_H. It was assumed that $K_T P_T << 1$, so that the TCE isotherm is linear. In this case, the parameters A, a_v, k and K_T appear in the same terms and were lumped together as follows

$$k_f = Aa_v k K_T RT \tag{4.18}$$

Equation (4.16) was solved numerically and the parameters k_f and K_H were found by fitting the calculated value of TCE partial pressure at the reactor outlet to experimental data. The fitting procedure was based on the minimization of total squared error between

predicted and measured values. Model simulations were performed to investigate the sensitivity of reactor performance to operational variables.

4.5 Results and discussion

4.5.1 Fuel cell performance curve

In the reactions of interest of a PEM fuel cell, H_2 is oxidized on the surface of anode catalyst, and O_2 is reduced on the surface of cathode catalyst. The reactions are

$$H_{2(g)} \rightarrow 2H^+ + 2e^-,\ E_a^o = 0\ V \tag{4.19}$$

$$\frac{1}{2}O_{2(g)} + 2e^- + 2H^+ \rightarrow H_2O,\ E_c^o = +1.23\ V \tag{4.20}$$

Theoretically, the open circuit potential (OCV) for the H_2/O_2 fuel cell under standard conditions is $OCV = E_c^o - E_a^o = +1.23$ V. In practice, the OCV for PEM fuel cells is around +1 V due to several non-idealities, including hydrogen crossover from the anode side to the cathode side, corrosion of electrode material, and oxygen reduction to hydrogen peroxide instead of water [102]. To obtain power from fuel cells, an electrical load is placed in the external circuit between anode and cathode. As current flows, the cell potential will deviate from the OCV due to activation overpotential, resistance loss, and mass transfer overpotential. A plot of cell potential vs. current density (current per unit nominal electrode area) is used to describe the performance of PEM fuel cell.

Performance curves depend on pressure, temperature, catalyst type and surface area, and membrane water content. Figure 4.4 shows the performance curve obtained in this work. The shape of the curve suggests that overpotential is strongly affected by PEM

limitations due to resistance to proton transport. There were no obvious mass transfer limitations to the catalytic surface in either electrode chamber. The activation overpotential was small, indicating that the Pt catalyst was in good condition.

More skillful construction of the MEA might have resulted in a less prominent overpotential loss due to trans-PEM charge transfer. However, the objective of this research was to study the feasibility and mechanism of TCE reduction using the MEA device. Therefore, no further effort was taken to optimize MEA design for high-energy generation performance.

4.5.2 TCE reduction products and conversion

The major product of TCE reduction in our experiments was ethane, counting for 95% or more of the carbon in the original TCE (data not shown). A small amount of ethylene (<5%) was also produced, which was not separated from the ethane in the GC FID used here. There were no other chlorinated intermediates observed, perhaps due to the low detection limit of the GC FID, around 10 ppmv. Under similar experimental conditions, trace amount of all three DCE isomers (<0.5% of the TCE transformed) have been detected, but no vinyl chloride has been measured by Liu et al. [10]. Since the effluent gas flow rate is generally higher than the influent flow rate due to hydrogen gas reformation in the cathode chamber, measurements of TCE and ethane concentrations (or partial pressures) in the effluent were used in this work to calculate TCE conversion,

$$\text{TCE conversion} = \frac{P_{T,e}}{P_{T,e} + P_{E,e}} \tag{4.21}$$

where the subscript e refers to effluent concentration and P_E is partial pressure of ethane.

4.5.3 TCE conversion as a function of cell potential

The measured relation between TCE conversion and cell potential is shown in Figure 4.5 for a fixed influent gas flow rate. Cell potential (Equation 4.1) has been chosen as independent variable instead of cathode potential because of the difficulty of providing a useful reference electrode within the solid electrolyte. Both TCE conversion efficiency and the cell current generally increased as the cell potential became more negative. It is important to remember that only a portion of the decrease in cell potential observed is due to a decrease in the cathode potential. That is, the cathode potential decreased along with the decreasing cell potential, but both the anode potential and IR drop increased as well. The IR drop could have been estimated from the measured current and fuel cell performance curve, but this was not attempted here.

Electrode kinetic performance is expected to follow the Butler-Volmer relation [103],

$$i = i_0\left[\exp\left(\frac{\alpha_A nF}{RT}\eta\right) - \exp\left(-\frac{\alpha_C nF}{RT}\eta\right)\right] \qquad (4.22)$$

where i_0 is exchange current density, i is net reaction current density, F is the Faraday constant, α_A and α_C are the transfer coefficients for the oxidation and reduction reactions, respectively, η is the activation overpotential, defined as $\eta = E - E_{eq}$, where E is the electrode potential, and E_{eq} is the equilibrium potential for the redox reaction.

For low overpotentials (magnitude less than 50 mV), equation (4.22) may be approximated by the linear relation

$$i = i_0 \frac{(\alpha_C + \alpha_A)nF}{RT} \eta \qquad (4.23)$$

whereas at high overpotentials (greater than 100 mV), equation (4.22) reduces to an exponential,

$$i = i_0 \exp(-\frac{\alpha_C nF}{RT} \eta) \qquad (4.24)$$

The results in Figure 4.5 show that current and cell potential are linearly related throughout most of the cell potential range employed, indicating that ionic resistance was the dominating factor in cell potential change when compared with electrode polarization. The change in slope at high currents might indicate that mass transfer limitations were reached. The monotonic increase in current with decreasing cell potential is due to hydrogen consumption in the anode chamber and hydrogen production in the cathode (see below).

The observed TCE conversion (Figure 4.5) increased with decreasing cell potential at first, reached a maximum of about 65% at -0.1 V, and then slowly decreased over the remaining range of cell potentials explored. The reformation of hydrogen gas in the cathode contributed significantly to the volume rate of flow in the effluent from the cathode. Thus, the decrease in TCE conversion at cell potentials below -0.1 V was a result of the total flow increase and the consequent decrease in residence time due to hydrogen evolution in the cathode chamber. It could be hypothesized, in addition, that the evolution of molecular hydrogen may have swept TCE away from reaction sites in the cathode.

Figure 4.5 also shows the fit of the mathematical model to the TCE conversion data. The fitted values of the two adjustable parameters were k_f =624 $atm^{-1/2}$mL/min·m and K_H =13.4 atm^{-1}. The model adequately represents the trends followed by the data, including the decrease in conversion at low potentials due to the decrease in residence time.

Current efficiency is defined as the fraction of total current that is accounted for by the observed rate of TCE reduction, assuming that ethane was the only product (8-electron transfer). The current efficiency (Figure 4.5) was highest at a cell potential of 0.1 V and decreased monotonically with decreases in cell potential. When the cell potential was lower than -0.1 V, the current efficiency was less than 0.1%. At a cell potential of -0.4 V, the exit flow rate reached 42 mL/min, or more than twice the influent value (18 mL/min). These results confirm that most of the current was a consequence of hydrogen gas reformation in the cathode. The measured gas flow rate at the cathode exit matched well with the total exit flow rate that was calculated based on the assumption that the entire cell current represents hydrogen reformation (Figure 4.6).

4.5.4 Heterogeneous catalytic reduction of TCE

TCE and other chlorinated solvents can be reduced by molecular hydrogen in the presence of a metallic catalyst that can stabilize atomic hydrogen [47]. As stated above, during electrochemical operation of the fuel cell, a relatively large amount of hydrogen gas was produced on the cathode surface. It seems possible that the observed reduction of TCE in those experiments was the catalyzed TCE reaction with hydrogen on the Pt

catalyst, as opposed to direct electron transfer. A pathway of this nature was also proposed by Li et al. [9] for TCE reduction on elemental iron in aqueous media. To test this hypothesis, the fuel cell cathode chamber was operated as a heterogeneous catalytic reactor. A gas-phase mixture of hydrogen, nitrogen and TCE served as reactor influent. Hydrogen was added at flow rates designed to mimic conditions present during electrochemical operation; that is, hydrogen addition was equivalent to the hydrogen gas produced electrochemically, measured as the difference between effluent and influent flow rates during electrochemical operation. The difference between electrochemical and heterogeneous catalytic operation was that hydrogen gas was reformed in the former, but was added with the cathode influent during catalytic operation. In the latter, the anode side of the unit cell was complete shut down (no flow).

TCE conversion as a function of the reactor effluent flow under both sets of conditions is shown in Figure 4.7, along with model predictions. Model calculations were performed with the fitted parameters reported above. The similarity of TCE conversions in the two operational modes and the ability of the model to predict conversions in the catalytic mode of operation suggest that heterogeneous catalysis, which was the only reaction pathway available when $H_{2(g)}$ was added with the reactor influent, is responsible for TCE conversion under both operating conditions.

4.5.5 Fixed cell potential operation

The calibrated model was used to predict reactor performance under different operating conditions for model verification, and simulation of process performance when there

were no empirical data. Specifically, the model was verified using data obtained during electrochemical operation at a fixed cell potential (0 V). The influent flow rate was varied to obtain different TCE conversions. Model predictions, along with experimental data, are shown in Figure 4.8. The model robustness is illustrated by its capability to adequately predict these results, along with those obtained in the catalytic mode of operation described above.

Model calculations were used to assess the effect of flow path length and cross sectional area of flow channel on reactor performance. The results are shown in Figure 4.9. Variations of cross sectional area are represented by changes in the parameter k_f, which is directly proportional to A. The results in Figure 4.9 show that conversions close to 100% can be obtained by a fuel cell that has a flow path about four times longer than the unit used in this work, or one that has an electrode area 3 to 4 times higher.

4.5.6 O_2 Effects

The electronegative character and abundance of oxygen in the atmosphere make O_2 a potential inhibitor for TCE reduction in contaminated SVE gases by means of the fuel cell reactor used in this work. There are two potential pathways through which oxygen may compete with TCE reduction in the cathode: first, oxygen consumption of electrons (reaction 4.20) could inhibit hydrogen reformation in the cathode; second, oxygen gas might react on the catalyst with reformed hydrogen to produce water.

The mole content of oxygen in the influent gas stream was varied from 0 to 21% to examine potential inhibitory effects. Experimental results show that TCE conversion was

essentially independent of the oxygen partial pressure (Figure 4.10), although cell current for a given degree of TCE conversion increased monotonically with O_2 addition (Figure 4.11), reflecting oxygen reduction to water in the cathode chamber. The nonzero currents measured at all potentials greater than zero in the presence of oxygen (Figure 4.11) are directly associated with oxygen reduction. The change in the slope of the curves at zero cell potential represents the onset of hydrogen reformation in the cathode, which is responsible for TCE conversion.

The results in Figure 4.10 show that oxygen reduction does not interfere, to an appreciable extent, with TCE conversion. Moreover, the presence of O_2 has no effect on the product distribution of TCE decomposition, since ethane was still the major product. In the study of aqueous-phase thermocatalytic reduction of TCE on γ-Al_2O_3-supported Pd, Lowry et al. [75] observed that dissolved oxygen reacted twice as fast as TCE but its presence had no effect on TCE conversion. This is consistent with the results presented here.

4.5.7 Change in reactor performance with time

A reduction in the levels of TCE conversion with operation time was observed during both electrochemical operation (Figure 4.12) and thermocatalytic operation (Figure 4.13). Reactor deactivation typically follows a pattern of initial rapid deactivation followed by slower loss of conversion, as is commonly observed in heterogeneous catalytic reactions [75,104].

Catalyst deactivation is a ubiquitous problem in heterogeneous catalytic hydrodechlorination. The deactivation mechanism has been attributed to catalyst sintering, coking [61,105] and poisoning due to chemisorption of chlorine to the metal [14,53]. Catalyst sintering occurs at high temperature, and is not a mechanism for catalyst deactivation in this work. Coking also occurs at relatively high temperature. Mass balances on gas-phase carbon forms during electrolytic operation accounted for >90% of the influent mass, suggesting that coking is not a major source of catalyst deactivation. Catalyst deactivation was attributed mainly to chlorine poisoning. The high solvation energy of chloride ion in water helps eliminate adsorbed chlorine from metal catalysts and makes poisoning effects reversible upon washing with DI water. In this work, treatment of the cathode with various gases (N_2, H_2, O_2 and O_2+ H_2) did not lead to reactivation (Figure 4.13), whereas a relatively quick wash with DI water was enough to bring TCE conversion back to its original level. It is interesting that reactor deactivation did not cause a complete loss of conversion capacity: the TCE conversion level remained at about 25% for 1200 min after the wash with DI water in Figure 4.13 (results not shown). This indicates that a steady state is reached in the blocking of active sites by chlorine poisoning.

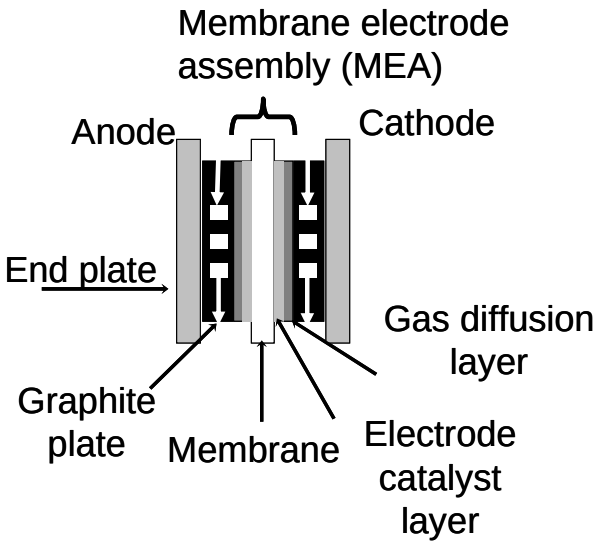

Figure 4.1. Polymer electrolyte membrane (PEM) fuel cell reactor. The fuel cell device was comprised of a membrane electrode assembly (MEA), two graphite plates with serpentine flow channels, and two end plates to support the whole device.

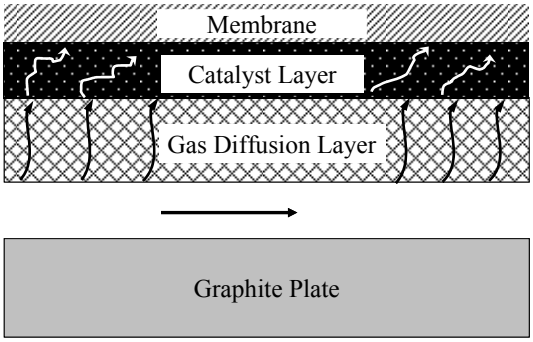

(a)

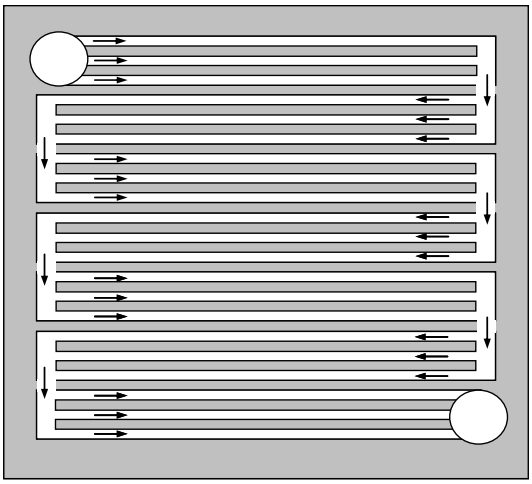

(b)

Figure 4.2. (a) Half of the MEA showing advective gas transport and the gas diffusion and (catalyst) reactive zones mounted on the PEM. (b) Serpentine channel configuration in the graphite plate.

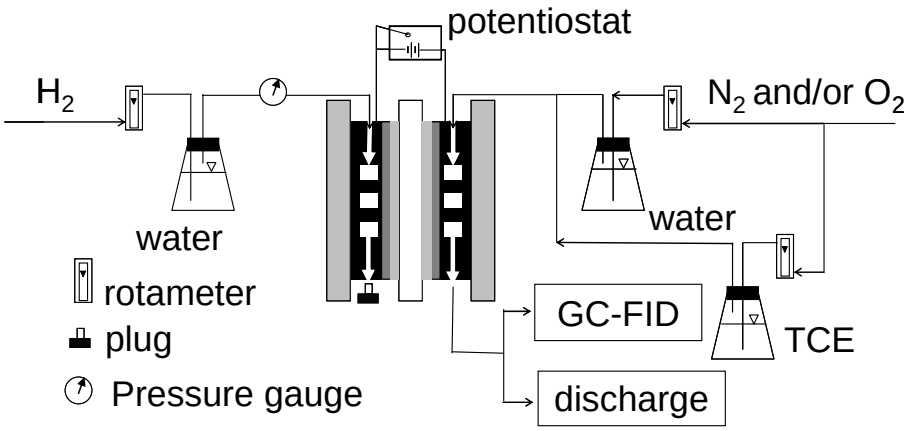

Figure 4.3. Experimental setup for fuel cell reactor system. Humidified hydrogen is fed to the anode chamber. Humidified nitrogen-containing gas-phase TCE flows through the cathode chamber. Reactants and products were monitored by gas chromatography using a flame ionization detector.

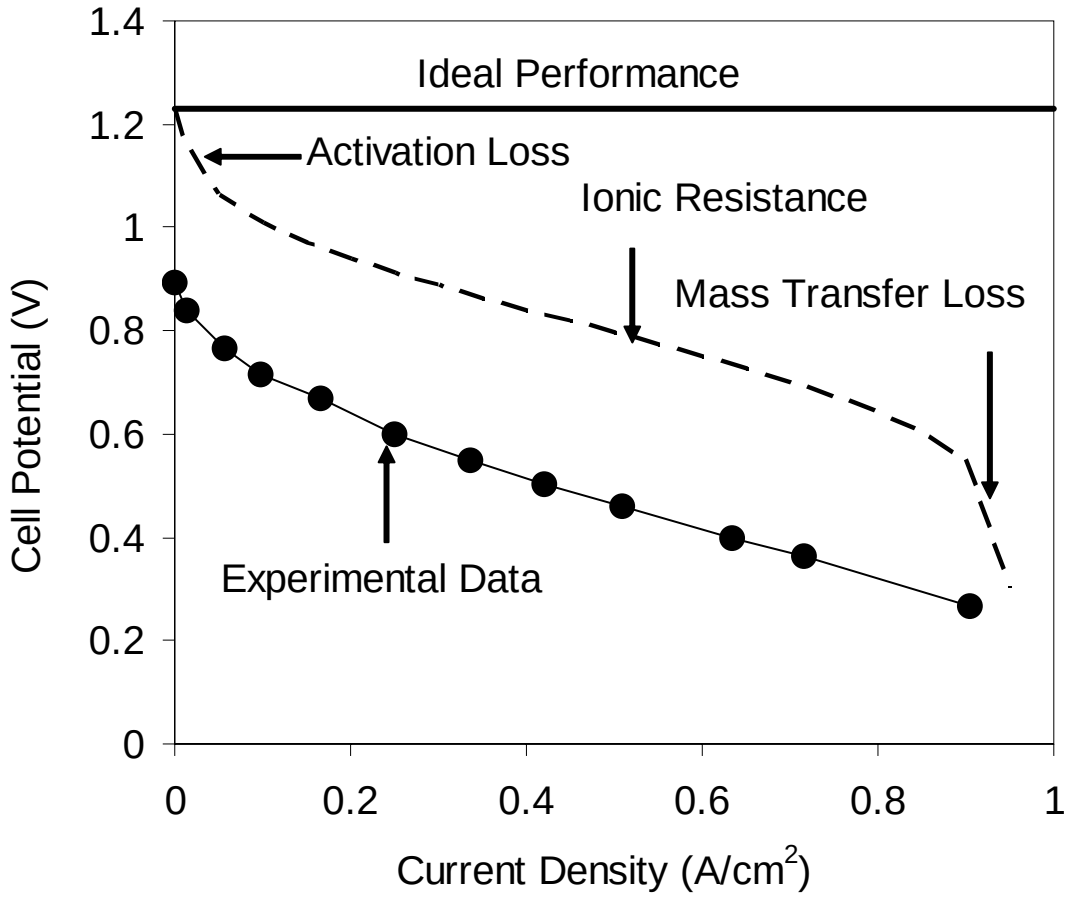

Figure 4.4. Current-potential performance curve for fuel cell operation. The solid line represents a theoretical ideal performance without any overpotential loss due to overpotential non-idealities. The dashed line illustrates the relation between typical or expected fuel cell performance and several sources of non-ideal behavior.

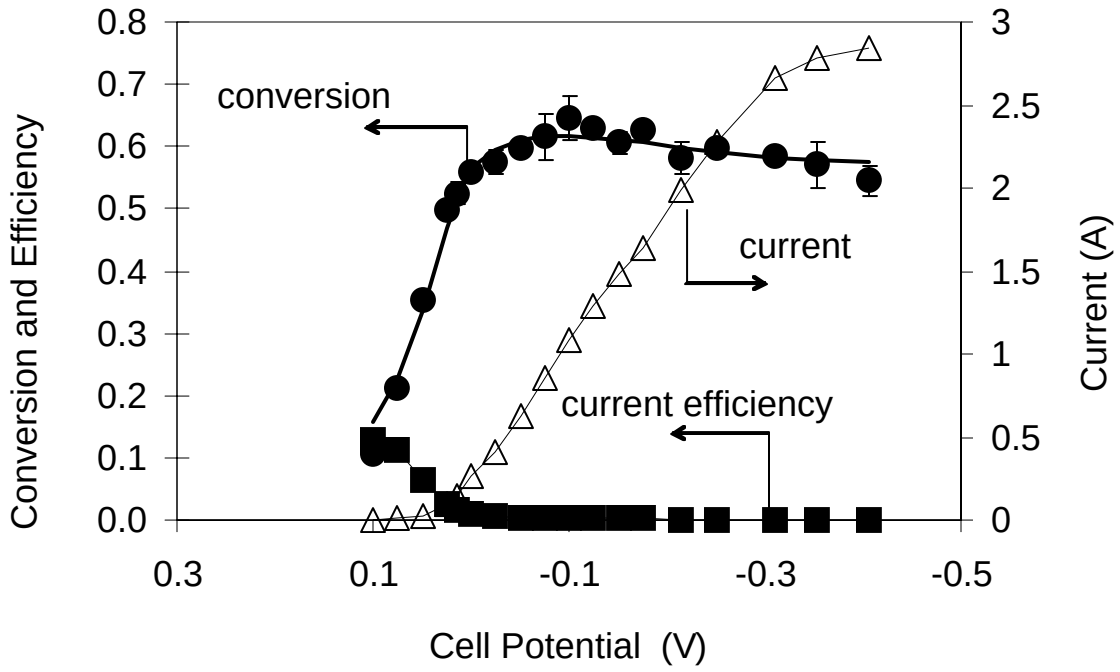

Figure 4.5. TCE conversion, current efficiency, and total current as a function of cell potential. The inlet flow rate to the cathode chamber was 18 mL/min, influent TCE concentration was 500 ppmv. The solid line through the TCE conversion data is a fit of the mathematical model (see text).

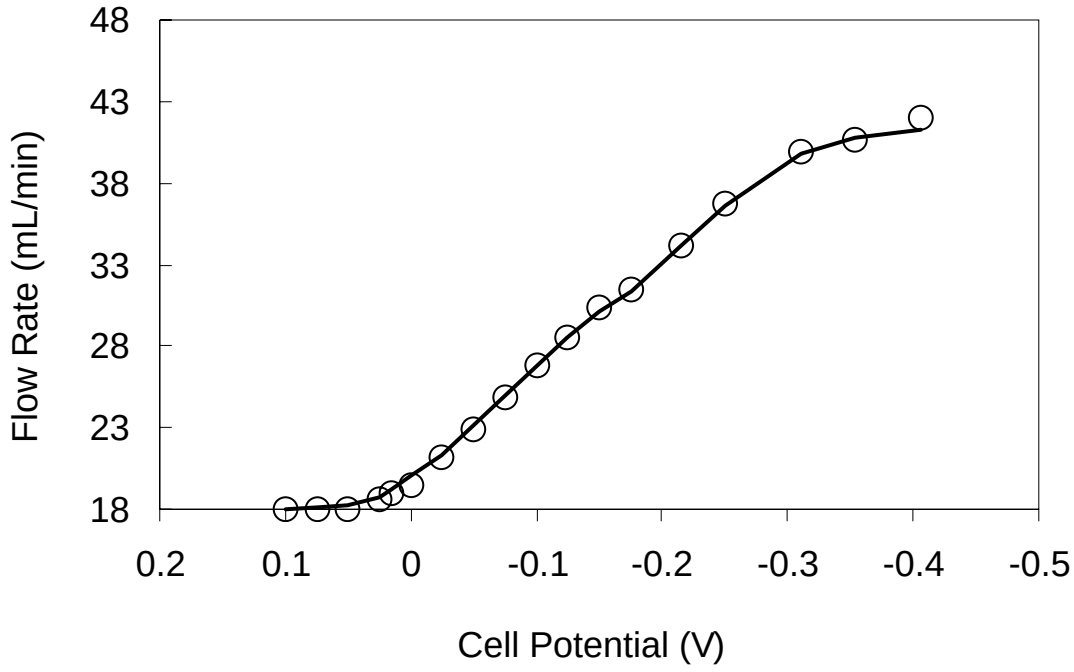

Figure 4.6. Measured exit flow rate (○) and calculated flow rate (—) as a function of cell potential. Calculations used Faraday's law and the ideal gas relation, assuming that the entire measured current represents hydrogen reformation in the cathode. The influent flow rate was 18 mL/min.

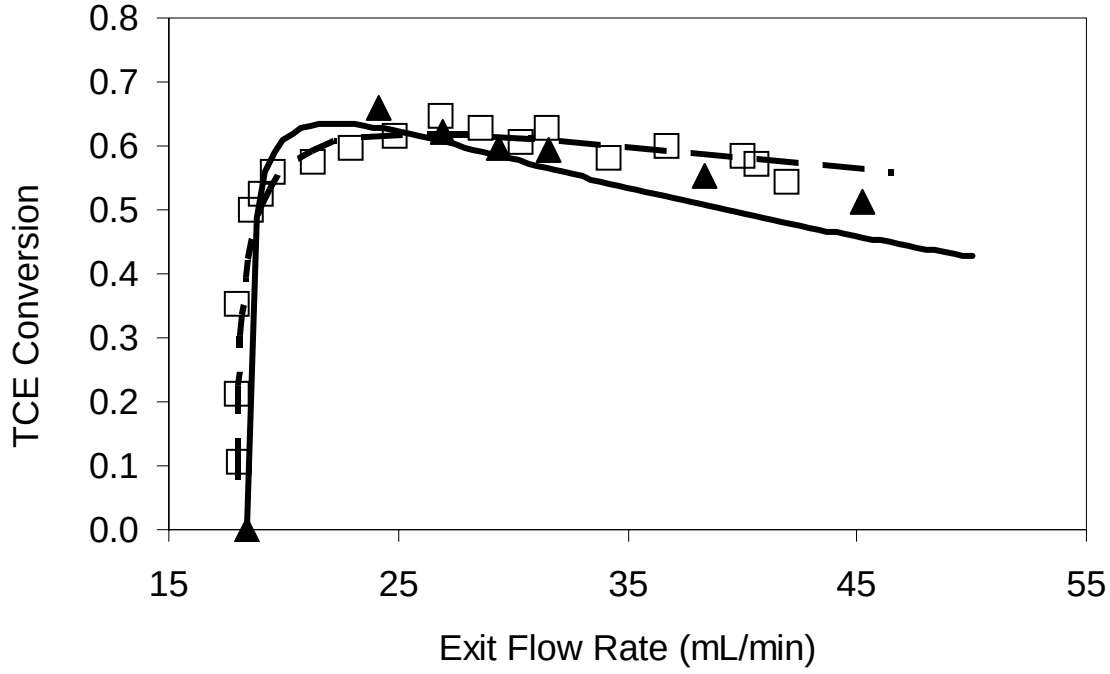

Figure 4.7. Experimental data (□, ▲) and model simulation (—, --) for electrochemical and catalytic operation, respectively. Electrochemical operation was conducted by varying cell potential from +0.1 V to -0.4 V while keeping the inlet flow rate at 18 mL/min. The exit flow rate changed with cell potential, reflecting hydrogen reformation on the cathode side (Figure 4.6). Catalytic operation was conducted by supplying both TCE and $H_{2(g)}$ with the influent to the cathode chamber while the anode and cathode were disconnected. The TCE inlet concentration was approximately 500 ppmv.

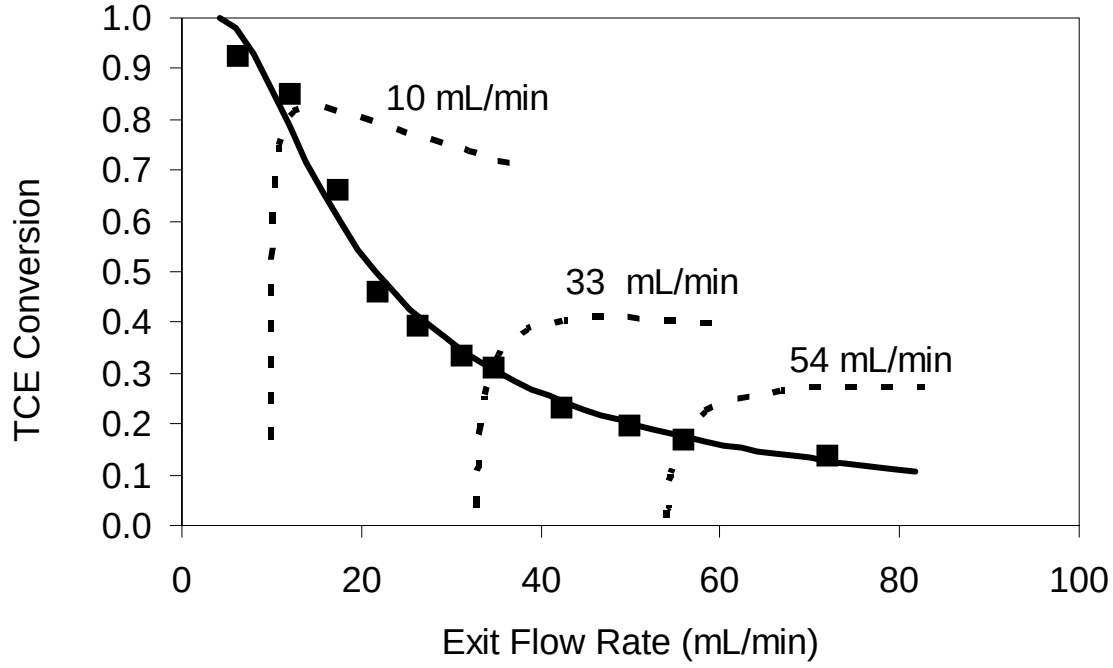

Figure 4.8. Experimental data (■) and model simulation (▬) for electrochemical operation with varying inlet flow rate and cell potential fixed at 0 V. The current, and thus hydrogen generation rate, were constant at 0.2 A and 1.6 mL/min, respectively, while the influent flow rate was varied. Dashed lines are model predictions for constant influent flow rate.

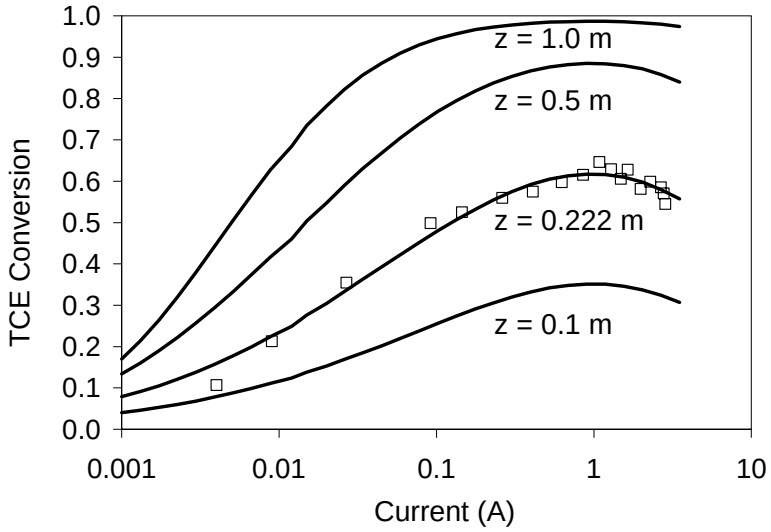

(a)

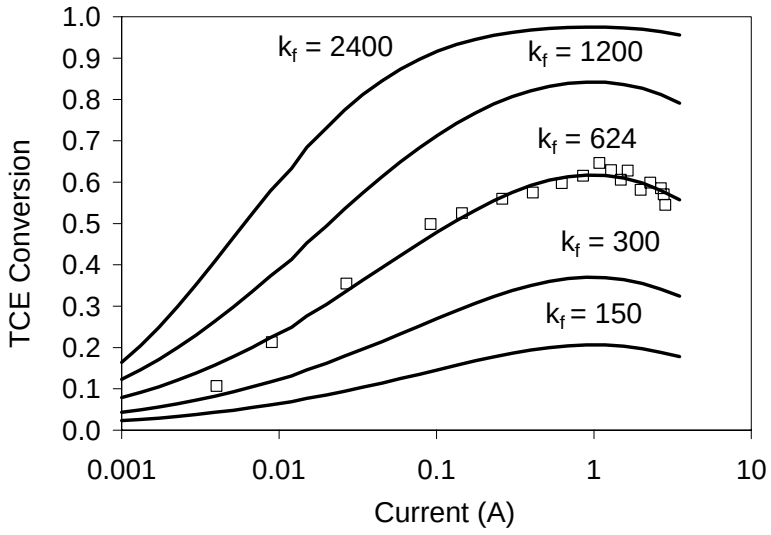

(b)

Figure 4.9. TCE conversion as a function of cell current and (a) reactor length, and (b) cross-sectional area of flow path, represented in terms of changes in k_f (atm$^{-1/2}$·mL/min m). The influent flow rate to the cathode was 18 mL/min, and the TCE influent concentration was 500 ppmv

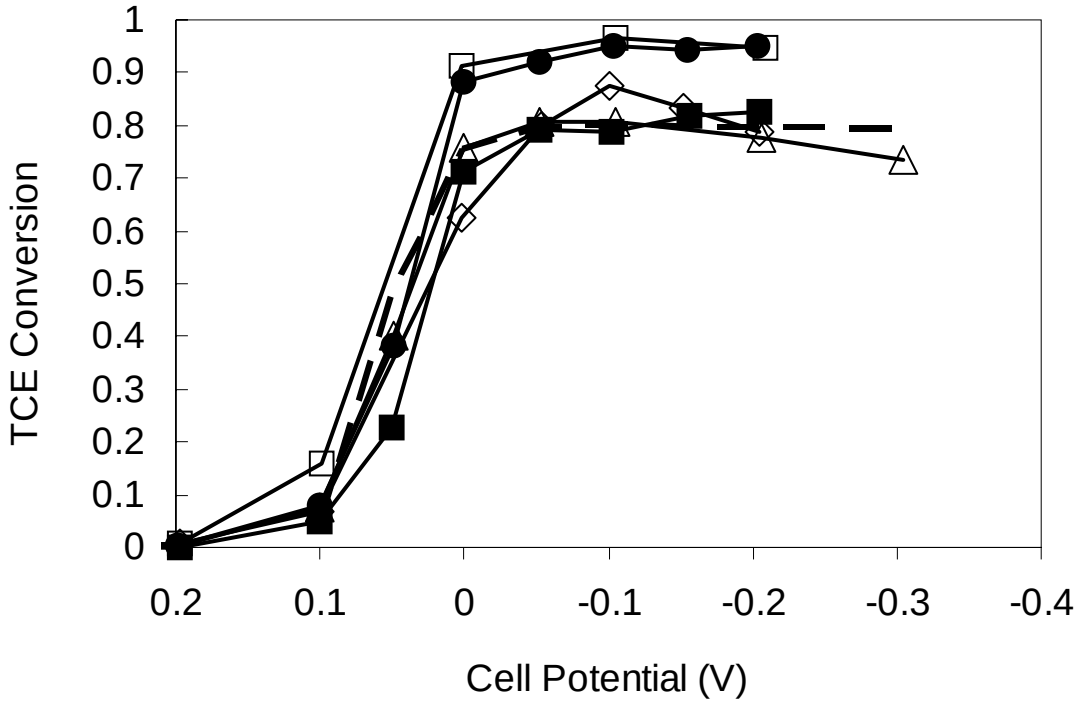

Figure 4.10. TCE conversion as a function of cell potential for: 0% O_2 (Δ), 5% (●), 10% (■), 15% (□), and 21% (◊). Dashed line is model simulation for the case without O_2. Solid lines are straight lines joining data points. Inlet flow rate is 10 mL/min.

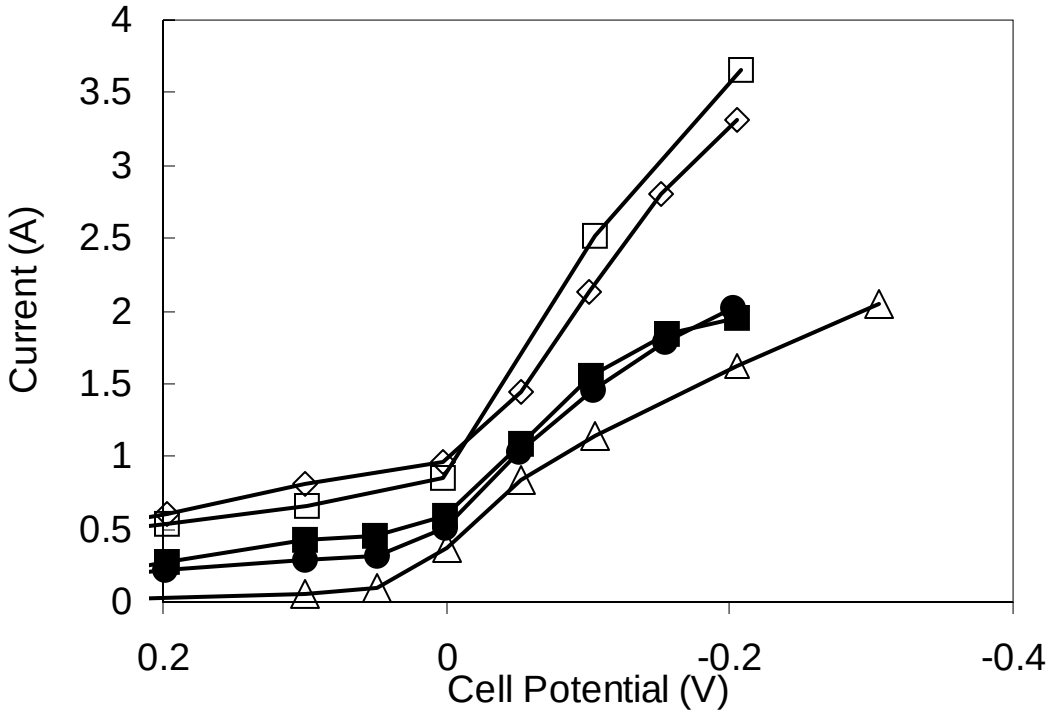

Figure 4.11 Current as a function of cell potential for TCE degradation experiments with: 0% O_2 (Δ), 5% (●), 10% (■), 15% (□), and 21% (◊). Solid lines are straight lines joining data points. Conditions are the same as in Figure 4.10.

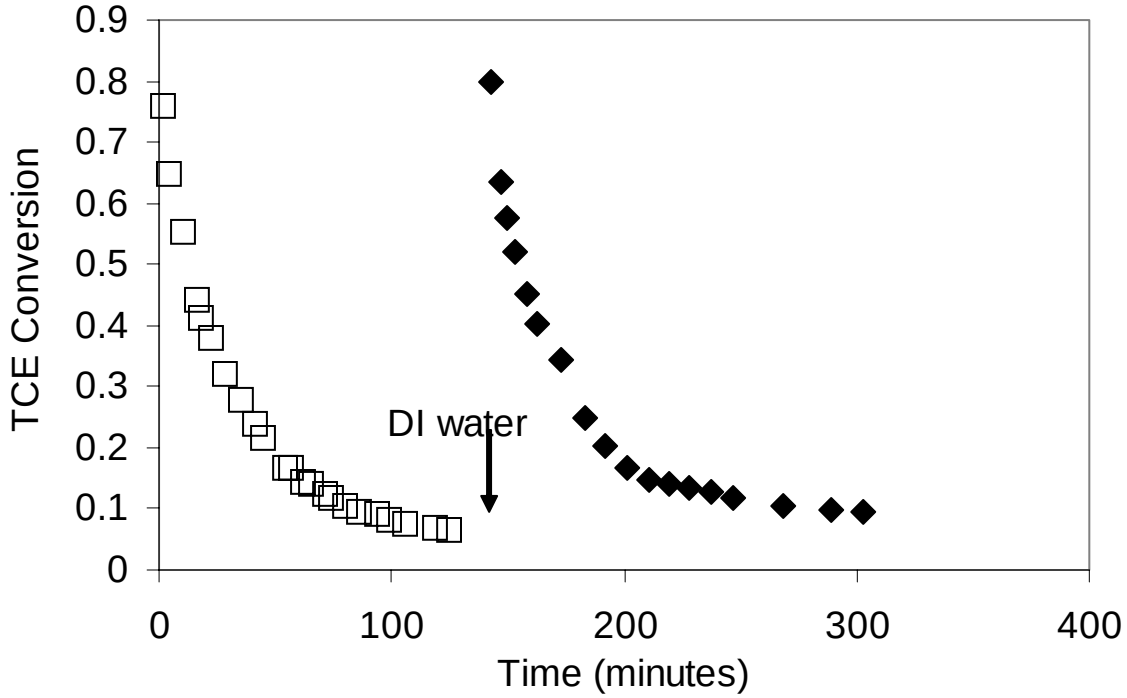

Figure 4.12. TCE conversion decrease with time in electrochemical operation. In these experiments, the cell potential was set at -0.1 V, the influent flow rate 40 mL/min, TCE influent concentration was 2000 ppmv. The cathode chamber was washed with 600 mL DI water at the indicated time.

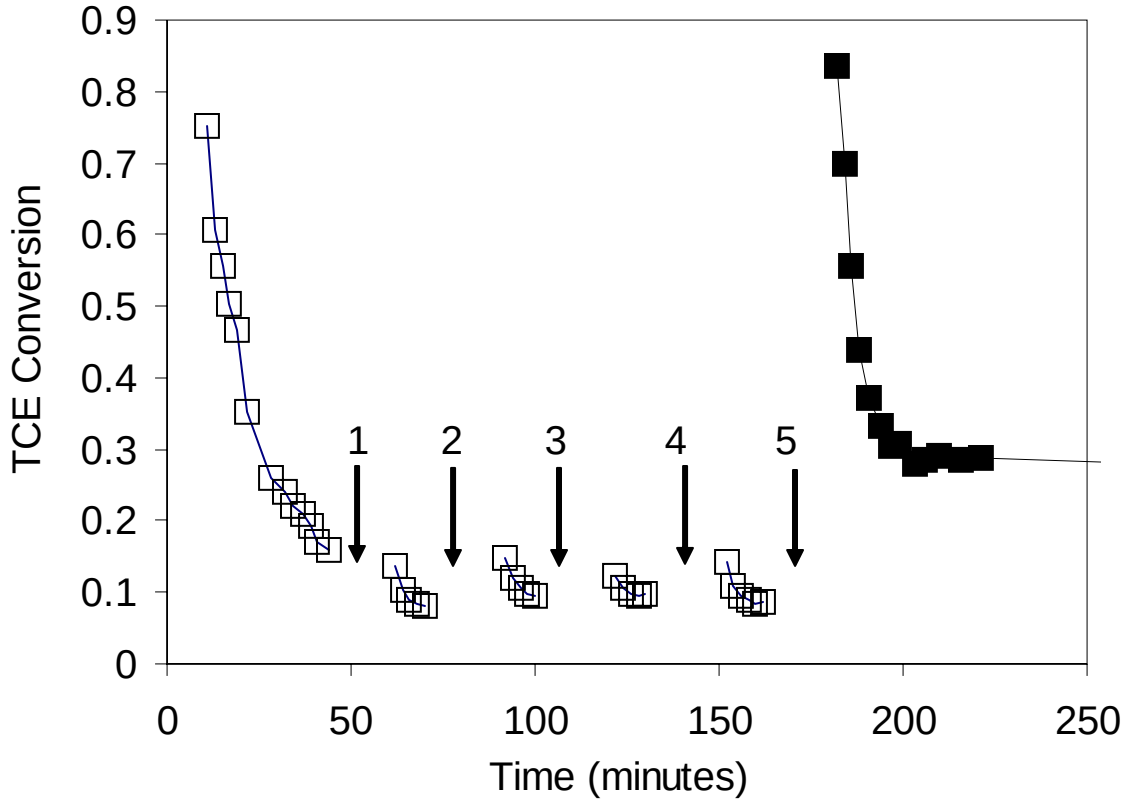

Figure 4.13. TCE conversion decrease with time in catalytic operation. The influent flow rate was 150 mL/min, the TCE influent concentration was 2000 ppmv, and influent gas was ~97% hydrogen. The indicated times 1, 2, 3, 4, 5 represent sequential treatment with 200 mL/min N_2, O_2, H_2, O_2+H_2 for 20 minutes, and 600 mL DI water, respectively.

CHAPTER 5

SUMMARY

5.1 Catalytic hydrodechlorination gas-phase TCE using packed-bed reactors

Catalytic hydrodechlorination (HDC) of gas-phase trichloroethylene (TCE) was investigated using 0.5 wt.% Pt/Al_2O_3 and 0.0025 wt.% Pt/SiO_2 in packed-bed reactors. TCE was efficiently transformed on the platinum surface using H_2 as reducing agent. The main products of the reaction were ethane and chloroethane. In the case of Pt/Al_2O_3, more than 94% TCE conversion efficiency was maintained for over 700 hours of operation with a residence time of 0.37 seconds at 100ºC. At this temperature, ethane was the sole observable product. At 22ºC, severe catalyst deactivation was observed, as TCE conversion efficiency dropped from 87% to 5% in 80 hours of operation. The catalyst deactivation rate constant for TCE hydrodechlorination at 22ºC (0.039 h^{-1}) was 162 times larger than that at 100ºC (0.00024 h^{-1}). That is, high temperature operation tended to extend catalyst life while improving both process kinetics and product selectivity (for ethane). Catalyst deactivation was attributed to coking and chlorine poisoning. A series of treatments including hydrogen treatment to remove chlorine and oxygen treatment to remove coke was attempted to regenerate the deactivated catalyst. Only hydrogen treatment partially restored catalyst activity.

When using Pt/SiO_2, catalyst deactivation was severe even at 100ºC, probably due to low surface area of Pt and the silica support. Amending 1 g powder KOH to 175 g Pt/SiO_2 reduced the catalyst deactivation rate constant by a factor of 4. The presence of O_2 in the gas stream had beneficial effects on TCE removal, increasing the temperature of the

catalyst surface due to the reaction with H_2, and/or preventing deposition of carbonaceous compounds on the catalyst.

5.2 Reductive destruction of gas-phase TCE using PEM fuel cell design

Reductive dehalogenation of gas-phase TCE was tested using a gas diffusion electrode in a design similar to a polymer electrolyte membrane (PEM) fuel cell. The critical part of the PEM fuel cell is the membrane electrode assembly (MEA) consisting of a proton-conducting membrane sandwiched by two gas diffusion electrodes serving as anode and cathode. In this research, both anode and cathode were made of carbon-black-supported Pt, deposited on a carbon cloth gas diffusion layer.

TCE was transformed to ethane and hydrochloric acid at the cathode Pt surface. The results obtained suggest that TCE reduction occurs by a catalytic reaction with atomic hydrogen that is reformed on the Pt surface beyond a certain applied cell potential, rather than reduction via direct electron transfer. Substantial conversion of TCE is obtained, even when oxygen reduction competes for hydrogen on the cathode surface. The process has been modeled successfully by conceptualizing the cathode chamber as a plug flow reactor with a continuous source of hydrogen emanating from the boundary.

REFERENCES

1. EPA *Cleaning Up the Nation's Waste Sites: Markets and Technology Trends*; EPA 542-R-04-015, 2004.

2. National Research Council *Alternatives for ground Water Cleanup*; National Academy Press: Washington D.C., 1994.

3. American Water Works Association *water quality and treatment*; 5th ed.; McGraw-Hill, INC., 1999.

4. Goldberg, S. J. *Journal of the American College of Cardiology* 1990, *16*, p155.

5. CBO *Cleaning Up Defense Installations: Issues and Options* Washington, D.C: Congressional Budget Office, 1995.

6. LaGrega, M. D.; Buckingham, P. L.; Evans, J. C.; Environmental Resources Management *Hazardous Waste Management*; 2nd ed.; McGraw-Hill, 2001.

7. Vogel, T. M.; Criddle, C. S.; McCarty, P. L. *Environ. Sci. Technol.* 1987, *21*, p722

8. Gillham, R. W.; O'Hannesin, S. F. *Ground Water* 1994, *32*, p958.

9. Li, T.; Farrell, J. *Environ. Sci. Technol.* 2001, *35*, p3560.

10. Liu, Z.; Arnold, R. G.; Betterton, E. A.; Smotkin, E. *Environ. Sci. Technol.* 2001, *35*, p4320.

11. Wang, J.; Farrell, J. *Environ. Sci. Technol.* 2003, *37*, p3891.

12. Bonarowska, M.; Burda, B.; Juszczyk, W.; Pielaszek, J.; Kowalczyk, Z.; Karpinski, Z. *Appl. Catal. B: Environ.* 2001, *35*, p13.

13. Bonarowska, M.; Malinowski, A.; Karpinski, Z. *Appl. Catal. A: Gen.* 1999, *188*, p145.

14. Bozzelli, J. W.; Chen, Y.-M.; Chuang, S. S. C. *Chem. Eng. Commun.* 1992, *115*, p1.

15. Campbell, J. S.; Kemball, C. *Trans. Faraday Soc.* 1961, *57*, p809

16. Keane, M. A.; Murzin, D. Y. *Chem. Eng. Sci.* 2001, *56*, p3185.

17. Habutsu, H.; Okazaki, S. *J. Fluorine Chem.* 1991, *54*, p385.

18. Kim, S. Y.; Choi, H. C.; Yanga, O. B.; Lee, K. H.; Lee, j. S.; Kim, Y. G. *J.Chem. Soc., Chem. Commun.* 1995, p2169

19. Dini, P.; Bart, J. C. J.; Giordano, N. *J. C. S. Perkin II* 1975, p1479.

20. Ahn, B. S.; Lee, S. C.; Moon, D. J.; Lee, B. G. *J. Mol. Catal. A: Chem.* 1996, *106*, p83.

21. Bonarowska, M.; Pielaszek, J.; Semikolenov, V. A.; Karpinski, Z. *J. Catal.* 2002, *209*, p528.

22. Cao, Y. C.; Jiang, X. Z. *J. Mol. Catal. A: Chem.* 2002, *184*, p183.

23. Gioia, F.; Gallagher, E. J.; Famiglietti, V. *J. Hazard. Mater.* 1994, *38*, p277.

24. LaPierre, R. B.; Guczi, L.; Kranich, W. L.; Weiss, A. H. *J. Catal.* 1978, *52*, p230.

25. Yuan, G.; Keane, M. A. *Catal. Commun.* 2003, *4*, p195.

26. Bae, J. W.; Kim, I. G.; Lee, J. S.; Lee, K. H.; Jang, E. J. *Appl. Catal. A: Gen.* 2003, *240*, p129.

27. Ordonez, S.; Diez, F. V.; Sastre, H. *Catal. Today* 2002, *73*, p325.

28. Johnstone, R. A. W.; Wilby, A. H.; Entwistle, I. D. *Chem. Rev.* 1985, *85*, p129.

29. Ukisu, Y.; Kameoka, S.; Miyadera, T. *Appl. Catal. B: Environ.* 2000, *27*, p97.

30. Ukisu, Y.; Miyadera, T. *Appl. Catal. B: Environ.* 2003, *40*, p141.

31. Shin, E.-J.; Keane, M. A. *J. Hazard. Mater.* 1999, *66*, p265.

32. Murena, F.; Gioia, F. *Appl. Catal. B: Environ.* 2002, *38*, p39.

33. Yuan, G.; Keane, M. A. *J. Catal.* 2004, *225*, p510.

34. Kim, D. I.; Allen, D. T. *Ind. Eng. Chem. Res.* 1997, *36*, p3019

35. Murwani, I. K.; Kemnitz, E.; Skapin, T.; Nickkho-Amiry, M.; Winfield, J. M. *Catal. Today* 2004, *88*, p153.

36. Thompson, C. D.; Rioux, R. M.; Chen, N.; Ribeiro, F. H. *J. Phys. Chem. B* 2000, *104*, p3067.

37. Anderson, J. R.; McConkey, B. H. *J. Catal.* 1968, *11*, p54.

38. Chen, N.; Rioux, R. M.; Ribeiro, F. H. *J. Catal.* 2002, *211*, p192.

39. Dal Santo, V.; Dossi, C.; Recchia, S.; Colavita, P. E.; Vlaic, G.; Psaro, R. *J. Mol. Catal. A: Chem.* 2002, *182-183*, p157.

40. Gomez-Sainero, L. M.; Seoane, X. L.; Fierro, J. L. G.; Arcoya, A. *J. Catal.* 2002, *209*, p279.

41. Weiss, A. H.; Gambhir, B. S.; Leon, R. B. *J. Catal.* 1971, *22*, p245.

42. Golubina, E. V.; Lokteva, E. S.; Lunin, V. V.; Turakulova, A. O.; Simagina, V. I.; Stoyanova, I. V. *Appl. Catal. A: Gen.* 2003, *241*, p123.

43. Delannoy, L.; Giraudon, J. M.; Granger, P.; Leclercq, L.; Leclercq, G. *Appl. Catal. B: Environ.* 2002, *37*, p161.

44. Bae, J. W.; Park, E. D.; Lee, J. S.; Lee, K. H.; Kim, Y. G.; Yeon, S. H.; Sung, B. H. *Appl. Catal. A: Gen.* 2001, *217*, p79.

45. Prati, L.; Rossi, M. *Appl. Catal. B: Environ.* 1999, *23*, p135.

46. Munakata, N.; Reinhard, M. Palladium Catalysis for the Treatment of Contaminated Waters: a Review. In *Physicochemical Groundwater Remediation*; Smith, J. A., Burns, S. E., Eds.; Kluwer Academic/Plenum Pub.: London 2001; pp 46-71.

47. Ordonez, S.; Sastre, H.; Diez, F. V. *Appl. Catal. B: Environ.* 2000, *25*, p49.

48. Ordonez, S.; Sastre, H.; Diez, F. V. *Appl. Catal. B: Environ.* 2003, *40*, p119.

49. Weiss, A. H.; Krieger, K. A. *J. Catal.* 1966, *6*, p167.

50. Farrauto, R. J.; Bartholomew, C. H. *Fundamentals of Industrial Catalytic Processes*; first ed.; Blackie Academic & Professional: London, 1997.

51. Gampine, A.; Eyman, D. P. *J. Catal.* 1998, *179*, p315.

52. Yuan, G.; Keane, M. A. *Appl. Catal. B: Environ.* 2004, *52*, p301.

53. Aramendia, M. A.; Borau, V.; Garcia, I. M.; Jimenez, C.; Lafont, F.; Marinas, A.; Marinas, J. M.; Urbano, F. J. *J. Mol. Catal. A: Chem.* 2002, *184*, p237.

54. Chang, C.-C.; Reo, C. M.; Lund, C. R. F. *Appl. Catal. B: Environ.* 1999, *20*, p309.

55. Coq, B.; Ferrat, G.; Figueras, F. *J. Catal.* 1986, *101*, p434.

56. Ribeiro, F. H.; Gerken, C. A.; Rupprechter, G.; Somorjai, G. A.; Kellner, C. S.; Coulston, G. W.; Manzer, L. E.; Abrams, L. *J. Catal.* 1998, *176*, p352.

57. Balko, E. N.; Przybylski, E.; Von Trentini, F. *Appl. Catal. B: Environ.* 1993, *2*, p1.

58. Hoke, J. B.; Gramiccioni, G. A.; Balko, E. N. *Appl. Catal. B: Environ.* 1992, *1*, p285.

59. Shin, E.-J.; Keane, M. A. *Appl. Catal. B: Environ.* 1998, *18*, p241.

60. Frankel, K. A.; Jang, B. W. L.; Spivey, J. J.; Roberts, G. W. *Appl. Catal. A: Gen.* 2001, *205*, p263.

61. Ordonez, S.; Sastre, H.; Diez, F. V. *Thermochimica Acta* 2001, *379*, p25.

62. Weiss, A. H.; Valinski, S.; Antoshin, G. V. *J. Catal.* 1982, *74*, p136.

63. Creyghton, E. J.; Burgers, M. H. W.; Jansen, J. C.; van Bekkum, H. *Appl. Catal. A: Gen.* 1995, *128*, p275.

64. Ordonez, S.; Diez, F. V.; Sastre, H. *Appl. Catal. B: Environ.* 2001, *31*, p113.

65. Wiersma, A.; van de Sandt, E. J. A. X.; den Hollander, M. A.; van Bekkum, H.; Makkee, M.; Moulijn, J. A. *J. Catal.* 1998, *177*, p29.

66. Marecot, P.; Akhachane, A.; Micheaud, C.; Barbier, J. *Appl. Catal. A: Gen.* 1998, *169*, p189.

67. Lerner, B. A.; Carvill, B. T.; Sachtler, W. M. H. *Catal. Today* 1994, *21*, p23.

68. Ren, X. H.; Bertmer, M.; Stapf, S.; Demco, D. E.; Blumich, B.; Kern, C.; Jess, A. *Appl. Catal. A: Gen.* 2002, *228*, p39.

69. Chambers, A.; Baker, R. T. K. *J. Phys. Chem. B* 1997, *101*, p1621.

70. Kulkarni, P. P.; Deshmukh, S. S.; Kovalchuk, V. I.; d'Itri, J. L. *Catal. Lett.* 1999, *61*, p161.

71. Zhang, Z. C.; Beard, B. C. *Appl. Catal. A: Gen.* 1998, *174*, p33.

72. Bradford, M. C. J.; Vannice, M. A. *Appl. Catal. A: Gen.* 1996, *142*, p73.

73. van de Sandt, E. J. A. X.; Wiersma, A.; Makkee, M.; van Bekkum, H.; Moulijn, J. A. *Appl. Catal. A: Gen.* 1998, *173*, p161.

74. Lowry, G. V.; Reinhard, M. *Environ. Sci. Technol.* 2000, *34*, p3217

75. Lowry, G. V.; Reinhard, M. *Environ. Sci. Technol.* 2001, *35*, p696

76. Mcnab, W. W., Jr.; Ruiz, R.; Reinhard, M. *Environ. Sci. Technol.* 2000, *34*, p149

77. Liu, Z.; Betterton, E. A.; Arnold, R. G. *Environ. Sci. Technol.* 2000, *34*, p804.

78. Chen, G.; Betterton, E. A.; Arnold, R. G.; Ela, W. P. *Journal of applied Electrochemistry* 2003, *33*, p161.

79. Farrell, J.; Melitas, N.; Kason, M.; Li, T. *Environ. Sci. Technol.* 2000, *34*, p2549.

80. Li, T.; Farrell, J. *Environ. Sci. Technol.* 2000, *34*, p173.

81. Costentin, C.; Robert, M.; Saveant, J. M. *J. Am. Chem. Soc.* 2003, *125*, p10729.

82. Al-Abed, S. R.; Fang, Y.; Kukainis, V. R. In *Presented at American Chemical Society National Meeting*: New Orleans, LA, 2003.

83. Fangmark, I. E.; Hammarstrom, L.-G.; Stromqvist, M. E.; Ness, A. L.; Norman, P. R.; Osmond, N. M. *Carbon* 2002, *40*, p2861.

84. Roh, Y.; Cho, K.-S.; Lee, S. *J. Environ. Sci. Health A* 2001, *36*, p923.

85. Nagaoka, T.; Yamashita, J.; Takase, M.; Ogura, K. *J. Electrochem. Soc.* 1994, *141*, p1522.

86. Tezuka, M.; Yajima, T. *Denki Kagaku oyobi Kogyo Butsuri Kagaku* 1991, *59*, p517.

87. Lipkowski, J.; Ross, P. N. *Electrocatalysis*; WILEY-VCH, 1998.

88. Sonoyama, N.; Sakata, T. *Environ. Sci. Technol.* 1998, *32*, p4005.

89. Sonoyama, N.; Sakata, T. *Environ. Sci. Technol.* 1998, *32*, p375.

90. Motoo, s.; Watanabe, m.; Furuya, n. *J. Electroanal. Chem.* 1984, *160*, p351

91. Lowry, G. V.; Reinhard, M. *Environ. Sci. Technol.* 1999, *33*, p1905

92. ATSDR "Toxicological Profile for Trichloroethylene," Atlanta, GA: U.S. Department of Health and Human Services, Public Health Service, 1997.

93. U.S. EPA "Toxics Release Inventory Public Data Release," 2005.

94. He, J.; Ela, W. P.; Betterton, E. A.; Arnold, R. G.; Sáez, A. E. *Ind. Eng. Chem. Res.* 2004, *43*, p7965.

95. He, J.; Saez, A. E.; Ela, W. P.; Betterton, E. A.; Arnold, R. G. *Ind. Eng. Chem. Res.* 2004, *43*, p913.

96. Liu, Z.; Arnold, R. G.; Betterton, E. A.; Festa, K. D. *Environmental Science Engineering* 1999, *16*, p1.

97. Farrell, J.; Kason, M.; Melitas, N.; Li, T. *Environ. Sci. Technol.* 2000, *34*, p514.

98. Roberts, A. L.; Totten, L. A.; Arnold, W. A.; Burris, D. R.; Campbell, T. J. *Environ. Sci. Technol.* 1996, *30*, p2654.

99. Lambert, F. L.; Hasslinger, B. L.; Franz, R. N. *J. Electrochem. Soc.* 1975, *122*, p737.

100. Wang, J.; Blowers, P.; Farrell, J. *Environ. Sci. Technol.* 2004, *38*, p1576.

101. Warren, K. D.; Arnold, R. G.; Bishop, T. L.; Lindholm, L. C.; Betterton, E. A. *Journal of Hazardous Materials* 1995, *41*, p217.

102. Hoogers, G. *Fuel Cell Technology Handbook*; CRC Press LLC, 2003.

103. Bard, A. J.; Faulkner, L. R. *Electrochemical Methods Fundamentals and Applications*; 2nd ed.; John Wiley & Sons, Inc., 2001.

104. Thomas, J. M.; Thomas, W. J. *Principles and Practice of Heterogeneous Catalysis*; VCH: New York, 1997.

105. Frankel, K. A.; Jang, B. W. L.; Roberts, G. W.; Spivey, J. J. *Applied Catalysis A: General* 2001, *209*, p401.